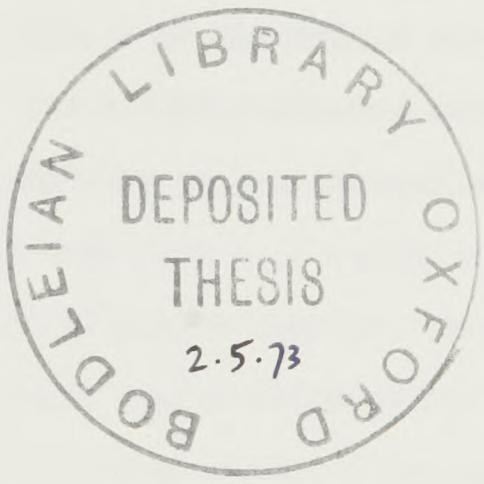
Electrical Conduction in Semiconductors at Low Temperatures

by

L. Eaves

A thesis submitted for the degree of
Doctor of Philosophy
at the
University of Oxford



Christ Church
November, 1972

ABSTRACT

This thesis is concerned with the study of the magnetophonon effect in a wide range of semiconductors. The five materials investigated are n-InP, n-CdSe, n-Ge, p-Ge and p-GaAs. The effect which was first predicted in a theoretical paper by Gurevich and Firsov (1961) arises from the resonant coupling of optical phonons with conduction electrons in an applied magnetic field. Extrema occur in the magnetoresistance when the phonon energy approaches an integral number of Landau level spacings. The resonance condition is

$$N\omega_c = \frac{NeB}{m^*} = \omega_\ell \; ; \; N = 1,2,3\ldots \qquad (1)$$

where ω_ℓ is the phonon frequency, ω_c the cyclotron frequency, m^* the carrier effective mass and B the applied magnetic field.

There are three main applications of the magnetophonon experiments to the study of the properties of conduction electrons. Firstly, equation (1) may be used to determine a precise value of the band edge effective mass provided that small corrections for band non-parabolicity and polaron effects are taken into account. Secondly, the data are a test of recent theories concerning the problem of electrical conduction in an applied magnetic field. Thirdly, the magnetophonon structure which appears in the non-ohmic magnetoresistance at low temperatures can reveal new mechanisms for the energy relaxation of warm electrons.

The first application of magnetophonon resonance is of particular relevence to the study of n-InP and n-CdSe since previously the conduction band effective masses had not been known precisely. In n-InP (Eaves et al., 1971) up to eleven extrema have been observed in the transverse orientation over the temperature range from 77 K to 300 K. The low frequency cyclotron effective mass deduced from the field positions of the peaks is $0.082\ m_0 \pm 0.001\ m_0$ at 77 K and $0.078\ m_0 \pm 0.001\ m_0$ at 300 K. The dependence of the peak amplitudes in InP on magnetic field and ionised impurity concentration are in agreement with the theoretical treatment of the transverse magnetophonon effect by Barker (1972). The magnetophonon structure in n-CdSe (Eaves et al., 1972) is considerably weaker in amplitude

and can only be observed in a limited temperature range around 80 K. After corrections are applied for band non-parabolicity and the polaron effect, the low frequency cyclotron masses are deduced to be 0.122 m_0 for $B \perp$ c-axis and 0.127 m_0 for $B \parallel$ c-axis. The relatively polar nature of both InP and CdSe provides a test of two recent theoretical studies of the magnetophonon effect. First, a comparison of the value of m^* derived directly from equation (1) with that obtained from recent cyclotron resonance experiments shows that the optical polaron correction factor by which m^* must be multiplied to obtain the low frequency cyclotron mass is $(1 + 0.73\ \alpha/3)^{-1}$, in excellent agreement with the predictions of Mears et al., (1968) and the theoretical estimate by Palmer (1970). Second, the displacement of the magnetic field positions of the minima in the longitudinal magnetoresistance ρ_{zz} away from the resonance fields given by equation (1) is in qualitative agreement with the damping theory of Barker (1972a).

The magnetophonon structure which has been observed in n- and p-Ge (Eaves et al., 1970) is the most extensive yet reported. In both materials the anisotropy of the peaks has been studied for orientations of $\underline{B}$ in the (110) crystal plane and accurate values are deduced for the cyclotron effective masses of both the electrons and holes over the temperature range from 55 K to 260 K. In n-Ge, the structure can be interpreted solely in terms of intravalley scattering by optical phonons at the centre of the Brillouin zone. No peaks can be identified as arising from intervalley transitions and such processes are estimated to be at least an order of magnitude weaker than intravalley scattering processes. This result is in opposition to that of Sokolov and Tsidil'kovskii (1967) who attributed some of the minima which they observed in the longitudinal magnetoresistance of n-Ge to intervalley optical phonon scattering. The striking series of peaks in p-Ge are the first definitive observation of the magnetophonon effect due to optical phonon transitions in the valence band of a semiconductor. The complex splitting of the harmonics at fields above 50 kG is rather difficult to interpret precisely but appears to reflect the complex dependence of the heavy hole Landau level energies on k_B, the hole wavevector in the direction of the applied field. A series of

magnetophonon peaks has also been observed in the transverse magnetoresistance of p-GaAs at a temperature of about 100 K. The magnetic field positions of the five light hole peaks provide an estimate of the band-edge light hole effective mass of 0.091 m_0.

In the ohmic electric field regime, the structure in the magnetoresistance disappears as the temperature is lowered below about 50 K due to the decreasing importance of optical phonon scattering in limiting the electron mobility. However, by applying electric fields of sufficient strength to heat the electron temperature above that of the lattice, extrema can be made to reappear in the magnetoresistance. The phonons responsible for the structure are those which dominate the energy relaxation of the electrons and the reappearance of the peaks arises from the oscillatory variation with magnetic field of the energy relaxation time of the electrons. In InP, at a temperature of about 10 K, the most prominent series of peaks is caused by electron capture at a shallow ionised donor site accompanied by the emission of a single L.O. phonon. At electric fields below about 5 V/cm a second series of five extrema, accurately periodic in $^1/B$, appears in the magnetoresistance. This structure is attributed to energy relaxation of electrons by the simultaneous emission of a pair of band-edge transverse acoustic phonons. The field positions of the peaks satisfy the condition

$$\frac{N\hbar eB}{m^*} = 2\hbar\omega_{(T.A.X)} \qquad (2)$$

where $\hbar\omega$ (T.A.X) is the T.A. phonon energy at the X-point of the Brillouin zone. In addition to the structure arising from phonon emission processes, additional peaks appear in the magnetoresistance of all the n-InP samples studied. The field positions of these extrema appear to correspond to an energy relaxation mechanism in which the electrons inelastically scatter from neutral donor sites which are thereby excited from the ground state to the lowest energy Landau state.

The energies of the donor states which are required for the interpretation of the warm electron magnetophonon data are deduced from a series of photoconductivity experiments on n-InP (Stradling et al., 1972).

This work involved the use of two cryostats designed for infra-red measurements at temperatures down to 1.2 K. The spectra reveal the presence of two shallow donor species whose ground states are separated in energy by an amount equivalent to 0.7 cm^{-1}. The mean ionisation energy of the two impurities is 61.0 cm^{-1}. The photoconductive response also shows an additional peak at 33.8 cm^{-1} which appears to have an intensity directly related to the width of the shallow donor lines.

Barker, J.R., J. Phys.C. Sol.St. Phys. 5, 1675, (1972).

Barker, J.R., J. Phys.C. Sol.St. Phys. to be published (1972a).

Eaves, L., Stradling, R.A. and Wood, R.A., Proc.Int. Conf. on Physics of Semiconductors (Boston), 816, (1970).

Eaves, L., Stradling, R.A., Askenazy, S., Leotin, J., Portal, J.C. and Ulmet, J.P., J. Phys.C. Sol.St.Phys. 4, L42, (1971).

Eaves, L., Stradling, R.A., Askenazy, S., Carrère, G., Leotin, J., Portal, J.C. and Ulmet, J.P., J. Phys.C. Sol.St. Phys. 5, L19, (1972).

Gurevich, V.L. and Firsov, Y.A., Sov. Phys. J.E.T.P. 13, 137 (1961).

Mears, A.L., Stradling, R.A. and Inall, E.K., J.Phys. C. Sol.St. Phys. 1, 821, (1968).

Palmer, R.J. D.Phil. Thesis, Oxford University (1970).

Sokolov, V.I. and Tsidil'kovskii, I.M. Sov.Phys. Semiconductors 1, 695 (1967).

Stradling, R.A., Eaves, L., Hoult, R.A., Miura, N., Simmonds, P.E. and Bradley, C.C., Proc.Int. Symposium on GaAs and related compounds (Boulder, Colorado) Publ: Inst. of Physics (1972).

ACKNOWLEDGEMENTS

I would like to express my thanks to Professor B. Bleaney for permitting me the use of the facilities in the Clarendon Laboratory.

I am also indebted to my supervisor Dr. R.A. Stradling for his constant help and encouragement during the past three years.

The pulsed field experiments described in this thesis were possible only with the help of Dr. S. Askenazy and the members of the semiconductor group at Toulouse University. I offer them my thanks for making my visits both worthwhile and enjoyable.

I am grateful to my past and present research colleagues and to the technical staff of the Clarendon Laboratory for many helpful discussions and much patient assistance.

My thanks are also due to
The President and Fellows of St. John's College, Oxford for a Senior Scholarship
The Ministry of Defence, Navy Department for a research grant and the N.A.T.O. Research Grants Programme for travel funds to visit Toulouse.

The samples of InP, CdSe and GaAs were kindly supplied by Mrs. L. Taylor, Drs. C. Clarke, B. Mullin and D. Joyce (R.R.E., Malvern), Mr. G. Bucknell and Dr. B.C. Cavenett (Hull University), and Dr. B. Wilson and Mr. M. Hales (Plessey Co., Towcester).

CONTENTS

		Page
1.	MAGNETOPHONON EFFECTS IN THE ELECTRICAL CONDUCTIVITY OF SEMICONDUCTORS	
1.1	Introduction	1
1.2	The Energy States of Conduction Electrons	1
1.3	Electron Transport in a Magnetic Field	3
1.4	The Magnetophonon Effect	
1.4.1	The Transverse Orientation	5
1.4.2	The Polaron Contribution to the magnetophonon effective mass	7
1.4.3	The Longitudinal Orientation	8
2.	EXPERIMENTAL TECHNIQUES	
2.1	Preparation of Samples	13
2.2	Magnetic Field Facilities	14
2.3	The Cryostat	15
2.4	Electrical Measurements	16
3.	THE MAGNETOPHONON EFFECT IN n-InP AT TEMPERATURES ABOVE 60 K	
3.1	Introduction	20
3.2	Sample Characteristics	20
3.3	Experimental Results in the Transverse Orientation	21
3.4	Experimental Results in the Longitudinal Orientation	23
3.5	Determination of Effective Mass	24
4.	THE MAGNETOPHONON EFFECT IN n-CdSe	
4.1	Introduction	29
4.2	Experimental Results in the Transverse Orientation	29
4.3	Determination of Effective Mass	30
4.4	Experimental Results in the Longitudinal Orientation	32

		Page
5.	THE MAGNETOPHONON EFFECT IN n-Ge	
5.1	Introduction	33
5.2	The Experimental Data	35
5.3	The Interpretation of the Data and the Determination of Effective Mass	36
5.4	The Line-Shape and Amplitude of the Magnetophonon Peaks	41
6.	THE MAGNETOPHONON EFFECT IN p-Ge AND p-GaAs	
6.1	Introduction	45
6.2	The Experimental Data in p-Ge	46
6.3	The Interpretation of the Magnetophonon Data in Terms of the Valence Band Structure in Ge	
6.3.1	The Determination of the Hole Effective Masses	50
6.3.2	Interpretation of the Splitting of the Magnetophonon Peaks	52
6.4	The Amplitudes of the Magnetophonon Structure	56
6.5	The Experimental Data for p-GaAs	57
6.6	The Interpretation of the Magnetophonon Structure in p-GaAs	58
7.	THE WARM ELECTRON MAGNETOPHONON EFFECT IN n-InP	
7.1	Introduction	61
7.2	Experimental Results	64
7.3	The Interpretation of the Hot Electron Magnetophonon Structure	
7.3.1	Structure Arising from the Emission of L.O. Phonons	66
7.3.2	Structure Arising from the Emission of Two T.A. Phonons	69
7.3.3	Unidentified Structure in the Magnetoresistance	71

		Page
8.	INFRA-RED PHOTOCONDUCTIVITY IN n-InP	
8.1	Introduction	75
8.2	The Apparatus for the Photoconductivity Experiments	77
8.3	Experimental Results and Discussion	80
	REFERENCES	84

CHAPTER 1

Magnetophonon effects in the Electrical Conductivity of Semiconductors

1.1 Introduction

This thesis is principally concerned with the magnetophonon effect, an aspect of the electrical conductivity of pure semiconductors in high magnetic fields which has received considerable experimental and theoretical attention in recent years. In this chapter an outline is given of the theory of electrical conduction in a magnetic field with particular reference to the development of the theory of magnetophonon resonance. The second chapter deals with the experimental arrangements employed in the observation of the effect in the magnetoresistance of semiconductors at high magnetic fields. In chapters 3 to 6 the observation of magnetophonon resonance is reported in five semiconductors n-InP, n-CdSe, n-Ge, p-Ge and p-GaAs. In this series of materials the energy-momentum relation $\mathcal{E}(\underline{k})$ and Landau level structure of the carriers becomes progressively complex with the result that the interpretation of magnetophonon structure requires increasing refinement. Chapter 7 examines the magnetophonon effect in high purity InP at low temperatures under non-ohmic conditions when the electron gas is heated above the temperature of the lattice. The data show that shallow donor impurities play an important part in relaxing the energy of the conduction electrons under such conditions. In chapter 8, the energies of electrons bound to these donor sites are obtained from a series of photoconductivity experiments in InP.

1.2 The Energy states of Conduction electrons

In the first of the materials studied in this thesis, n-InP, the lowest energy conduction band at the Γ point of the Brillouin zone is spherical. The electron energy is given by

$$\mathcal{E}(k) = \frac{\hbar^2 k^2}{2m^*} \qquad (1.1)$$

where $\underline{k}$ is the electron wave-vector and m^*, the effective mass of the band, is a scalar quantity. In the presence of an applied magnetic field ($\underline{B}$) the electron states are redistributed into Landau levels given by

$$\mathcal{E} = \left(n+\tfrac{1}{2}\right)\frac{\hbar e B}{m^*} + \frac{\hbar^2 k_B^{\,2}}{2m^*} \qquad (1.2)$$

$n = 0, 1, 2 \ldots\ldots$

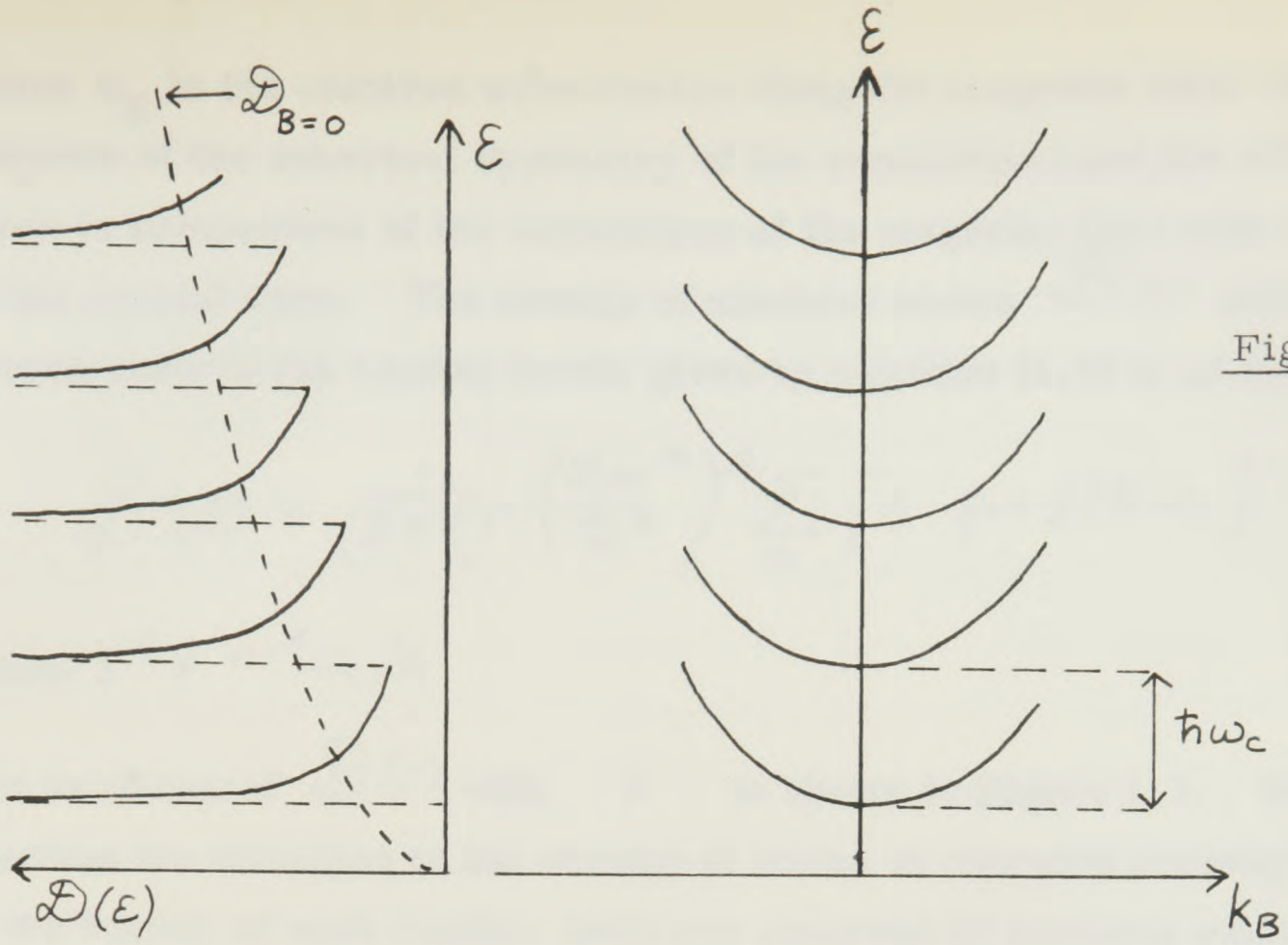


Figure 1.1

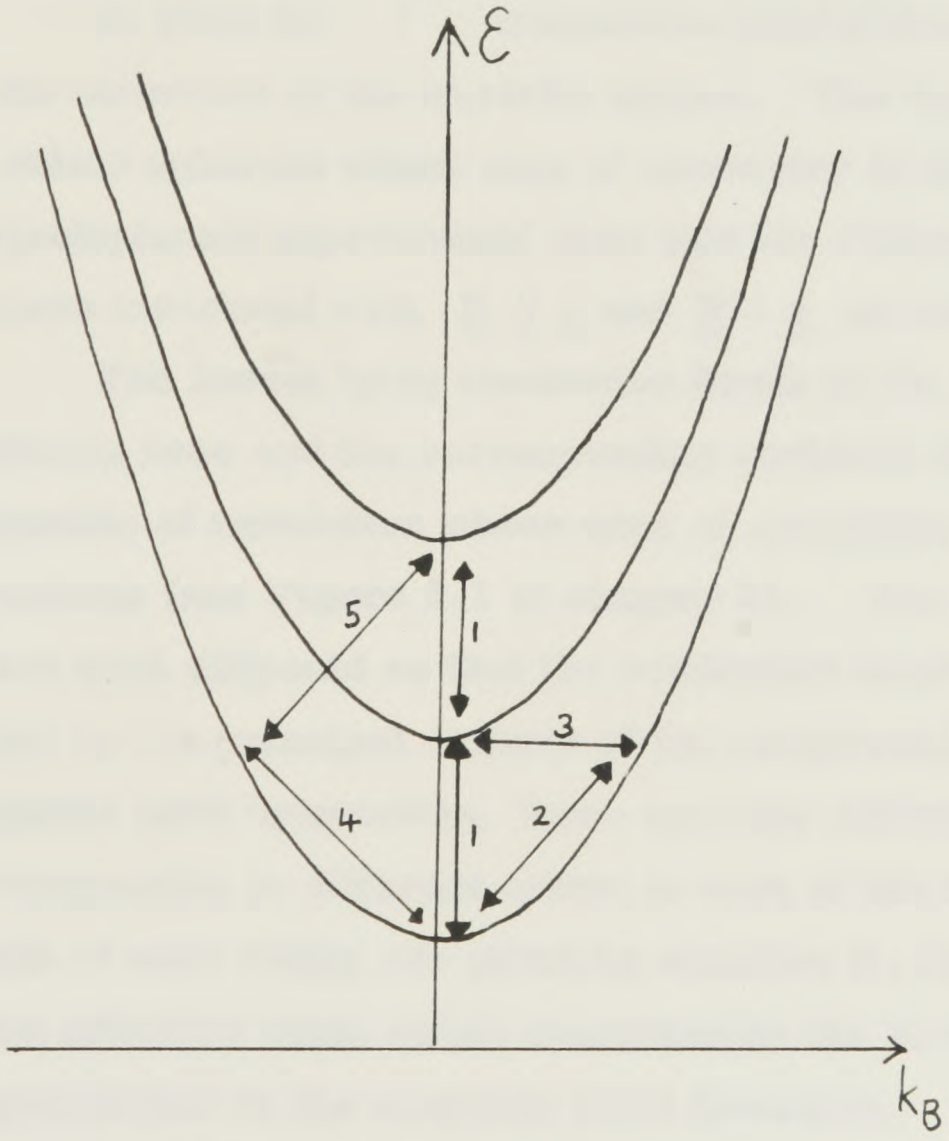


Figure 1.2

The mixed scattering processes (2 & 3) and (4 & 5) which give rise to the longitudinal magnetophonon structure

where k_B is the electron wave-vector along the magnetic field direction. Because of the spherical symmetry of the conduction band, the effective mass is independent of the orientation of the magnetic field with respect to the crystal axes. The density of electron states $\mathcal{D}(\varepsilon)$ which corresponds to the Landau levels given by equation (1.2) is of the form

$$\mathcal{D}(\varepsilon) = \frac{1}{(2\pi l)^2}\left(\frac{2m^*}{\hbar^2}\right)^{1/2}\sum_n \left[\varepsilon - (n+\tfrac{1}{2})\hbar\omega_c\right]^{-1/2} \qquad (1.3)$$

where $l^{-2} = m^*\omega_c/\hbar$

The variation of $\mathcal{D}(\varepsilon)$ with ε is shown in Figure 1.1. In practice the infinities in the density of states at energies corresponding to the bottom of each Landau level are removed by electron scattering processes.

In CdSe the Γ conduction band shows a slight anisotropy due to the structure of the wurtzite lattice. The constant energy surface is an oblate spheroid whose axis of symmetry is the crystalline c-axis. The magnetophonon experiments show that the difference between the cyclotron masses measured with $\underline{B} \parallel \underline{c}$ and $\underline{B} \perp \underline{c}$ amounts to 4%.

The lowest lying conduction bands in Ge are at the L-point of the Brillouin zone and the corresponding surfaces of constant energy are ellipsoids of revolution whose axes of symmetry are parallel to the (111) directions (see Figure 5.1 of chapter 5). The faces of the Brillouin zone bisect each ellipsoid so that the conduction band consists of 8 half-ellipsoids linked by the principal vectors of the reciprocal lattice. For an arbitrary magnetic field orientation, there are four different cyclotron masses corresponding to different orbits in each of the four ellipsoids. The Landau levels of each valley are given by equation (1.2) with appropriate values of the effective mass which characterise the motion parallel and perpendicular to the magnetic field direction.

In the p-type materials discussed in chapter 6 the $\mathcal{E}(\underline{k})$ function close to the valence band edge can be represented by the equation

$$\mathcal{E}(\underline{k}) = \frac{\hbar^2}{2m_0}\left\{Ak^2 \pm \left[B^2k^4 + C^2(k_1^2k_2^2 + k_2^2k_3^2 + k_3^2k_1^2)\right]^{1/2}\right\} \qquad (1.4)$$

where the suffices 1, 2, 3 refer to the (100) directions. The constants A (a negative number), B and C determine the effective masses of the holes. Equation (1.4) describes two bands occupied by light (- ve sign) and heavy (+ ve sign) holes. Both constant energy surfaces are warped but exhibit cubic symmetry. In the presence of a magnetic field the hole energies cannot be accurately described by equally spaced Landau levels with a quadratic k_H-dependence. Luttinger and Kohn (1955) first pointed out that as a consequence of the degeneracy of the light and heavy hole bands at the Γ -point, the separation of the low lying Landau levels is markedly non-uniform. In addition, the energy dependence of individual Landau levels on k_B is no longer quadratic. Calculations of the valence band states show that Landau level energy is a complex function of k_B with turning points occurring both at $k_B = 0$ and at finite k_B. (Evtuhov, Wallis and Bowlden; Hensel and Suzuki). As a result of the complex dependence of energy on k_B, the density of states function given by equation (1.3) is inapplicable to the holes. The results described in chapter 6 show that these characteristic features of the hole states in a magnetic field lead to striking complexity of the magnetophonon structure.

1.3 Electron Transport in a Magnetic Field

In most galvanomagnetic measurements, including the ones described in this thesis, the current density is maintained constant, and the electric field, which is permitted to adjust itself, is determined from measurements of potential difference. These voltages are proportional to the components of the resistivity tensor ρ . The theory of electrical conduction, however, is usually presented in terms of the magneto-conductivity tensor σ . The two tensors are related by

$$\rho\sigma = I$$

In an isotropic medium with the magnetic field along the z-axis i.e. $H = (0, 0, H_z)$

$$\sigma_{xx} = \sigma_{yy},\ \sigma_{xy} = -\sigma_{yx},\ \sigma_{xz} = \sigma_{zx} = \sigma_{yz} = \sigma_{zy} = 0$$

and the conductivity and resistivity tensors are related by

$$\sigma_{xx} = \frac{\rho_{yy}}{\rho_{xx}\rho_{yy} - \rho_{xy}\rho_{yx}} = \frac{\rho_{xx}}{\rho_{xx}^2 + \rho_{xy}^2}$$

$$\sigma_{xy} = \frac{-\rho_{xy}}{\rho_{xx}\rho_{yy} - \rho_{xy}\rho_{yx}} = \frac{-\rho_{xy}}{\rho_{xx}^2 + \rho_{xy}^2}$$

$$\sigma_{zz} = 1/\rho_{zz} \qquad (1.5)$$

Recent quantum mechanical approaches to the problem of electrical conduction in an applied magnetic field have been based on the calculation of the density matrix which can be expanded in powers of the scattering potential (see Roth and Argyres, 1966 for a list of references). Such a treatment by Argyres and Roth (1959) to second order in the potential yields for both elastic and inelastic scattering in the transverse orientation

$$\sigma_{xx} = \frac{e^2}{2kT\Omega} \sum_{\mu\nu} f_\mu (1-f_\nu) W_{\mu\nu} (X_\mu - X_\nu)^2$$

$$W_{\mu\nu} \sim |\langle \mu | V | \nu \rangle|^2 \qquad (1.6)$$

where Ω is the volume, X_μ is the centre of the electron motion in the x-direction when the electron is in state μ and $W_{\mu\nu}$ is the transition probability. For phonon scattering equation (1.6) can be written

$$\sigma_{xx} = \sum_q \int d\varepsilon \sum_{nn'} \frac{G_{nn'}(\varepsilon) f(\varepsilon) \left[1 - f(\varepsilon \pm \hbar\omega_q)\right]}{\left[\varepsilon - (n+\tfrac{1}{2})\hbar\omega_c\right]^{1/2} \left[\varepsilon \pm \hbar\omega_q - (n'+\tfrac{1}{2})\hbar\omega_c\right]^{1/2}} \qquad (1.7)$$

where the summation is over phonon wave-vector $\underline{q}$ and the integration is over the electron energy. $G_{nn'}(\varepsilon)$ is a smoothly varying function of energy. The terms in the denominator give the initial and final density of electron states from equation (1.3). Equation (1.7) states that the contribution to the electrical conductivity of electrons with energy ε in a level with quantum number n is proportional to the number of such electrons, the transition probability to all other states and to the number

of unoccupied final states.

A more general solution of the density matrix equation to all orders in V has been obtained by Kubo et al. (1965). This approach is particularly valuable at high magnetic fields when the electron wave function is greatly elongated in the field direction. If the length of the wave packet approaches the mean separation between scattering events, the electron can undergo multiple scattering and the kinetic-type transport equation is no longer valid. The Kubo formulation of the transport problem at high magnetic fields has been employed extensively in the theoretical treatment of the magnetophonon effect.

1.4 The Magnetophonon Effect

1.4.1 The Transverse Orientation

The magnetophonon effect was first predicted in a theoretical paper by Gurevich and Firsov (1961) and has since been observed in a wide range of semiconductors (see Stradling 1971; Harper, Hodby, Stradling 1972 for a list of references). The effect arises from the resonant coupling of optical phonons with conduction electrons in an applied magnetic field. The law of crystal momentum conservation limits the wave vector of the optic phonons that can interact with the electrons in one-phonon processes to a region close to the centre of the Brillouin zone. Such phonons are highly monoenergetic and for the purpose of considering scattering by the optic mode the phonon energy $\hbar\omega_q$ appearing in equation (1.7) can be replaced by a constant $\hbar\omega_l$. Each term in the denominator of the equation then contains an integrable singularity with the exception of magnetic fields such that

$$\omega_c(n-n') = \omega_c N = \omega_l \qquad N = 0, 1, 2 \ldots . \qquad (1.8)$$

As the resonance condition is approached, both terms in the denominator of equation (1.7) are simultaneously close to zero and the transverse conductivity shows a logarithmic divergence of the form

$$\Delta\sigma_{xx} \sim \log\left[\frac{\hbar\omega_c}{kT}\,\delta(1-\delta)\right] \qquad (1.9)$$

where

$$\delta = \left| M - \frac{\omega_l}{\omega_c} \right|$$

In practice other scattering mechanisms such as that due to ionised impurities remove the divergence in σ_{xx}. The electron - L.O. phonon interaction itself will also act to broaden the Landau levels when the resonance condition is satisfied. The effect of collision broadening in limiting the amplitude of the magnetophonon structure has been considered in detail by Barker (1970, 1972) who approximates the electron self energy by

$$\Sigma = \Delta + i\Gamma \tag{1.10}$$

where Δ and Γ are real constants determined by the parameters of the electron scattering potentials. Harmonic analysis on σ_{xx} shows the oscillatory part of the magnetoresistance to be

$$\rho_{osc} \sim \sum_{r=1}^{\infty} r^{-1} \exp(-2\pi r\gamma) \cos\left(\frac{2\pi r \omega_e}{\omega_c}\right) \tag{1.11}$$

where γ is in general a complex function of magnetic field and damping parameters. The first term of this expression can be identified with the empirical formula developed by Stradling and Wood (1968)

$$\rho_{osc} \sim \exp(-\bar{\gamma}_{M.P.R}\, \omega_e/\omega_c) \cos(2\pi \omega_e/\omega_c) \tag{1.12}$$

which is found to fit the magnetic field dependence of the magnetophonon amplitudes in a wide range of semiconductors. From experiment, $\bar{\gamma}_{MPR}$ is independent of magnetic field and is a weak function of temperature and impurity content. A similar exponential damping term $\exp(-2\pi\gamma_{d.H.S.})$ appears in the theory of the magnetic field variation of the amplitude of the de Haas-Shubnikov oscillations. However, in this case the damping term is simply related to the Hall mobility by the equation

$$\gamma_{d.H.S.} = \frac{1}{\omega_c \tau} = \frac{2\pi}{\mu B}$$

Calculations by Barker (1972) have shown that scattering of electrons by ionised impurities plays an important part in damping the magnetophonon oscillations, a result which corresponds closely with experiment. It appears that at high fields, band tailing, essentially a multiple scattering event in which the electron wave function overlaps two

impurities at a time, is most consistent with the experimental data for the damping in GaAs. The effect of impurity scattering on the magnitude of the magnetophonon structure has a weak temperature dependence compared to its strongly temperature dependent effect on the Hall mobility. According to theory, the damping factor γ due to single ionised impurity scattering is temperature independent and that due to multiple scattering (band tailing) varies as $T^{1/4}$. In simple terms, this is because magnetophonon transitions occur principally between states close to $k_B = 0$ and the broadening effect of ionised impurity scattering should be evaluated at the bottom of each Landau level irrespective of the thermal excitation of carriers to higher states. The damping theory predicts accurately the experimentally observed temperature variation of the magnetophonon amplitude. At low temperatures the amplitude falls because optic phonon scattering ceases to be the dominant mechanism in limiting the mobility. At sufficiently high temperature, the broadening of the Landau levels becomes so great that all magnetophonon structure is smeared out. Calculations in the case of GaAs (Barker 1972) show that the two competing effects lead to a peak in the magnetophonon amplitude at a temperature of 140 K, in excellent agreement with experimental observation.

1.4.2 The polaron contribution to the magnetophonon effective mass

A further aspect of the magnetophonon effect that has recently received theoretical attention is the enhancement of the electron effective mass as a result of the polaron interaction. The resonant polaron effect detected in magneto-optical experiments (Dickey and Larson 1968; Harper et al. 1970; McCombe and Kaplan 1968) is observed at precisely the magnetic fields given by the magnetophonon condition in equation (1.8) and it is therefore likely that the magnetophonon mass m^* will differ from the low frequency mass measured in cyclotron resonance where $\omega \ll \omega_c$. The polaron enhancement of the magnetophonon mass was first observed by Mears et al. 1968 in experiments on n-CdTe. Recently, Palmer has calculated the magnetic field dependent transport

coefficients by a perturbation expansion of the Kubo formula. He finds that the magnetophonon mass deduced from the N = 1 harmonic exceeds the bare electron mass by a factor $(1 + n\alpha/2)$ where α is the Frohlich coupling constant and n is a numerical factor equal to 0.83. As will be discussed in chapters 3 and 4, this value is in excellent agreement with the magnetophonon mass values obtained in polar materials.

1.4.3 The Longitudinal Orientation

The theoretical description of the magnetophonon effect in the longitudinal configuration is complicated by the problem of solving the transport equation when competing scattering processes are present. In the transverse orientation, if there are several independent scattering mechanisms, their contributions to the scattering probability and hence the conductivity σ_{xx} are additive and can be regarded independently. However, in the longitudinal orientation the various scattering mechanisms do not contribute additively to the current. Moreover the strong scattering (process 1 in figure 1.2) which occurs between states close to $k_B = 0$ and which produces extrema in σ_{xx} is ineffective in relaxing the longitudinal current. Indirect processes (for example 2 and 3 in figure 1.2) which involve an appreciable change in k_B and which link two high-density of states regions are therefore responsible for limiting the longitudinal currents. The requirement of two simultaneous scattering processes to link the high density of states regions makes the magnetophonon structure in the longitudinal orientation an order of magnitude weaker than that in the transverse orientation and may cause the extrema to be displaced from the resonance fields given by equation 1.8.

The first theoretical paper to appear on the longitudinal effect was that of Gurevich and Firsov (1964) who considered the combined effect of acoustic and polar optic phonon scattering. The first of these processes (for example the transition marked 3 in figure 1.2) produces sharp changes in the relaxation time for electrons whose energy coincides with the high density of states region at $k_B = 0$. Although the relaxation time $\tau(\mathcal{E})$ for electrons in a particular Landau level is thus a saw-tooth function with minima at energies $\mathcal{E} = (n + \frac{1}{2})\hbar\omega_c$, σ_{zz} is the integral of $\tau(\mathcal{E})$

multiplied by a smoothly varying function of energy and is a non-oscillatory function of magnetic field. If, however, optical phonon scattering is introduced into the integrand then oscillations can be expected in σ_{zz}. The behaviour of σ_{zz} near the resonance condition depends critically on which type of scattering process is dominant. By solving the kinetic equation, Gurevich and Firsov obtained a criterion for observing maxima or minima at resonance depending on the magnitude of a parameter Γ^{-1} which determines the relative strengths of optic and acoustic phonon scattering. Γ^{-1} is given by

$$\Gamma^{-1} = \frac{3\sqrt{\pi}}{4} \frac{kT}{\hbar\omega_c} \left(\frac{\hbar\omega_e}{kT}\right)^{1/2} \alpha \frac{\mu_a}{u_0} \qquad (1.13)$$

where α = Frohlich constant

μ_a = acoustic phonon scattering mobility

u_0 = $e/m_0\omega_e$

ω_e = L.O. phonon frequency

When $\Gamma^{-1} \lesssim 1$ there should be a minimum in $\rho_{zz} (= 1/\sigma_{zz})$ at resonance which changes to a maximum at sufficiently large values of Γ^{-1}. This result is in conflict with experimental data as in the majority of materials studied (Stradling and Wood 1968) there is a minimum in ρ_{zz} very close to the resonance field even though the parameter Γ^{-1} is considerably greater than unity.

More recently, Kharus and Tsidil'kovskii have considered in greater detail the solution of the Boltzmann equation for mixtures of non-polar and polar optical phonon scattering and elastic scattering by acoustic phonons and ionised impurities. They find that the sign and position of the extrema depend on the magnitude of a parameter λ which characterises the relative strengths of inelastic and elastic scattering. If there are several types of elastic scattering processes present, the resultant value of λ is given by

$$\lambda^{-1} = \sum_i \lambda_i^{-1}$$

λ_{ac} for acoustic phonon scattering is 2 Γ^{-1} where Γ^{-1} is the Gurevich-Firsov parameter. If λ_{ac} is less than a certain critical value (λ_0), which is calculated to be between 10 and 100 for all materials considered, then a minimum should occur in the longitudinal magneto-resistance at resonance. When ionised impurity scattering is also appreciable, λ will decrease and the condition for minima is even better satisfied. Kharus and Tsidil'kovskii have calculated λ for several materials and find that it is much greater than λ_0 only for CdTe. If $\lambda_{ac} \gg \lambda_0$ and $\hbar\omega_c/kT \gg 1$, their equations predict a maximum at resonance, with the maxima moving to higher fields as either inequality is weakened. Although Kharus and Tsidil'kovskii claim that in CdTe maxima have been observed at resonance (Mears et. al. 1968), this is in fact not the case as the resonance fields are approximately midway between adjacent maxima and minima found in the longitudinal orientation and the experimental displacements appear to be independent of temperature. This has also been found to be the case in the two polar materials, CdSe and InP, which are discussed in this thesis. The theory of Kharus and Tsidil'kovskii also appears to predict incorrectly the sign of the longitudinal extrema in n-GaAs where minima are found close to the resonance condition (equation 1.8) over a range of temperature from 50 K to 300 K.

Peterson (1972) has recently used the displaced Maxwellian distribution to examine the effect of adding other scattering mechanisms (ionised impurity, piezo-electric and deformation potential acoustic phonon) in varying strengths to optical phonon scattering in polar semi-conductors. The result of this analysis is that in the longitudinal configuration at resonance, maxima occur for predominantly optic phonon scattering and remain maxima as other scattering is added until eventually they disappear. According to Peterson, the strong electron-electron scattering implied by the distribution is the factor which prevents the theoretical description of minima at resonance. More recently, Peterson has resorted to a Boltzmann equation approach (Peterson 1972) and claims that in addition to the normal longitudinal extrema, an additional series of peaks, termed pseudoresonances, appears at magnetic

fields given by

$$\frac{(2n+1)}{2}\,\omega_c = \omega_\ell \qquad n = 0, 1, 2 \ldots \tag{1.14}$$

The existence of an additional series of extrema in the longitudinal orientation has been reported in several materials (Stradling and Wood, 1968, 1970; Akselrod and Tsidil'kovskii, 1969; Eaves et al. 1971). This structure was originally interpreted as involving the simultaneous scattering by a pair of optic phonons (processes 4 and 5 in figure 1.2) which at relatively high temperatures can compete with mixed optic phonon and elastic scattering (processes 2 and 3). Both types of combined scattering process can produce resonant structure in the longitudinal orientation as they link two sets of infinities in the density of states while at the same time relaxing the longitudinal electron momentum. The resonance condition for the indirect process involving the combination of two optic phonon scattering events is

$$n\omega_c = 2\omega_\ell \qquad n = 1, 2, 3 \ldots \tag{1.15}$$

Its relative probability is

$\exp(-2\hbar\omega_\ell/kT)$ as compared to $\exp(-\hbar\omega_\ell/kT)$

for the single optic phonon process. These expressions predict qualitatively the relative amplitudes of the two series in all the materials studied to date. The series given by equation (1.15) contains the field positions of Peterson's pseudo-resonances (equation 1.14) and the normal magneto-phonon series (equation 1.8). Analysis of the summations over Landau states which are involved in Peterson's calculation of σ_{zz} indicates that his description of the additional structure in the longitudinal orientation is probably equivalent to that originally made by Stradling and Wood.

Very recently, Barker (1972a) has extended the theoretical description of the longitudinal magnetophonon effect to treat collision broadening. The inclusion of Landau level broadening at the start of the

calculation ensures the occurrence of minima close to resonance. When the modification of the density of states by broadening is considered in detail, the minima are found to be shifting away from the resonance fields and in the strong coupling limit

$$\rho_{zz} \sim \frac{1}{A + B\cos\left(\frac{2\pi\omega_e}{\omega_c} - \frac{\pi}{2}\right)} \qquad (1.16)$$

where A and B are slowly varying functions of magnetic field. The equation shows that the minima should be displaced to lower fields by an amount which is qualitatively in agreement with the results for the two polar materials studied in chapters 3 and 4 of this thesis.

CHAPTER 2

Experimental Techniques

2.1 Preparation of Samples

Following a preliminary X-ray diffraction experiment to determine the orientation of the crystal axes, the samples were cut into the form of long rectangular bars by means of an oil/water lubricated rotating carborundum wheel. Before alloying metallic electrical contacts to the sample, its surface was ultrasonically cleaned in distilled water followed by washes in alcohol and trichloroethylene. In the case of germanium, it was found that a preliminary etch in CP4 generally improved the quality of the electrical contacts. The contacts were formed by placing small cubic cuttings of the metal on the sample and fusing them onto the surface by heating in a reducing atmosphere of pure hydrogen for about 10 minutes. The 'wetting' of the sample surface by the molten metal was generally facilitated by injecting a small amount of hydrogen chloride into the reducing atmosphere when the sample was at a temperature just above the melting point of the metal. The chemical composition of the metallic contact and the degree of heating required to produce consistently low resistance electrical contacts for the various semiconductors studied in this thesis are given in Table 2.1.

Table 2.1

Method of producing electrical contacts

Semiconductor	Metal for Contact	Maximum Temperature	Etch
CdSe	pure In	230 K	-
n-InP	"	300 K	-
p-GaAs	In + 1% Cd	350 K	-
p-Ge	pure In	250 K	CP4
n-Ge	Sn + 5% Sb	250 K	CP4

Each sample carried at least four electrical contacts which were arranged in a geometrical configuration suitable for the measurement of the sample resistance by the standard four contact technique. An additional pair of contacts were attached to several of the samples for measurements of the Hall voltage. In all cases the metal contacts were

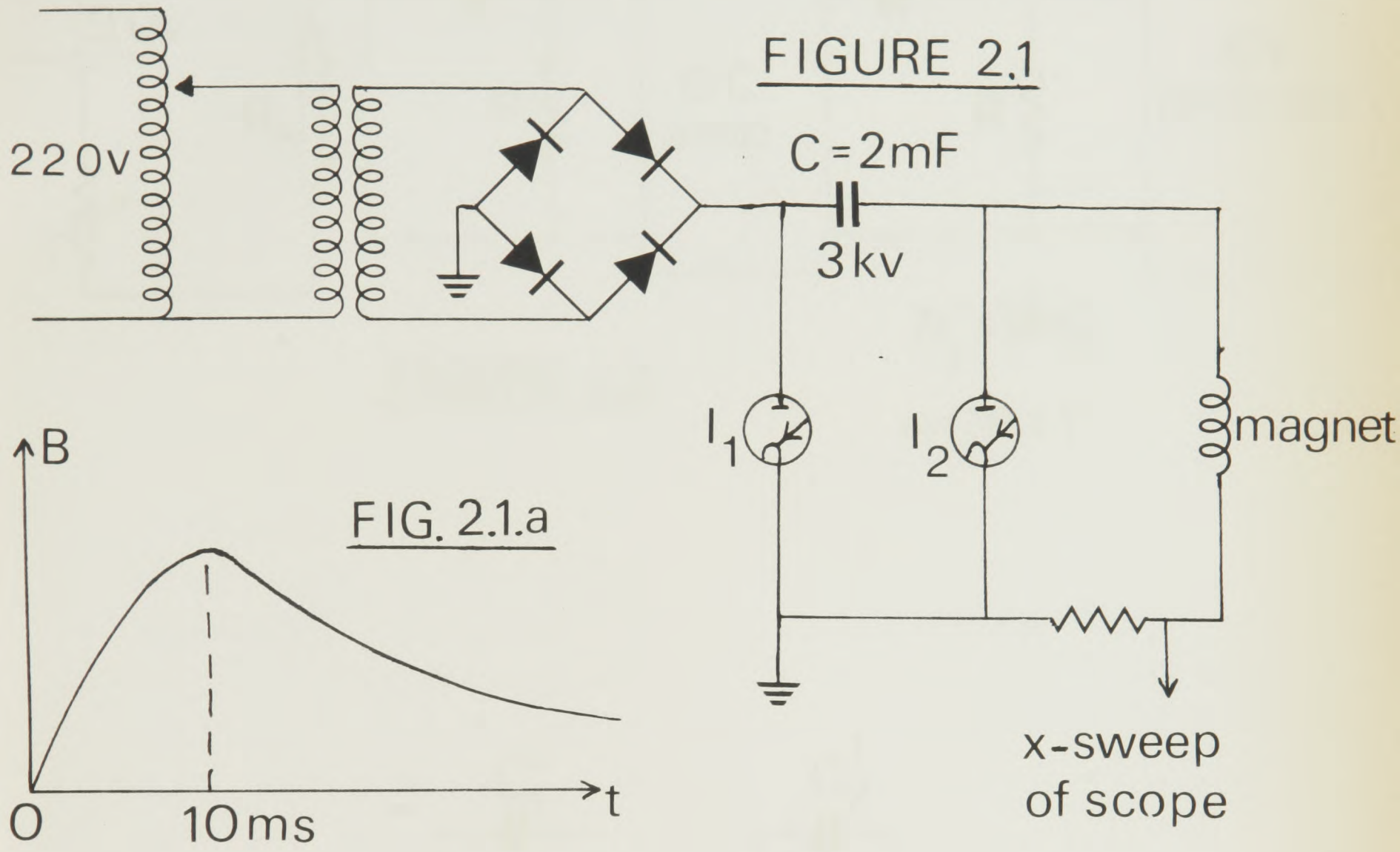


FIGURE 2.1

FIG. 2.1.a

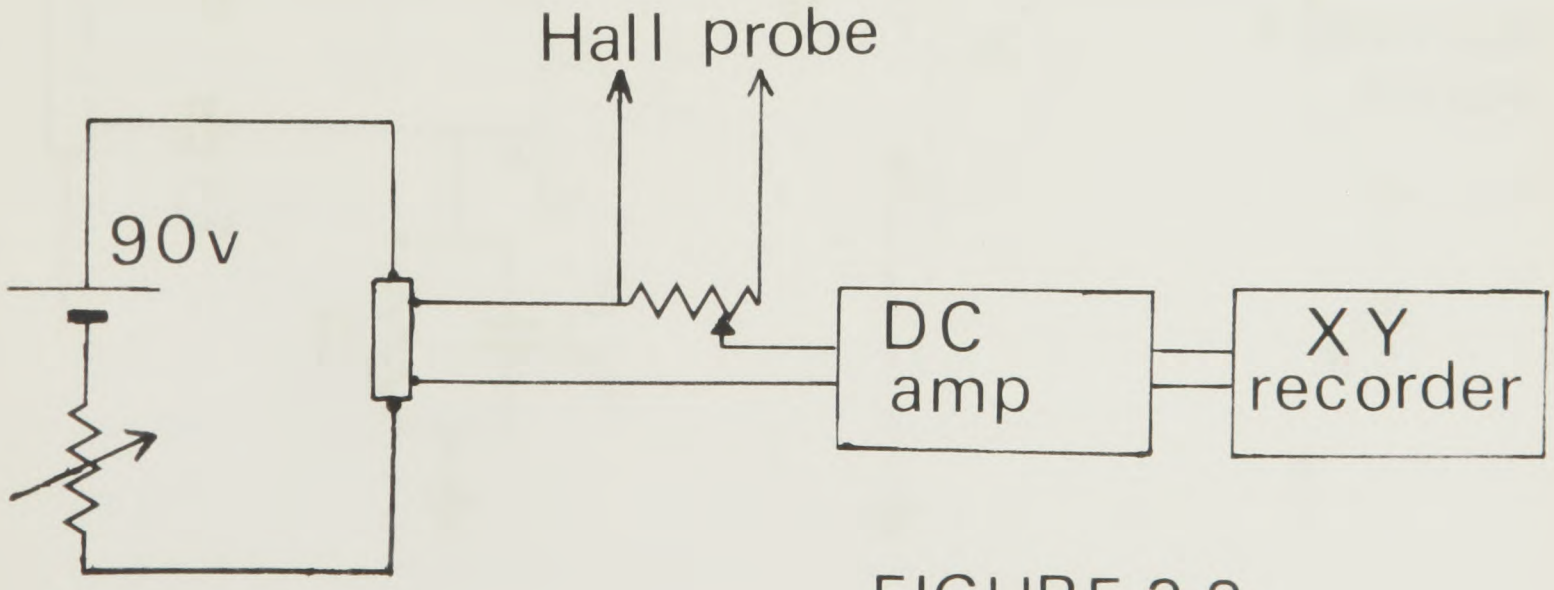
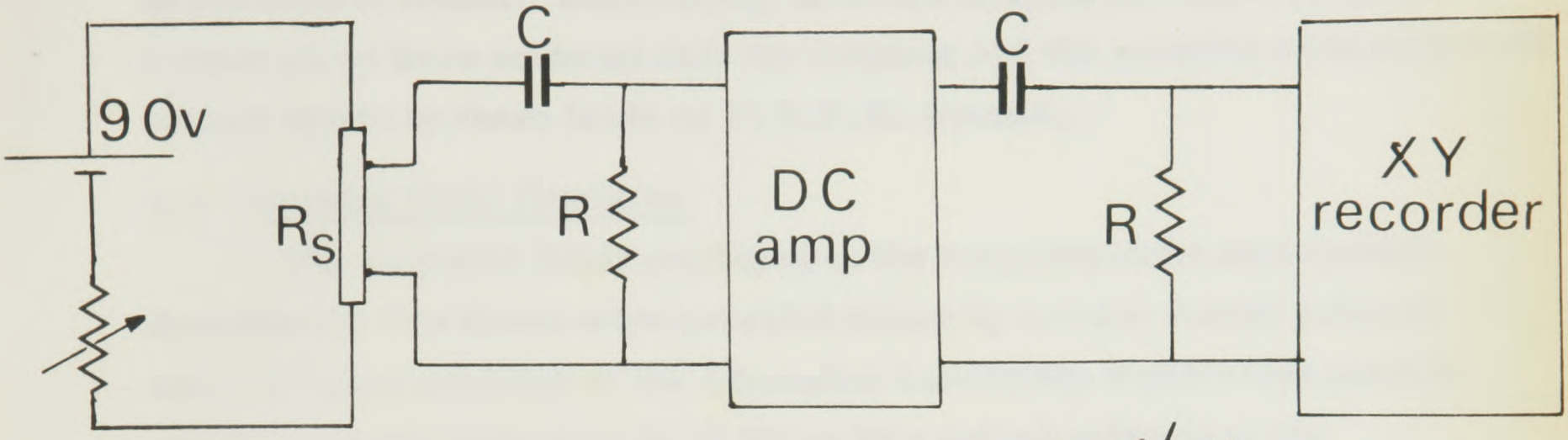


FIGURE 2.2



$R_s \ll 1/\omega C$

$\omega CR \ll 1$

FIGURE 2.3

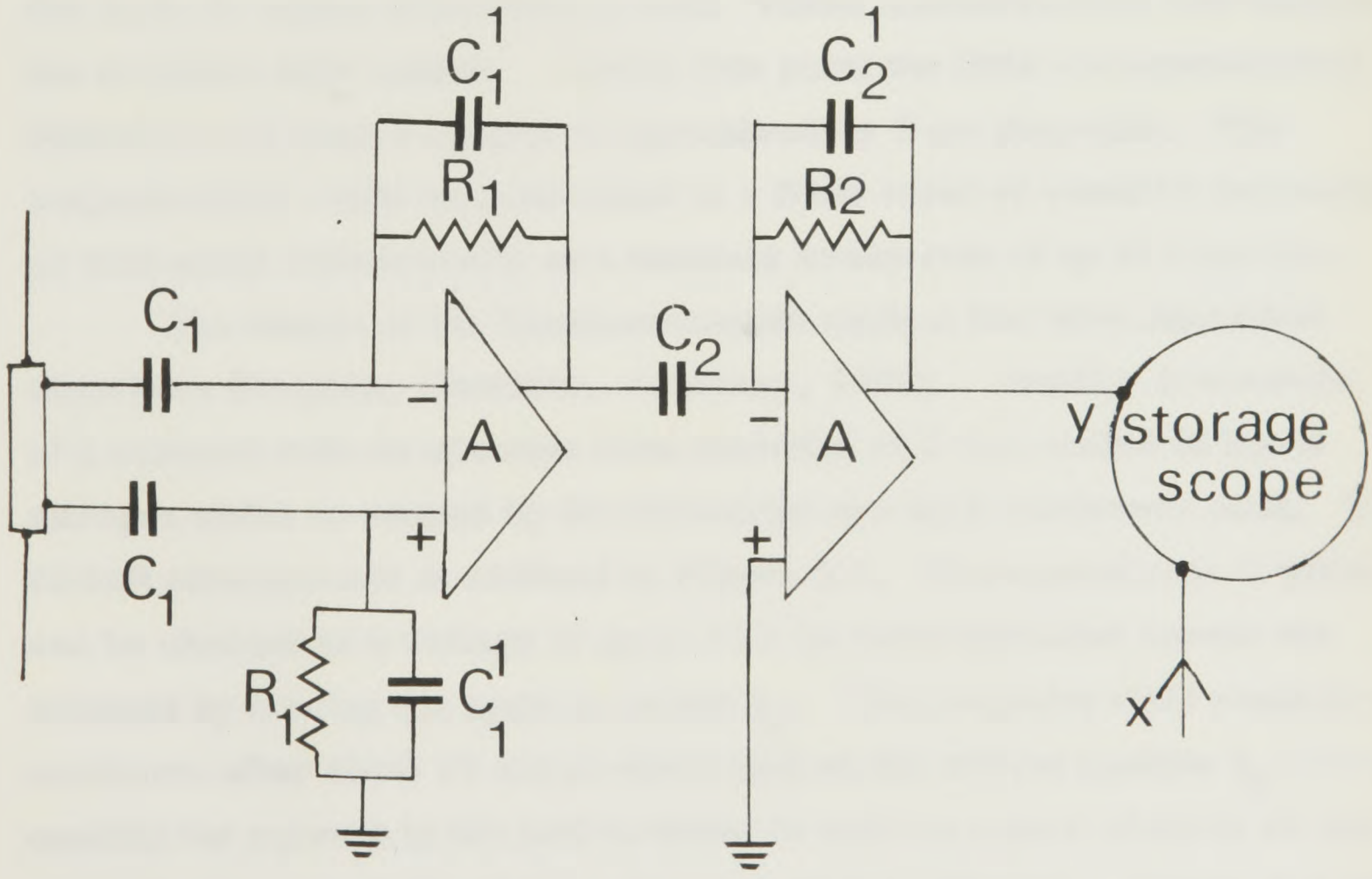


FIGURE 2.4

made as small as conveniently possible ($\sim \frac{1}{2}$ mm diameter) so as to prevent the distortion of the current lines due to the shorting effect of the contact areas. Immediately after the alloying process 44 s.w.g. copper wires were soldered onto the contacts and the samples were supported without strain by these leads on P.T.F.E. mounts.

2.2 Magnetic Field Facilities

The magnetic fields employed in the magnetophonon experiments described in this thesis were provided either by a water cooled solenoid with a 2" bore diameter at the Clarendon Laboratory which could produce steady magnetic field of up to 90 kG or by a pulsed solenoid at the Laboratoire de Physique des Solides of the University of Toulouse which could generate fields of up to 350 kG.

The current supplied to the Oxford magnet was electronically stabilised to the order of 1 part in 10^5 (Smith 1967) and could be measured to an accuracy of better than 0.1% by means of a digital voltmeter connected across a low impedance shunt in series with the magnet. The solenoid was calibrated (in gauss/amp) to accuracy of 0.1% by measuring the N.M.R. signal of protons in wax. These measurements also determined the magnetic field centre. Around this point the field homogeneity was better than $\frac{1}{2}$% over a sphere of approximately 2 cm diameter. The magnetic field could be maintained at a fixed value or could be increased or decreased automatically at a constant sweep rate of up to 3 kg/sec.

The design of the Toulouse magnet system has been described elsewhere (Prajoux, Gaechter, Askenazy, 1969). Briefly, it consists of a solenoid with an effective bore diameter of 6 mm cooled in liquid nitrogen which is excited by the discharge of a 2mF condensor bank. The circuit arrangement is outlined in Figure 2.1. The capacitance C which can be charged to a voltage of up to 3 kV is short circuited across the solenoid by closing the ignitron switch I_1. The magnetic field rises to a maximum after about 10 ms at which instant the second ignitron I_2 closes causing the current in the coil to decay to zero in a time of about 40 ms which is characteristic of the L/R value of the solenoid. Figure 2.1 (a) shows the variation of magnetic field with time. The feature of the

Toulouse magnetic system which is essential to the relatively long duration of the magnetic field pulse is the high self inductance and hence large size of the solenoid. The accompanying disadvantage of using a large mass of copper is the delay between pulses which is necessary to allow for the dissipation of Joule heating.

2.3 The Cryostat

The large 2" bore diameter of the Oxford magnet permitted the installation of a sample rotation system inside the cryostat. The P.T.F.E. mount to which each sample was attached was fixed in a turntable which could be rotated about a horizontal axis by means of a worm-gear mechanism. This facility enabled studies to be made of the anisotropy of the magnetophonon structure for various orientations of the crystallographic axes relative to the vertical magnetic field. The sample temperature could be varied between 300 K and 77 K by syphoning the appropriate amount of liquid nitrogen into the cryostat and allowing thermal equilibrium to be reached. In this way the sample temperature could be kept constant to within about 5 K for periods of up to 20 minutes, thus allowing sufficient time for magnetoresistance measurements at the temperature of interest. Lower temperatures were obtained either by pumping on liquid nitrogen or by using liquid helium or hydrogen refrigerants. The latter was used extensively in the warm electron experiments at 11 K and 20 K which are described in Chapter 7. The sample temperature was measured either by the thermo-e.m.f. of a copper versus gold-cobalt thermocouple or else by the forward junction voltage at constant current of a Unitrode silicon diode. The latter thermometer provided the greater sensitivity at temperatures below about 20 K.

In the Toulouse system, the sample container was surrounded by the liquid nitrogen refrigerant which cooled the solenoid. The temperature of the sample could be varied between 60 K and 350 K by means of a heater coil and was stabilised to within about 5^{o}K using a feed-back circuit which was regulated by the thermo-e.m.f. of a thermocouple junction mounted close to the specimen.

2.4 Electrical Measurements

The magnetophonon effect was measured in the transverse and longitudinal magnetoresistance tensors ρ_{xx} and ρ_{zz} ($\underline{B} \parallel$ z-axis) by passing a constant current through the two outer electrical contacts and measuring the voltage developed across the inner contacts. The advantage of the four contact technique is that provided the input impedance of the voltage measuring device is much greater than the sample impedance then the effects of contact resistance can be neglected.

The major problem associated with the measurement of magnetophonon structure is that its amplitude is seldom more than a few percent of the resistivity of the sample. For this reason, a constant current source with a stability of 1 part in 10^4 or better is essential. This can be most conveniently obtained from a 90 V dry cell in series with a low noise resistor whose resistance is much greater than that between the outer pair of contacts of the sample. Such a source was used in all the experiments described in this thesis except some of the warm electron measurements in n-InP (Chapter VII). In this material the non-ohmic magnetoresistance at 11 and 20 K is particularly rich in magnetophonon structure at electric field strengths above 5 V/cm. In order to make measurements at these fields without causing significant Joule heating of the sample it was necessary to use pulsed electric fields. The current stability necessary for observing the magnetophonon effect was obtained using a circuit (Wood, 1970) which switched the current periodically between the sample and a dummy load. The voltage signal generated across the two inner contacts which consisted of a series of rectangular pulses was fed into a sample and hold circuit synchronised with the current pulses through the sample. The output D.C. signal voltage was proportional to the magnetoresistance of the sample.

Even under optimum conditions, the magnetophonon structure is seldom more than a few percent of the total resistivity of the sample. An additional difficulty is that the peaks appear as small oscillations superposed on a magnetoresistance background which increases monotonically with increasing field. In the transverse configuration the magnetoresistance is at least an order of magnitude greater than the zero

field resistance at fields of about 100 kG. Because of distortion of the current lines or else warped energy bands, the magneto-resistance in the longitudinal configuration is also a significant fraction of the zero field resistance. In order to make a detailed study of the magnetophonon structure, it is necessary to suppress the slowly varying background magnetoresistance.

This can be achieved either by subtracting from the magneto-resistance ρ (B) a signal of appropriate magnitude which is proportional to the magnetic field or else by generating the second derivative of ρ (B) with respect to magnetic field. Both techniques have been employed in the experiments carried out at Oxford. In the pulsed field experiments, the double differentiation method has proved to be the more convenient and effective technique of studying the magnetophonon structure.

The circuit arrangement for the first method is shown in Figure 2.2. The voltage proportional to B is obtained from the Hall contacts of a degenerate sample of n-InSb which is mounted in the magnetic field at the base of the cryostat. A degenerate sample is used because this provides a Hall voltage which is insensitive to fluctuations of temperature. The difference signal ρ (B) - αB is amplified by a Keithley 150A D.C. amplifier and the output is displayed on the Y-axis of an X-Y recorder, the X-axis being driven by a voltage proportional to the magnet current which is obtained from a low resistance shunt in series with the magnet. The advantage of the linear biassing technique is that it displays the magnetophonon structure directly and permits an accurate estimate to be made of the amplitude of the extrema. Its principal disadvantage is that in a single sweep of magnetic field it is possible to study the magneto-phonon structure only over a limited range of magnetic field in which the gradient of the difference signal is small. From Figure 5.2 (ii) which shows recordings taken in n-Ge with the linear biassing techniques it can be seen that several field sweeps are required to study the magneto-phonon structure over a complete range of magnetic field. This is a serious limitation in the pulsed field experiments where a considerable delay ($\sim$ 40 minutes) occurs between successive runs due to the time taken to dissipate the Joule heating of the solenoid caused by the magnet

current pulse.

In the second method of studying magnetophonon structure, using the double differentiation technique, the voltage generated between the inner contacts of the sample is passed into a pair of differentiation circuits. When the magnetic field is swept linearly with time, the output signal is proportional to the second derivative of the magneto-resistance with respect to magnetic field. The differentiation process eliminates from the magnetoresistance any terms linear or quadratic in B and the oscillatory components may be amplified and plotted on the Y-axis of a chart recorder or storage oscilloscope. The circuit arrangements employed in the differentiation technique at Oxford and Toulouse are shown in Figures 2.3 and 2.4. In the Oxford measurements the differentiators are simple C.R. high pass filters each with a gain of $j\omega CR/(1+j\omega CR)$ Such a filter differentiates accurately provided that the magnetic field is swept sufficiently slowly for the condition $\omega CR \ll 1$ to be satisfied. An important feature of the double differentiators is that their gain-frequency response $G \sim \omega^2 C^2 R^2$ accentuates high frequency components. This is particularly valuable in revealing any sharp structure which may be present in the magnetophonon series as can be seen by comparing traces 5.2 (i)(a) and 5.2 (ii)(a) for n-Ge with B $\|$ (001). In the recording obtained with linear biassing, the oscillations appear to be a damped sinusoidal series of peaks whereas the double differentiation recordings reveal that the high field maxima are considerably sharper than the neighbouring minima. It should be noted that the operation of double differentiation inverts the extrema in ρ (B) so that for the sake of convenience all the experimental recordings using double differentiation which are presented in this thesis are plotted as $-\partial^2\rho/\partial B^2$ versus B.

With the differentiation technique, the experimental traces of the magnetophonon structure recorded on sweeping the magnetic field upward were slightly displaced along the X-axis relative to those obtained on the downsweep due to the finite time constants of the differentiators and amplifier. As the shifts of the peaks on the up and down sweeps are equal

and opposite, the magnetic field positions of the magnetophonon structure were calculated by taking the mean of the two sets of recordings.

The circuit employed in the pulsed field experiments (Figure 2.4) consists of two differential differentiating amplifiers with gain-frequency characteristics of $\omega C_1 R_1$ and $\omega C_2 R_2$ up to a value of ω determined by the integrating capacitances $C_1^{\,1}$ and $C_2^{\,1}$. Further high frequency attenuation can be provided by the internal filters of the storage oscilloscope. The C, R values of the circuit are chosen so that the frequency of the magnetophonon oscillations fall on the linear portion of the gain-frequency response curve. As a typical example, consider the structure in n-CdSe obtained in an upward pulse to 350 kG (Figure 4.3). By calculating the time interval between the minima on either side of the N=2 harmonic, this peak is estimated to appear in the magnetoresistance signal at a frequency of 500 Hz. The appropriate C-R values for such a trace would be $C_1 = 0.01\mu F$, $R_1 = 200k\,\Omega$, $C_1^{\,1} = 500\ pF$, $R_2 = 100\ k\,\Omega$, $C_2 = 1\mu F$ and $C_2^{\,1} = 1200\ pF$. After double differentiation the signal pulse is displayed on a storage oscilloscope whose X-sweep is developed by a voltage proportional to B from a low resistance shunt in series with the magnet. Because of the time constants of the differentiators and filters the recordings obtained on the upsweep are displaced to higher magnetic fields relative to their true field positions. A similar and opposite shift occurs for recordings made on the downsweep. The shift of a given peak can be obtained by estimating the frequency at which it appears in the signal pulse and reading off the corresponding angular phase shift from a graph of the phase-frequency response of the circuit. In order to check the accuracy of the phase shift corrections, recordings were usually made both using the upsweep and downsweep. It is estimated that the correction for phase shift can be made sufficiently accurately to determine the peak positions in the pulsed field experiments to within about 2%.

CHAPTER 3

The Magnetophonon Effect in n-InP at temperatures above 60K

3.1 Introduction

Indium phosphide is a material which has recently attracted interest following the paper by Hilsum and Rees (1970) suggesting its suitability as a three-level Gunn oscillator. This device potential has led to a rapid development in growth technology and workers at the Royal Radar Establishment, Malvern have produced high quality epitaxial layers of n-InP on semi-insulating substrates which have peak mobilities in excess of 80,000 $cm^2/V.s$. The availability of this material has made possible a series of resonance experiments involving electronic transitions between Landau states of well defined energy which yield an accurate value of the conduction band effective mass. One of these experiments, magnetophonon resonance, is the subject of this chapter. The value of effective mass obtained is considerably higher than that derived from earlier experimental work and from k.p. perturbation theory (see Table 3.2).

The experiments were carried out on several different epitaxial specimens at temperatures between 60K and 300K using steady magnetic fields of up to 90 kG and pulsed magnetic fields of up to 350 kG with the current direction ($\underline{j}$) oriented either parallel or perpendicular to the applied magnetic field ($\underline{B}$).

3.2 Sample Characteristics

The samples used in the experiments were cut from three high purity epitaxial slices. Slice A proved to be very inhomogeneous with the impurity concentration increasing steadily along its length. Thus a specimen (A1) taken from one end of the slice had a resistivity more than an order of magnitude greater and a peak mobility four times greater than one taken from the other end. The characteristics of sample A1 obtained from conventional Hall and resistivity measurements are $N_D - N_A = 4 \times 10^{15} cm^{-3}$; $\mu(300K) = 3,500\ cm^2/V.s$; $\mu(77K) = 33,000\ cm^2/V.s$. All samples from slice A showed a decrease in electrical resistance as the temperature was raised above about 250K, indicating the presence of a deep donor level with an activation energy of about 0.15 eV. Slices B and C were considerably more homogeneous than slice A and had a Hall mobility

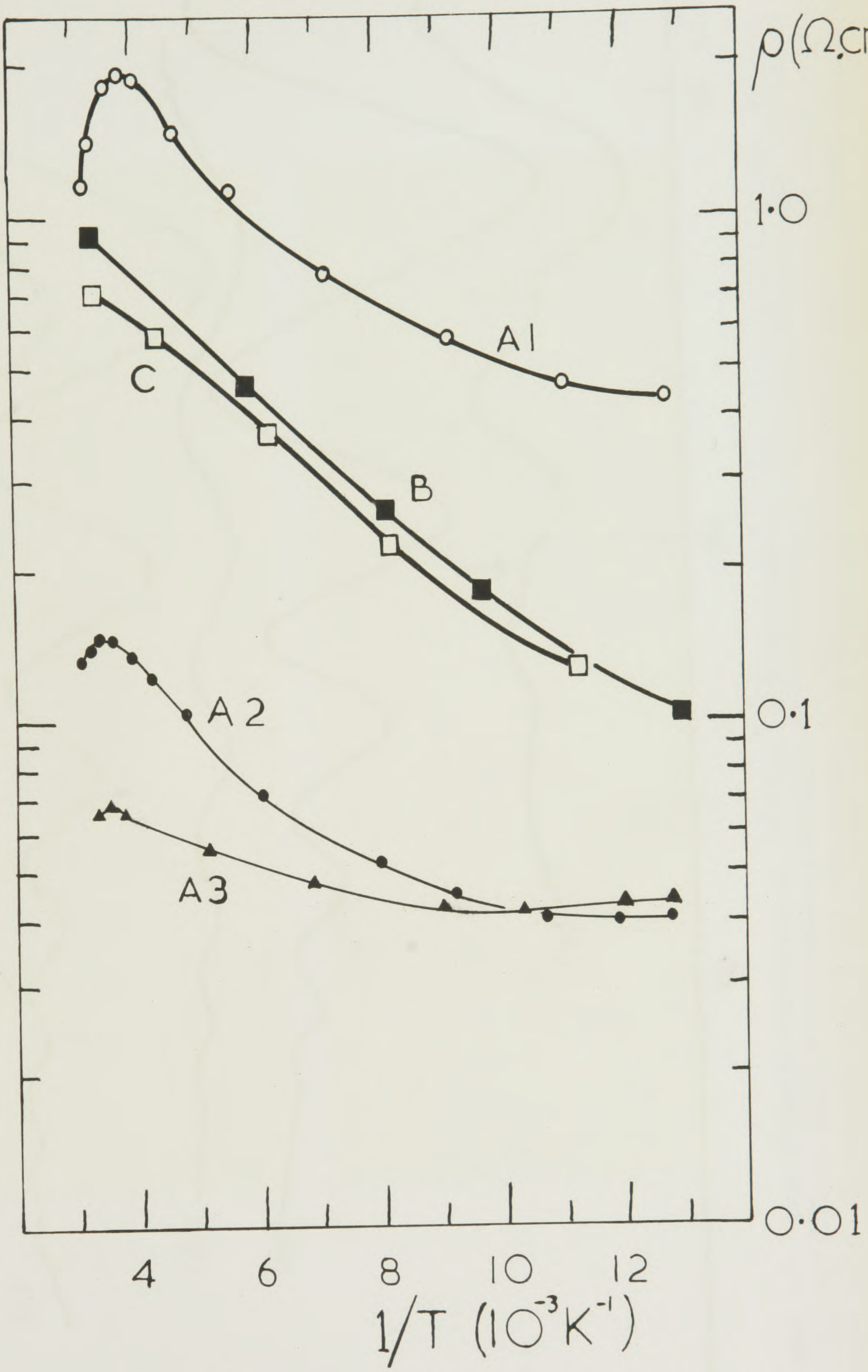


Figure 3.1 Temperature dependence of the resistivities of the n-InP samples used in the magneto-phonon experiments.

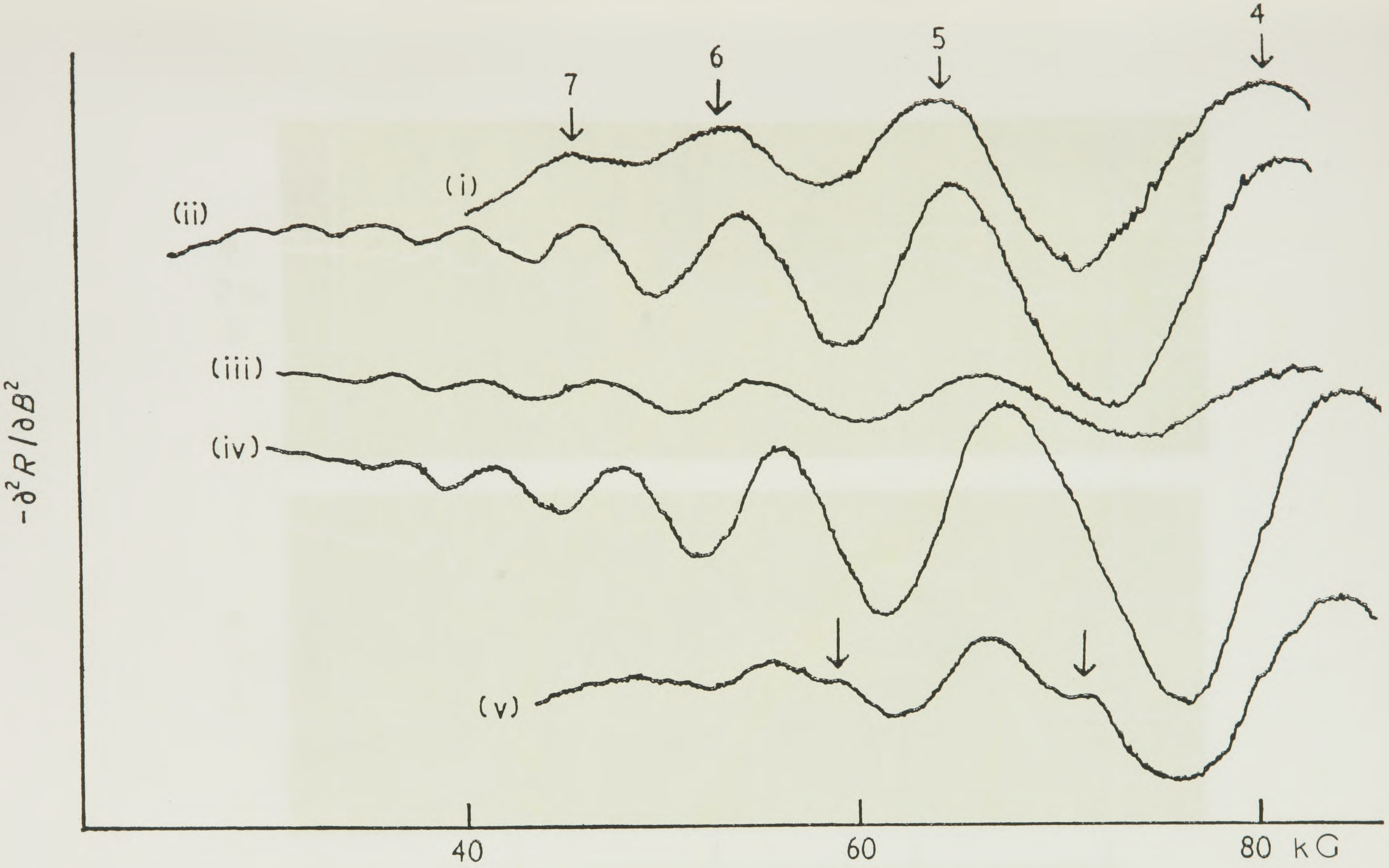


Figure 3.2. Experimental recordings of $-\partial^2 R/\partial B^2$ against magnetic field for fields up to 90 kG. Curves (i), (ii) and (iii) are taken with sample A1 in the transverse orientation at temperatures of 290, 175 and 85 K respectively. Curves (iv) and (v) are with sample B in the longitudinal orientation at 180 and 270 K respectively. The latter curve shows structure (indicated by arrows) attributed to two simultaneous L.O. scattering processes.

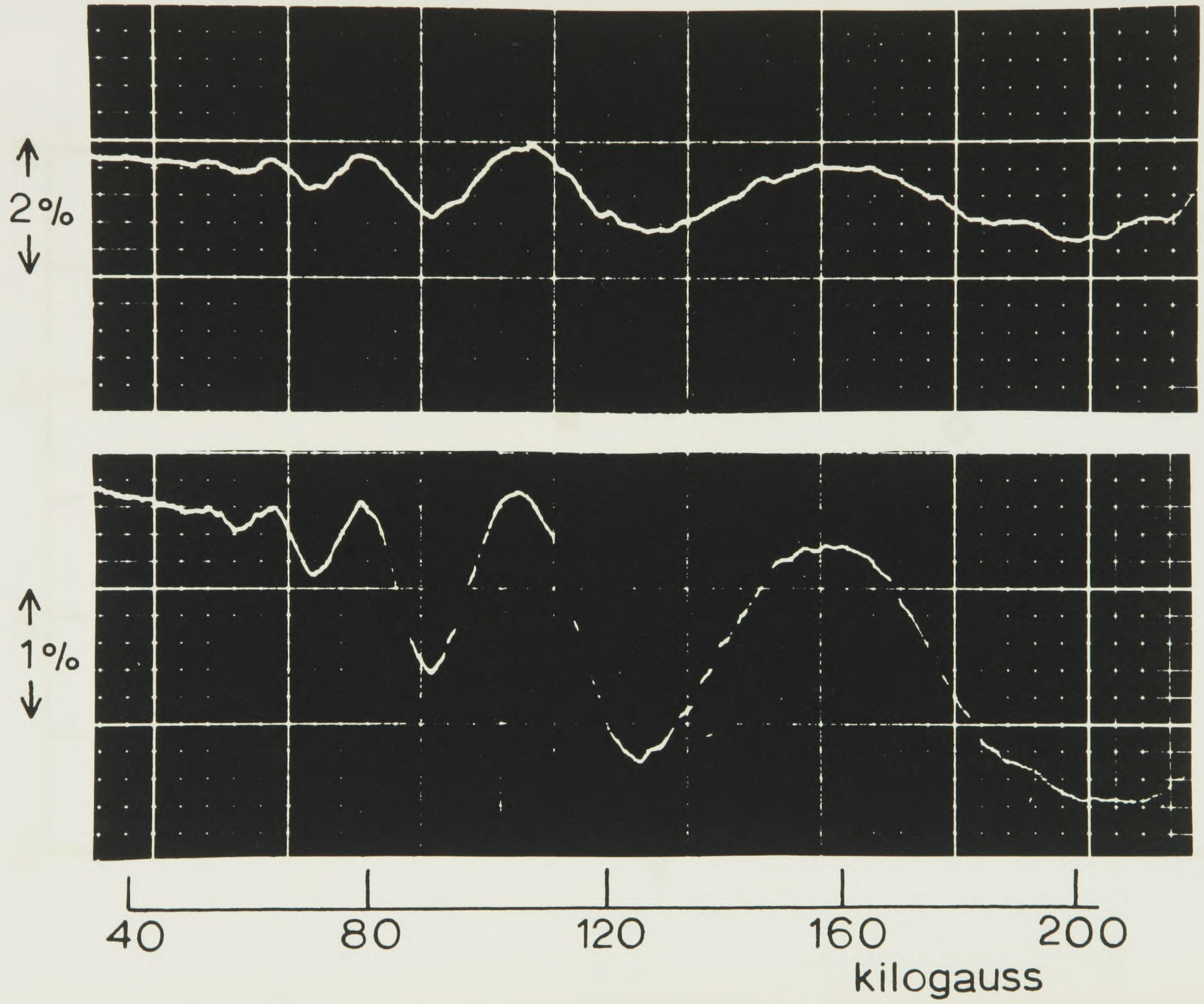


Figure 3.3 The experimental recordings of $-\partial^2 R/\partial B^2$ with ($\underline{j} \perp \underline{B}$) at a temperature of 160K for InP samples from slice A.

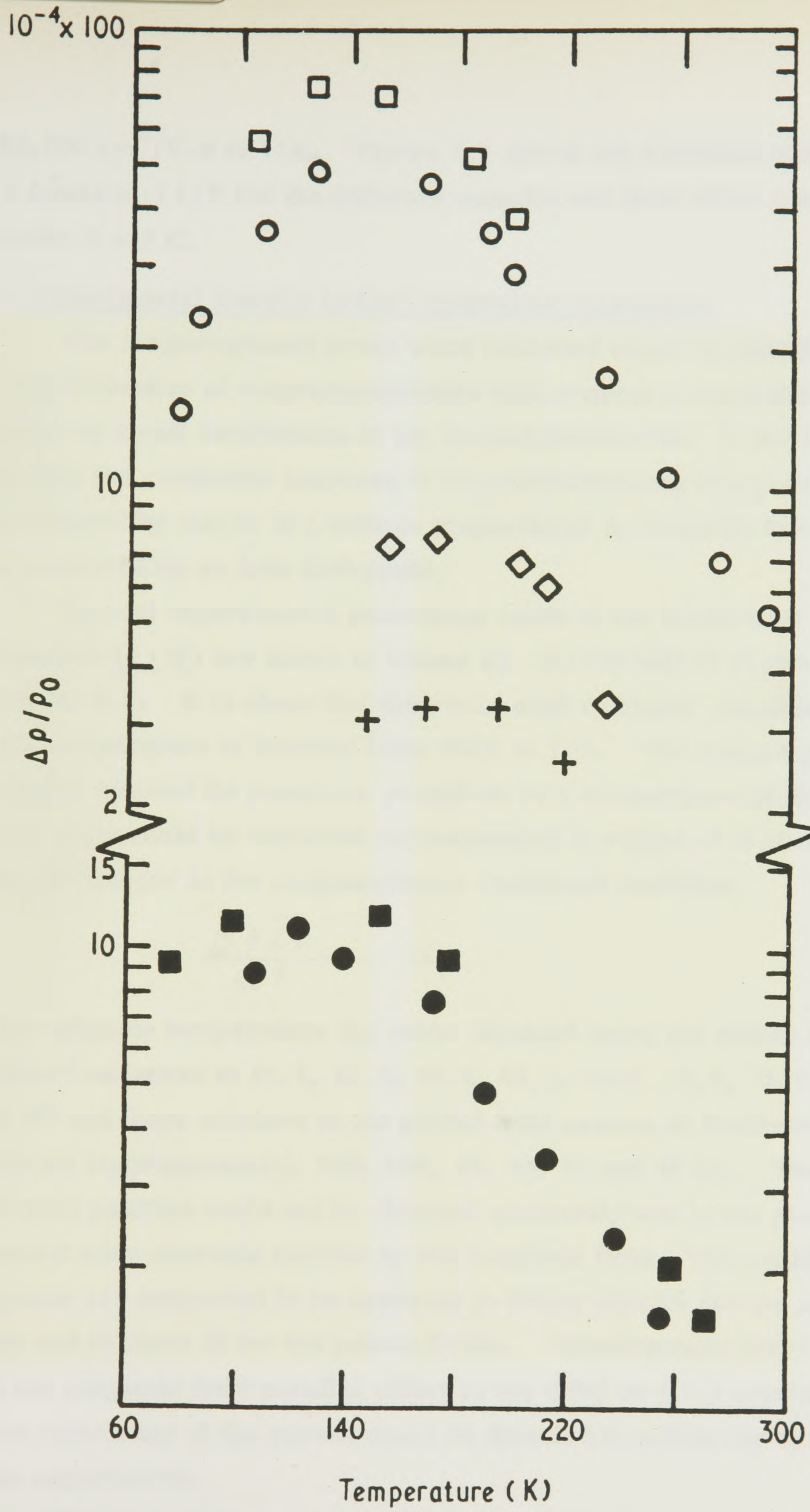


Figure 3.4 The temperature dependence of the amplitude of the N=5 extremum for the following samples and orientations. (i) transverse (□) and longitudinal (■) orientations for sample B, $\mu(77\,K) = 60,000\ cm^2\ V^{-1}s^{-1}$; (ii) transverse (○) and longitudinal (●) orientation for sample A1, $\mu(77\,K) = 32,000\ cm^2\ V^{-1}s^{-1}$; (iii) transverse orientation for sample A2 (◇), $\mu(77\,K) = 13,000\ cm^2\ V^{-1}s^{-1}$; (iv) transverse orientation for sample A3 (+), $\mu(77\,K) = 5000\ cm^2\ V^{-1}s^{-1}$.

of 60,000 $cm^2/V.s$ at 77K. Figure 3.1 shows the variation of resistivity as a function of 1/T for the different samples cut from slice A and for samples B and C.

3.3 Experimental Results in the Transverse Orientation

The magnetophonon peaks were observed either by plotting the second derivative of magnetoresistance with respect to magnetic field or directly as small oscillations in the magnetoresistance. In the latter technique the monotonic increase in magnetoresistance was partially compensated by means of a voltage proportional to magnetic field which was generated by an InSb Hall probe.

Typical experimental recordings taken in the transverse orientation ($\underline{j} \perp \underline{B}$) are shown in traces (i), (ii) and (iii) of Figure 3.2 and in Figure 3.3. It is clear that the peaks shift to higher magnetic fields as the temperature is lowered from 300K to 77K. The magnetophonon structure reached its maximum amplitude at a temperature of about 130K where peaks could be observed corresponding to values of N of up to 11, N being the integer in the magnetophonon resonance condition

$$\frac{N q B_N}{m^*} = \omega_\ell \qquad (3.1)$$

At the optimum temperature the peaks obtained using the steady fields at Oxford occurred at 81.7, 65.2, 54.2, 46.3, 40.4, 35.6, 31.9 and 28.5 kG and those obtained in the pulsed field system at Toulouse were at 320 kG (approximately), 160, 106, 80, 64, 53 and 45 kG. The highest field peak position could not be obtained accurately due to the presence of transient eddy currents induced by the magnetic field. The positions of the peaks are estimated to be accurate to better than 1% for the steady fields and to about 2% for the pulsed fields. Measurements were made with the magnetic field parallel either to the (100) or (111) crystal axis but no anisotropy of the curves could be detected to within the accuracy of the experiments.

The magnetophonon peaks showed no sign of sharpening at the highest fields and could accurately be described by the relation

$$\Delta\rho \sim \exp(-\gamma\omega_e/\omega_c)\cos(2\pi\omega_e/\omega_c) \qquad (3.2)$$

which was developed empirically by Stradling and Wood. In this equation γ is a numerical factor which describes the damping of the magnetophonon oscillations with decreasing magnetic field. Barker (1970, 1972) has recently derived equation (3.2) in a theoretical treatment of the magnetophonon effect where the role of collision broadening in determining the amplitude of the magnetophonon peaks has been considered in detail.

Figure 3.4 shows the variation with temperature of the amplitude (defined as $\Delta\rho/\rho_o$ where ρ_o is the zero field resistance) of the N = 5 extremum for a number of samples. It is clear that the amplitudes of the peaks for the low mobility samples A2 and A3 are an order of magnitude smaller than those for the high purity samples and that at temperatures above 250K the peaks have disappeared into the noise background even though at these temperatures the mobilities of all samples are quite comparable. Thus, as was found in GaAs (Stradling and Wood, 1968) instead of depending simply on the low field mobility determined by L.O. phonon scattering, the peak amplitude appears to be inversely proportional to the concentration of ionised impurities. One can understand qualitatively why the ionised impurities should have a temperature independent effect on the amplitude of the magnetophonon peaks whereas their contribution to the low field Hall mobility varies as $T^{3/2}$: the optical phonon scattering which leads to the transverse magnetophonon effect occurs mainly between states close to $k_B = 0$ and the broadening effect of ionised impurity scattering is important at the bottom of each Landau level irrespective of the thermal excitation of electrons to higher energy states.

The temperature dependence of the amplitude of the magnetophonon peaks for a given sample is similar to that observed in other materials. At low temperatures the optical phonon vibration mode freezes out and optical phonon scattering is dominated by ionised impurity and acoustic phonon scattering processes which take over to limit the mobility. At high temperatures optical phonon scattering becomes so strong that the

Landau levels broaden and the magnetophonon peaks are smeared out.

3.4 Experimental Results in the Longitudinal Orientation

The nature of the scattering processes discussed previously in the theory of the longitudinal magnetophonon effect leads to three important features that distinguish the experimental results in the longitudinal orientation from those in the transverse orientation. Firstly, as can be seen from Figure 3.2, the extrema in the longitudinal orientation are displaced from the magnetic field positions of the maxima in the transverse orientation. Secondly, the amplitudes of the peaks in ρ_{zz}, plotted against temperature in Figure 3.4, are an order of magnitude weaker in amplitude than those in ρ_{xx} at the same temperature because the strong scattering processes between the high density of states regions near $k_z = 0$ are unable to relax the longitudinal current appreciably. Thirdly, at temperatures above about 200K, an additional series of minima, indicated by arrows in Figure 3.2, can be observed in the purest samples (B and C) at high magnetic fields. This structure has been observed in the longitudinal magnetoresistance of other materials (Stradling and Wood, 1968, 1970; Akselrod and Tsidilkovskii, 1969) and is due to the two-stage optical phonon scattering process discussed in Chapter 1.

Table 3.1 : Positions of Extrema in $-\partial^2 R/\partial B^2$ at 130K

	Magnetic Field kG
Transverse maxima, samples A1, B, C.	320 160 106 81.7 65.2 54.2 46.3 40.4 35.6 31.9 28.5
Longitudinal maxima, sample A1.	180 119 88 68.1 56.0 47.8 41.3
Longitudinal maxima, samples B, C.	86.4 67.5 56.5 48.3 41.8
Longitudinal minima, sample A1.	141 101 77.1 61.6 51.7 44.5 38.7
Longitudinal minima, samples B, C.	78.3 61.7 52.2 44.8

In table 3.1 the positions of the longitudinal extrema are compared with the positions of the transverse maxima for samples A and B. The positions of the peaks in samples B and C agreed to within experimental error. The interesting feature of the results is that the longitudinal extrema do not coincide with those observed in the transverse orientation even at high values of N. This is in contrast with the results obtained for other III-V compounds where minima are found in the longitudinal configuration at fields close to but slightly lower than the maxima observed with $j \perp B$ (Stradling and Wood, 1968; Askenazy et al. 1969). However, the large displacement of the minima which is also observed in CdTe (Mears et al. 1968) and CdSe (Eaves et al. 1972 and chapter 4) suggests that this is a feature common to polar materials, a proposition which is supported by the result obtained by Barker (1972a) for the effect of Landau level broadening in the limit of strong polar coupling of the electron to the L.O. phonon.

The longitudinal peak positions observed in samples cut from slice A were found to be displaced slightly to lower fields relative to those observed for samples B and C. It is difficult to account for this small discrepancy but it may be connected with the inhomogeneity of the epitaxial slice A. The large longitudinal magnetoresistance which was found in all samples cut from this slice suggests that the inhomogeneity, which was found over the length of the slice, was also present in individual samples cut from it. Any such spatial variation of the conductivity would bend the current lines so that the magnetoresistance measured with $j \parallel B$ would consist of an admixture of ρ_{zz} and ρ_{xx}. As these components are not exactly 180° out of phase, they will not cancel completely and the resulting magnetophonon extrema may be displaced from the longitudinal peak positions observed in a homogeneous sample.

3.5 Determination of Effective Mass

Earlier work (Stradling and Wood, 1968, 1970) has established magnetophonon resonance as a reliable method of obtaining the electronic effective mass. In deriving accurate effective mass values from the

experimental recordings, account must be taken of the small shift in the positions of the maxima from the resonance fields which is caused by the exponential damping term in equation 3.2. By differentiating this equation, it can be shown that the N^{th} peak in the magnetoresistance curve is shifted by an amount

$$\delta = \frac{100}{2\pi N} \tan^{-1} \frac{\gamma}{2\pi} \quad \%$$

to higher magnetic fields. When the peaks are observed in the second derivative of the magnetoresistance with respect to field, the expression for the shift is more complicated but can be approximated by

$$\delta' = \frac{100}{2\pi N} \tan^{-1} \frac{3}{2\pi} \left(\gamma - \frac{2}{N}\right)$$

for small damping and large N (Wood, 1970). At room temperature γ = 1.6 for sample A1 and the correction is 1.8% for the N = 5 peak, whereas at 150K γ has decreased to 1.1 so that the correction is 1% for the N = 5 peak and 0.7% for the N = 8 peak.

The magnetophonon effective mass derived from equation (3.1) can be converted into a band-edge value by applying a correction arising from the non-parabolicity of the conduction band using the method described by Stradling and Wood (1968, 1970a). In indium phosphide the correction for the N = 4 peak is about 5% at 300K and 3½% at 100K. After reducing the magnetic field positions of the maxima by these amounts, the values of the product NB_N at a given temperature were independent of N to within 1% for values of N from 4 to 11. The average value of NB_N was then used to calculate the band-edge effective mass using the temperature dependent values of the optical phonon frequency given by the Raman data of Mooradian and Wright (1966).

In order to compare the effective mass values obtained from the magnetophonon data with those obtained by means of other experiments, a further correction arising from the polaron effect must be considered. The magnetic fields at which magnetophonon peaks are found in the transverse magnetoresistance are precisely those at which resonant polaron effects have been detected in magneto-optical experiments and

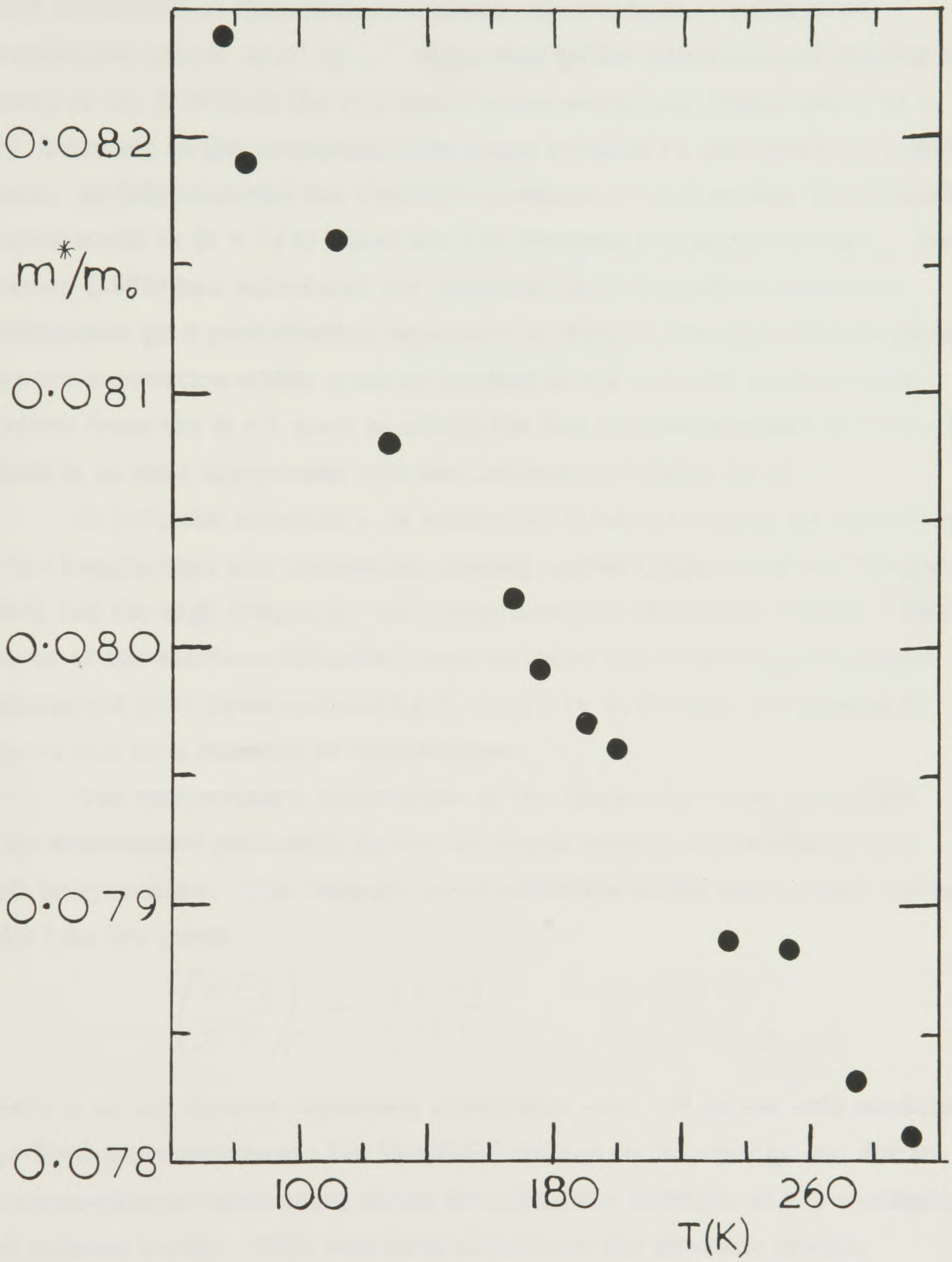


Figure 3.5 The temperature dependence of the low frequency band-edge effective mass of the electrons in InP obtained from the positions of the magnetophonon peaks in the transverse orientation.

it can be expected that the effective mass deduced from magnetophonon experiments using Equation (3.1) may be different from the low frequency mass measured in cyclotron resonance experiments at millimetre wavelengths where $\omega \ll \omega_c$. According to the experimental results of Mears et al. (1968) on the relatively polar compound CdTe, there is a 13% increase in the magnetophonon mass relative to the cyclotron resonance mass. In this material the Frohlich constant $\alpha = 0.4$ so that the magnetophonon mass is $(1 + \alpha/3)$ times the low frequency cyclotron mass. Recently, Palmer (1970) has calculated the magnetic field dependent transport coefficients by a perturbation expansion of Kubo's formula and has shown that the correction which must be applied to the magnetophonon mass derived from the N = 1 peak to obtain the low frequency mass is $0.73\alpha/3$ which is in good agreement with the estimate of Mears et al.

In InP, the constant α is estimated to be 0.12 from the frequencies of the longitudinal and transverse optical modes (Mooradian and Wright, 1966) and the high frequency dielectric constant (Newman, 1958). The values of the electron effective mass deduced from the magnetophonon experiment have been reduced by $0.73\ \alpha/3$ (= 2.7%) and are plotted in Figure 3.5 as a function of temperature.

The temperature dependence of the band-edge mass is thought to be determined primarily by the dilational change in the energy gap with temperature. The temperature coefficient of the energy gap can be split into two parts

$$\left(\frac{\partial E_g}{\partial T}\right)_P = \left(\frac{\partial E_g}{\partial T}\right)_V - \frac{\alpha}{\beta}\left(\frac{\partial E_g}{\partial P}\right)_T \qquad (3.3)$$

where α is the volume expansion coefficient and β is the bulk modulus. The first term expresses the 'explicit' change in the energy gap due to electron-phonon interaction which broadens the extrema of the conduction and valence bands. This was first calculated for acoustic phonon scattering by Fan (1951). In indium phosphide an additional narrowing of the gap can be expected from polar optic phonon scattering. The second term in equation (3.3) is the dilational contribution resulting from the

change of the lattice constants with temperature.

Knowing the values of the expansion coefficeint (Bernstein and Beal, 1961), the bulk modulus (Hickernell and Gayton, 1966) and the variation of energy gap with pressure (Pitt, 1970), the dilatational change in the energy gap is estimated to decrease the band-edge mass by 3.8% as the temperature is increased from 100K to 300K which is in quite good agreement with the 5%change observed experimentally. The observed variation of the optical energy gap would, however, predict an 8% change of effective mass in the same temperature range. The temperature dependence of m^* for InP is similar to that obtained by Stradling and Wood (1970a) in InSb and GaAs where the observed change in effective mass with temperature is approximately equal to, but slightly larger than, the amount predicted from the dilatational change in energy gap with temperature.

The value of the band-edge mass of $0.082\ m_0 \pm 0.001\ m_0$ at 77K and $0.078\ m_0 \pm 0.001\ m_0$ at 300K is considerably higher than the theoretical estimate of $0.0545\ m_0$ derived from the $\underline{k}.\underline{p}$ theory of Pollak et al. (1966). This discrepancy is surprising in view of the success of these calculations in predicting the experimentally determined electron and hole effective masses in GaAs. Some early experimental determinations of the effective mass together with recent values deduced from cyclotron resonance and the Zeeman effect in shallow donors are compared with the present magnetophonon estimate in Table 3.2.

The experiments described in this chapter have been repeated recently by Bashirov et al. (1972). They observed five peaks in the transverse orientation at a temperature of 300K and deduced from the magnetic field positions an electronic effective mass of $0.082\ m_0$.

Table 3.2 : The electronic effective mass in InP

Method	Reference	T (K)	m^*/m_0
Magnetophonon resonance	Eaves, 1971	77	0.082 ± 0.001
		290	0.078 ± 0.001
Cyclotron resonance	Chamberlain, 1972a	9	0.0803 ± 0.0003
" "	Simmonds, 1972	55	0.080 ± 0.001
" "	"	300	0.080 ± 0.003
Cyclotron resonance	Palik, 1961	77-300	0.077 ± 0.005
Zeeman effect in shallow donors	Chamberlain, 1971	4	0.0810 ± 0.0005
	Eaves (Chapter 8)	4	0.0802 ± 0.0003
Shubnikov-de Haas	Askenazy, 1971	2-25	0.084 ± 0.004
Infra-red reflectivity	Köhl, 1971	300	0.077
Temperature dependence of mobility	Glicksman, 1958	-	0.05
	Folberth, 1955	-	0.05
Faraday rotation	Moss, 1959	300	0.073 ± 0.007
	Kesamanly, 1964	300	0.066 ± 0.003
$\underline{k}.\underline{p}$ perturbation theory	Pollak, 1966	-	0.0545

CHAPTER 4

The Magnetophonon Effect in n-CdSe

4.1 Introduction

Cadmium selenide has two interesting features which can be investigated by the magnetophonon experiments described in this chapter. Firstly, since the compound has a wurtzite crystal structure there should be an anisotropy of the conduction band of a similar nature to that in cadmium sulphide. The amount of anisotropy and the band edge effective mass have not previously been measured precisely. Secondly, the relatively polar nature of the compound (α = 0.46) provides a test of recent theoretical predictions concerning the magnetic field positions of the magnetophonon extrema in both the longitudinal and transverse magnetoresistance.

The experiments were performed on high purity samples prepared at the University of Hull in the form of thin platelets deposited from the vapour phase. The Hall mobility which was measured over a temperature range from 20 K to 300 K is shown in Figure 4.1 and is the highest yet reported for cadmium selenide, reaching a peak of 11,000 $cm^2/V.s.$ at 40 K.

4.2 Experimental Results in the Transverse Orientation

In order to determine the anisotropy of the conduction band, experiments were performed with the magnetic field ($\underline{B}$) applied transverse to the current direction ($\underline{j}$) and either parallel or perpendicular to the c-axis of the crystal. The samples were cut in the form of rectangular bars which had the long current carrying dimension either parallel or perpendicular to the c-axis so that all orientations of the magnetic field with respect to the current direction and crystal axes could be studied. The magnetophonon peaks in the magnetoresistance were of maximum amplitude at a temperature of about 80 K when, in the transverse orientation with $\underline{B} \perp \underline{c} \parallel \underline{j}$, six maxima were observed at magnetic fields of 53.2, 63.4, 81.4, 107, 157 and about 320 kG. The recordings shown in Figure 4.2 were obtained using the steady fields at Oxford and those in Figure 4.3 with the pulsed fields at Toulouse. The peaks were considerably weaker in amplitude than those obtained in n-InP and could only be observed in the temperature interval between 70 K and 90 K. In this range the amplitude (defined as $\Delta\rho/\rho_0$ where ρ_0 is the zero

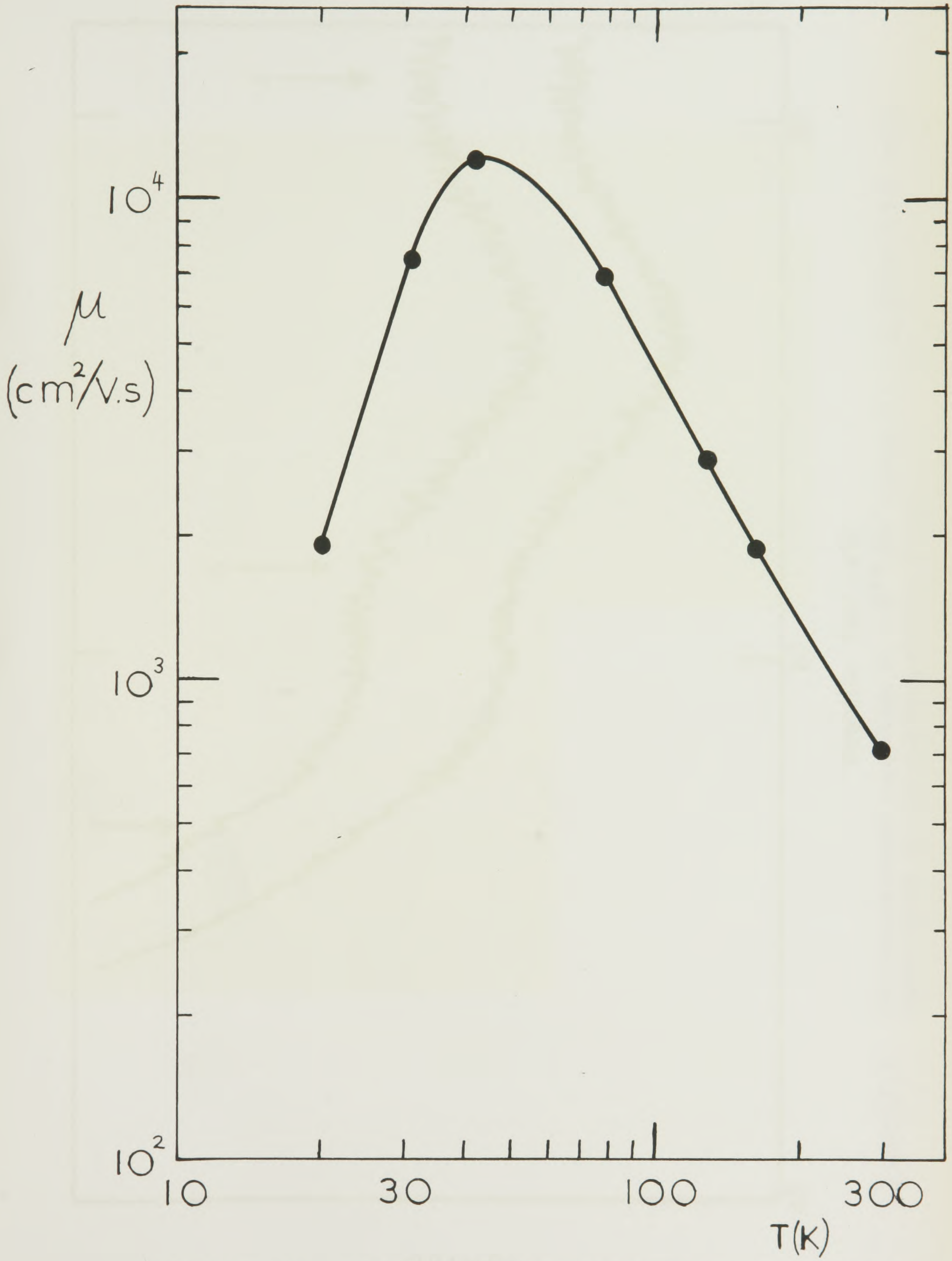


Figure 4.1 The Hall mobility of the CdSe samples prepared at Hull University.

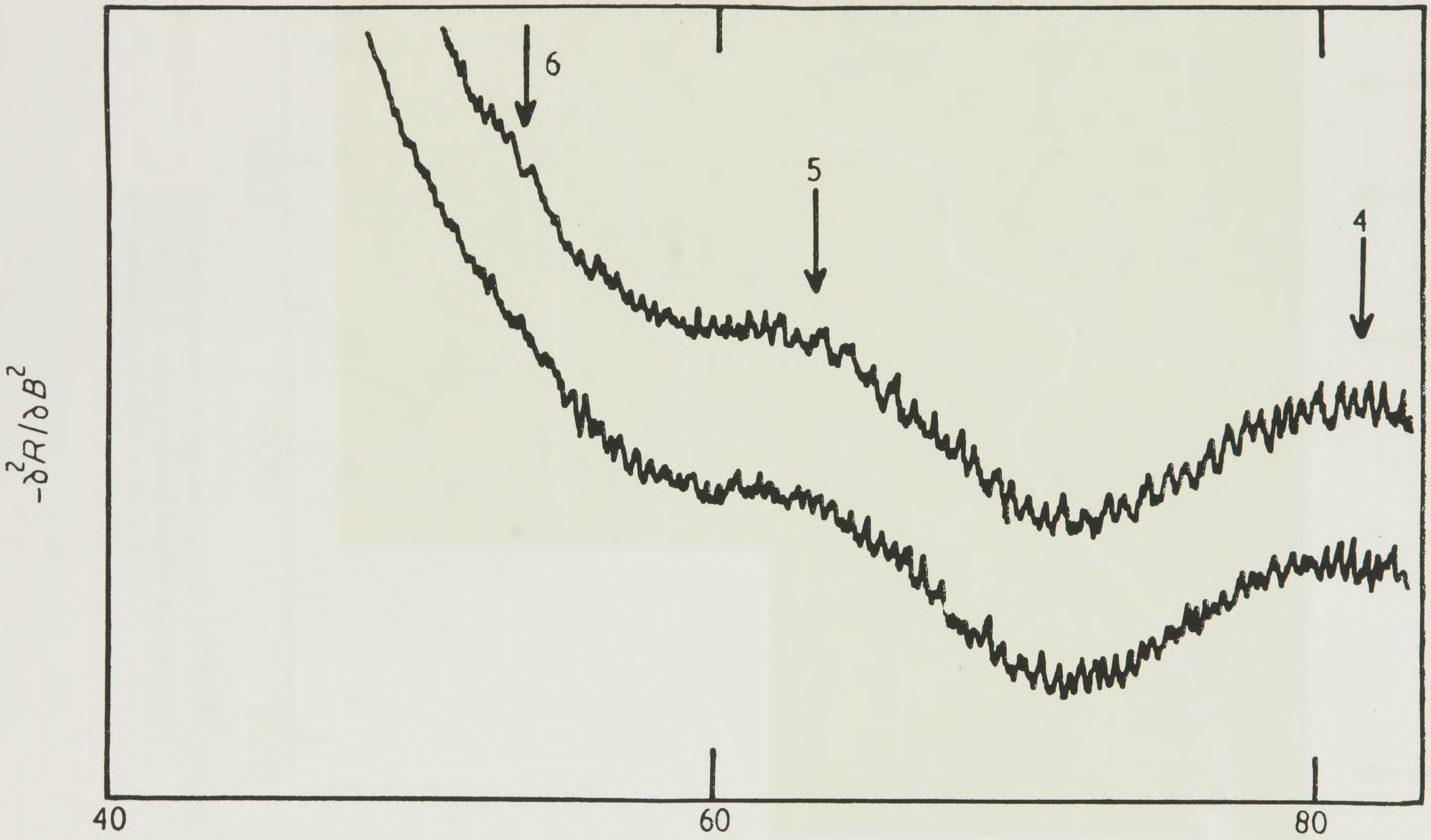


Figure 4.2 The experimental recordings of $-\partial^2 R/\partial B^2$ against B ($\underline{j} \perp \underline{B}$) for Cd Se using steady fields at a sample temperature of 80K

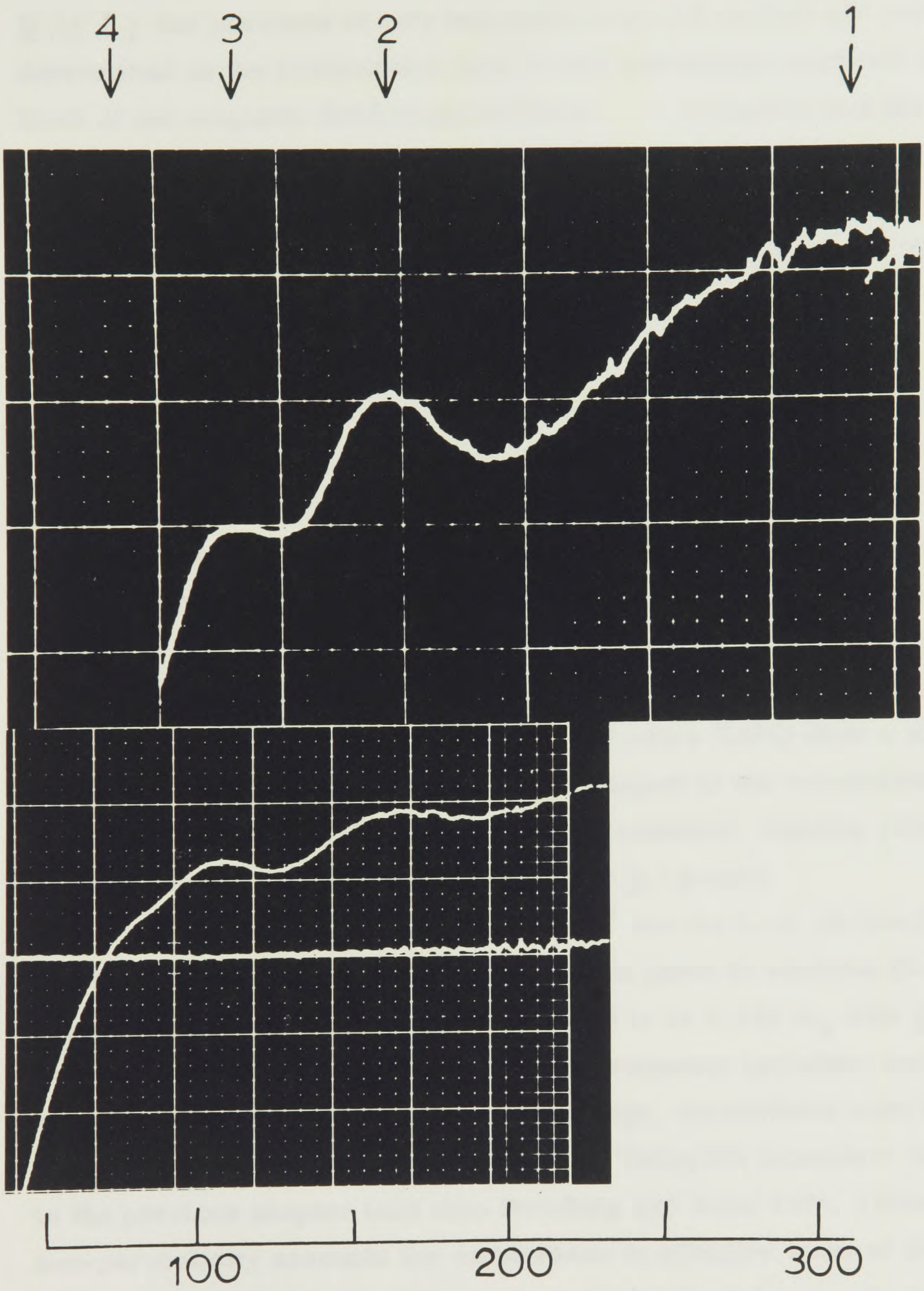


Figure 4.3 The experimental recordings of $-\partial^2 R/\partial B^2$ against B for Cd Se using pulsed fields at a sample temperature of 80K ($B \perp j \parallel c$)

field resistance) of the N = 5 harmonic was about 3×10^{-5}. With $\underline{B} \parallel \underline{c} \perp \underline{j}$ the positions of only two maxima at 113 and 162 kG could be determined as the fundamental peak in this orientation occurred at the limit of the magnetic field range available. A comparison of the magnetic field positions of the peaks in the two orientations shows that the effective mass is about 4% higher with $\underline{B} \parallel \underline{c}$ than with $\underline{B} \perp \underline{c}$ indicating that the conduction band is a slightly oblate spheroid whose symmetry axis is the crystalline c-axis.

4.3 Determination of Effective Mass

In order to determine the conduction band effective mass from the magnetophonon data, a precise value is required for the energy of the L.O. phonon mode at the Brillouin zone centre. In general, the most accurate estimate of the frequency of such phonons is obtained from Raman scattering and these experiments (Parrish et al., 1968) indicate a value of 213 cm^{-1} at 80 K. This value is supported by that obtained from luminescence measurements (Langer et al., 1966) which give 214 cm^{-1} at 4 K. The reflectivity data of Mitra (1966) show a slight anisotropy of the phonon frequency with respect to the orientation of the electric field vector of linearly polarised radiation, yielding values of 210 cm^{-1} for $\underline{E} \parallel \underline{c}$-axis and 212 cm^{-1} for $\underline{E} \perp \underline{c}$-axis.

On substituting a value of 213 cm^{-1} for the L.O. phonon frequency into the magnetophonon resonance condition given by equation (3.1), the magnetophonon effective mass m^* is found to be 0.140 m_0 with $\underline{B} \perp \underline{c}$. In order to determine the 'bare' and low frequency cyclotron resonance effective masses at the conduction band edge, corrections must be applied for non-parabolicity and polaron effects. Using the procedure discussed in the previous chapter (see also Stradling and Wood 1968, 1970a) the non-parabolicity accounts for an increase in effective mass of 3% at 80K. At the energy of an L.O. phonon above the band minimum, the piezoelectric polaron contribution to the effective mass (Mahan and Hopfield 1964; Mikaye, 1968) should be negligible. However, the increase in effective mass due to the optical polaron contribution will be important in the relatively polar CdSe. Employing the values of the high and low frequency dielectric constants derived by Mitra (1966), α is estimated to be 0.45.

As discussed in the previous chapter, Palmer (1970) has shown that the optical polaron correction factor that must be applied to the observed magnetophonon mass is $(1 + 0.73\alpha/3)^{-1}$ so that the low frequency cyclotron effective masses are estimated to be $0.122\ m_0$ for $\underline{B} \perp \underline{c}$ and $0.127\ m_0$ for $\underline{B} \parallel \underline{c}$. The corresponding ba e masses are $0.115\ m_0$ and $0.120\ m_0$.

The error in the determination of the magnetic field positions from which the effective mass values are derived is 1% for fields less than 100 kG and 2% for higher fields. In assessing the final accuracy of the quoted effective masses, the systematic error arising from the application of polaron and non-parabolicity corrections is difficult to estimate. This is particularly true for the 13% polaron correction not only because of the uncertainty in the values of the dielectric constant used to derive α but also because the only calculation of the polaron correction at present available (Palmer 1970) applies only to the N = 1 peak. However, earlier work on the magnetophonon effect in the polar materials CdTe (Mears et al., 1968) and InP (Eaves et al., 1971 and Chapter 3 of this thesis) have shown that after applying a correction of the size estimated by Palmer, the effective masses agree with the low frequency cyclotron resonance data to within the limit of experimental error. Hence, at the time of publication of the work described in this chapter (Eaves et al., 1972) when no precise cyclotron resonance data was available, it was felt that the systematic error in the effective masses was probably no more than 2%.

Recently, Chamberlain et al. (1972a) have performed a series of cyclotron resonance experiments using an HCN infra-red gas laser both in transmission and photoconductivity and obtain a band edge effective mass of $0.118 \pm 0.002\ m_0$ at 4 K with $\underline{B} \perp \underline{c}$-axis. This result clearly demonstrates the validity of the polaron correction applied to obtain the effective mass from the magnetophonon data.

These recent magnetophonon and cyclotron resonance results are in good agreement with the values of $0.13\ m_0$ at 1.8 K derived from the Zeeman splitting of exciton spectra (Wheeler and Dimmock, 1962;

Reynolds et al., 1968), 0.15 ± 0.01 m_0 determined at 300 K from free carrier absorption and reflectivity (Kubo and Onuki, 1965) and of 0.120 ± .005 m_0 obtained from cyclotron resonance (Button and Lax, 1970). In addition, the observed anisotropy in the magnetic field positions of the magnetophonon peaks agrees closely with that obtained from plasma reflectivity experiments at 300 K (Ginter, 1965) which indicate a mean effective mass of 0.125 m_0 and a mass anisotropy of 3.5%.

4.4 Experimental Results in the Longitudinal Orientation

Magnetophonon peaks were also visible in the longitudinal magnetoresistance of CdSe when the magnetic field was applied parallel to the current direction. However, their amplitudes were about an order of magnitude weaker than the corresponding peaks in the transverse orientation and structure could only be observed at magnetic fields above 100 kG. With $\underline{B} \parallel \underline{c} \parallel \underline{j}$ minima in ρ_{zz} were observed at 148 kG and 230 kG and a maximum at 127 kG, while with $\underline{B} \parallel \underline{j} \perp \underline{c}$ the corresponding extrema were displaced by about 4% to lower fields. Reference to the magnetic field positions of the extrema given in section 4.2 shows that the resonant fields at which maxima occur in the transverse orientation are approximately midway between adjacent maxima and minima found in the longitudinal magnetoresistance. As was discussed in section 3.4 of the previous chapter, this result appears to be common to magnetophonon resonance in the three polar materials so far studied.

CHAPTER 5

The Magnetophonon Effect in n-Ge

5.1 Introduction

For materials having a single spherical or spheroidal energy band at the centre of the Brillouin zone, the magnetophonon effect consists of a single series of peaks in the magnetoresistance which are periodic in $^1/B$ and which occur at magnetic fields given by the equation

$$\omega_c = \frac{NeB}{m^*} \qquad N = 1,2,3... \qquad (5.1)$$

N-type germanium, whose conduction bands have a more complex structure was first investigated by Sokolov and Tsidil'kovskii (1967) who reported observing about thirteen minima in the longitudinal magnetoresistance measured at fields of up to 220 kG. Because of the difficulty in eliminating the monotonically increasing part of the magnetoresistance, peaks were only visible for one orientation, $\underline{B} \parallel (100) \parallel \underline{j}$. This work was later extended by the observation of magnetophonon extrema in the transverse magnetoresistance (Gluzman and Tsidil'kovskii, 1969a) and in the longitudinal thermoelectric power (Gluzman and Tsidil'kovskii, 1969b) using samples with $N_D - N_A \sim 10^{15}$ cm^{-3} and magnetic fields of up to 180 kG. Later experiments carried out at Oxford (Wood, 1970) yielded results which appeared to differ from the Russian work in several important respects. The experiments described in this chapter extend the work by Wood by making a detailed investigation of the dependence of the magnetophonon peaks on the direction of current ($\underline{j}$) and magnetic field ($\underline{B}$) relative to the crystal axes for a range of sample purity from 2×10^{12} cm^{-3} to 10^{15} cm^{-3}. In addition, the use of double differentiation techniques has detected structure considerably weaker in amplitude than that obtained by Tsidil'kovskii and co-workers so that for certain magnetic field orientations more than twenty peaks have been observed in the transverse magnetoresistance.

The large anisotropy of the magnetophonon structure observed in n-type Ge arises from the complexity of the conduction band. Cyclotron resonance experiments (see Levinger and Frankl, 1961, for a summary of this work) have established that the constant energy surfaces near the conduction band edge consist of four ellipsoids of revolution about the

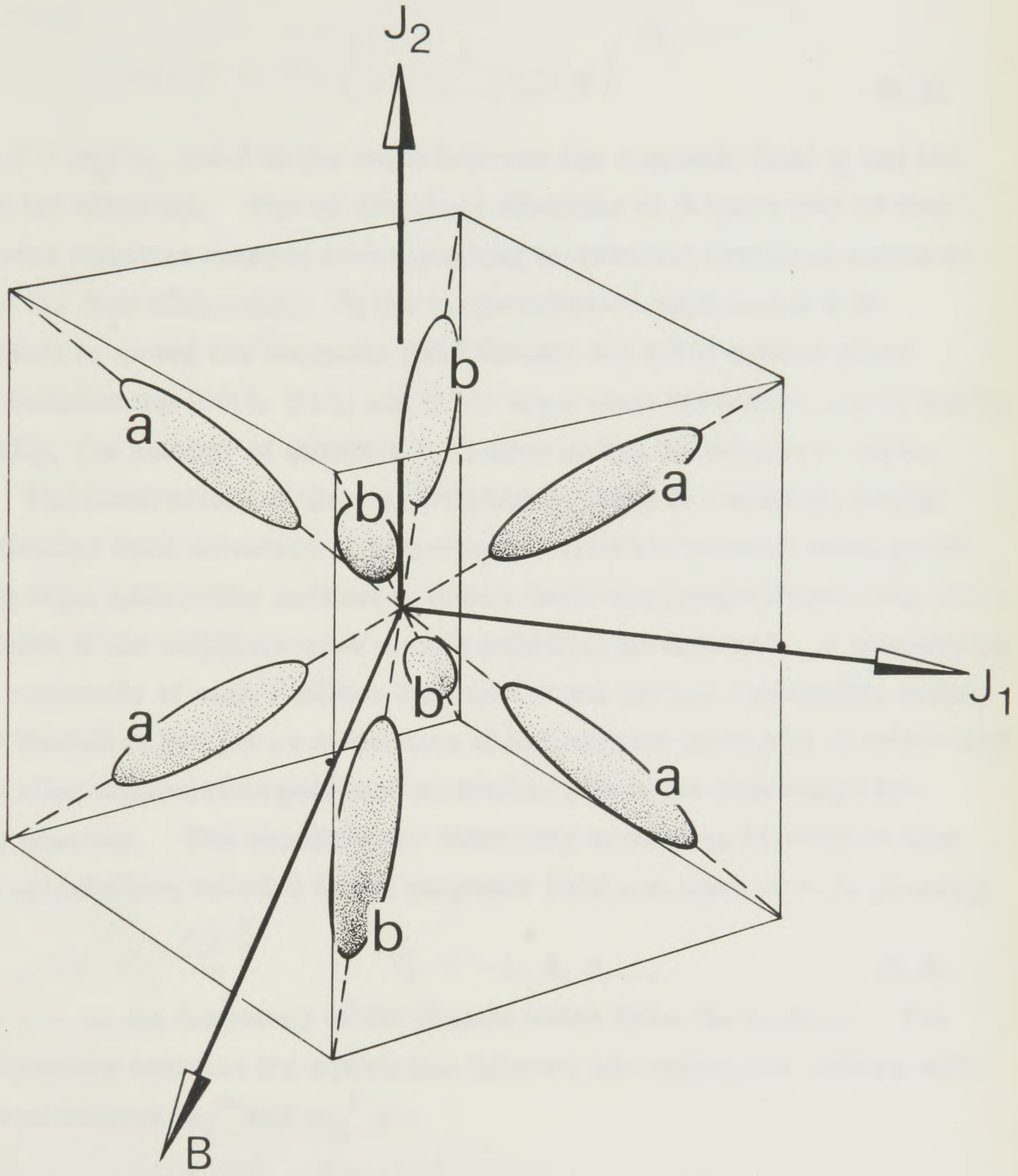


Figure 5.1 The conduction band ellipsoids in n-Ge

(111) crystal axes as shown in Figure 5.1. The cyclotron mass for any ellipsoid is given in terms of the principal masses m_l (longitudinal) and m_t (transverse) by the equation

$$m(\theta) = m_t \left[\frac{K}{1 + (K-1)\cos^2\theta} \right]^{1/2} \qquad (5.2)$$

where $K = m_l/m_t$ and θ is the angle between the magnetic field $\underline{B}$ and the axis of the ellipsoid. For an arbitrary direction of B there will be four electronic effective masses corresponding to different cyclotron orbits in each of the four ellipsoids. In the magnetophonon experiment it is convenient to sweep the magnetic field through the (110) crystal plane which contains the (001), (111) and (110) symmetry directions and in which, generally, the number of different cyclotron orbits is reduced to three.

The observation of the magnetophonon effect in materials having a multivalley band structure is of particular interest because extra peaks arising from intervalley scattering events involving phonons well away from the centre of the Brillouin zone may in principal be detected. A comparison of the amplitude of such a series with that of the normal intravalley series should therefore permit an estimation of the relative strengths of inter- and intra-valley deformation potential scattering processes involving high energy phonons. The condition for observing scattering between valleys whose orientations relative to the magnetic field are equivalent is given by

$$\omega_q = \frac{NeB}{m^*} \quad , \; N = 1, 2, 3 \ldots \qquad (5.3)$$

where ω_q is the frequency of the phonon which links the valleys. The corresponding equation for scattering between non-equivalent valleys with cyclotron masses m_1^* and m_2^* is

$$\omega_q = \left(N + \tfrac{1}{2}\right)\frac{eB}{m_1^*} - \left(M + \tfrac{1}{2}\right)\frac{eB}{m_2^*} \quad N, M = 0, 1, 2 \ldots \qquad (5.4)$$

According to Lax (1961), only the degenerate L.O. and L.A. phonons at the X-point in the Brillouin zone can assist in inter-valley transitions in Ge and the frequency ω_q of such phonons is about 70% of that at the zone centre. Thus the magnetic field positions of peaks given by equations (5.2) and (5.3) should differ significantly from those for intravalley processes involving optic phonons at the zone centre for which the resonance condition is equation 5.1. Tsidil'kovskii and co-workers claim to have

observed, in addition to an intravalley series, extra peaks occurring at fields given by equations (5.3) and (5.4). One of the important features of the results described in this chapter is that all the observed extrema can be fitted accurately by an interpretation involving intravalley scattering processes alone.

5.2 The Experimental Data

The germanium crystals used in the experiments were of very high purity except for some samples with an impurity concentration of about 10^{15} cm^{-3} which were studied in an attempt to repeat the experiments of Sokolov and Tsidil'kovskii. The highest purity sample (1) was intrinsic at temperatures above about 220K and had $N_D - N_A = 2 \times 10^{12}$ cm^{-3}. It was cut in the form of a long rectangular bar in which the current carrying axis was parallel to the $(\bar{1}10)$ crystal axis. The magnetophonon peaks were studied for different orientations of $\underline{B}$ by mounting the sample in the transverse orientation, $\underline{B} \perp \underline{j} \parallel (\bar{1}10)$, and rotating it about the current direction relative to the vertical magnetic field. A set of traces of $-\partial^2 R/\partial B^2$ versus magnetic field for different orientations of $\underline{B}$ is shown in figure 5.2 (i).

At an arbitrary direction of magnetic field the oscillatory terms are complex and difficult to analyse completely because of the strong interference and beating between magnetophonon series arising from the three possible orientation of $\underline{B}$ relative to the conduction band ellipsoids. However, with $\underline{B}$ along the (001) direction and also along the (110) direction the experimental recordings are much simpler. In the (001) direction, where all the conduction band valleys are equivalent, the observed peaks can be accounted for by a single series corresponding to a fundamental field of 423 kG. In the (110) direction two well separated series which have fundamental fields of 1.175 Megagauss and 338 kG are observed. Along the other directions the peaks are more complex but in all cases it is possible to distinguish magnetophonon series, characterised by their $^1/B$ periodicity, particularly when the fundamental fields of the different components are well separated. Thus for curve d in figure 5.2 at fields below 50 kG, a series with a fundamental field of 528 kG is dominant whereas at higher fields a series, marked by arrows, with a fundamental of 1.04

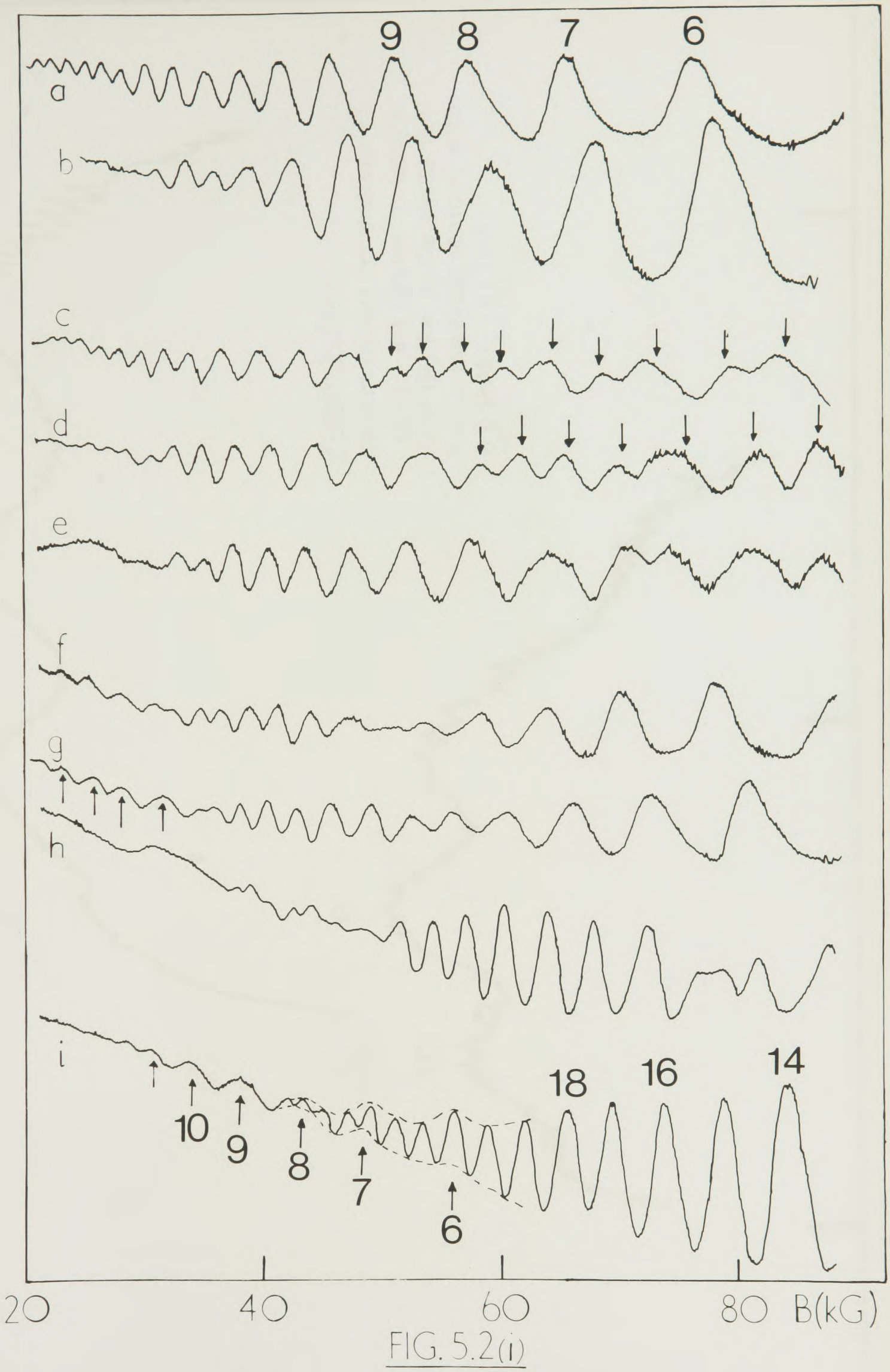


FIG. 5.2(i)

Experimental recordings in n-Ge at 120K for following orientations of B in transverse $(\bar{1}10)$ plane:- (a) (001); (b) (001) + 14°; (c) (001) + 26°; (d) (001) + 30°; (e) (001) + 38°; (f) (001) + 54°; (g) (111); (h) (001) + 80°; (i) (110), $j \parallel (\bar{1}10)$.

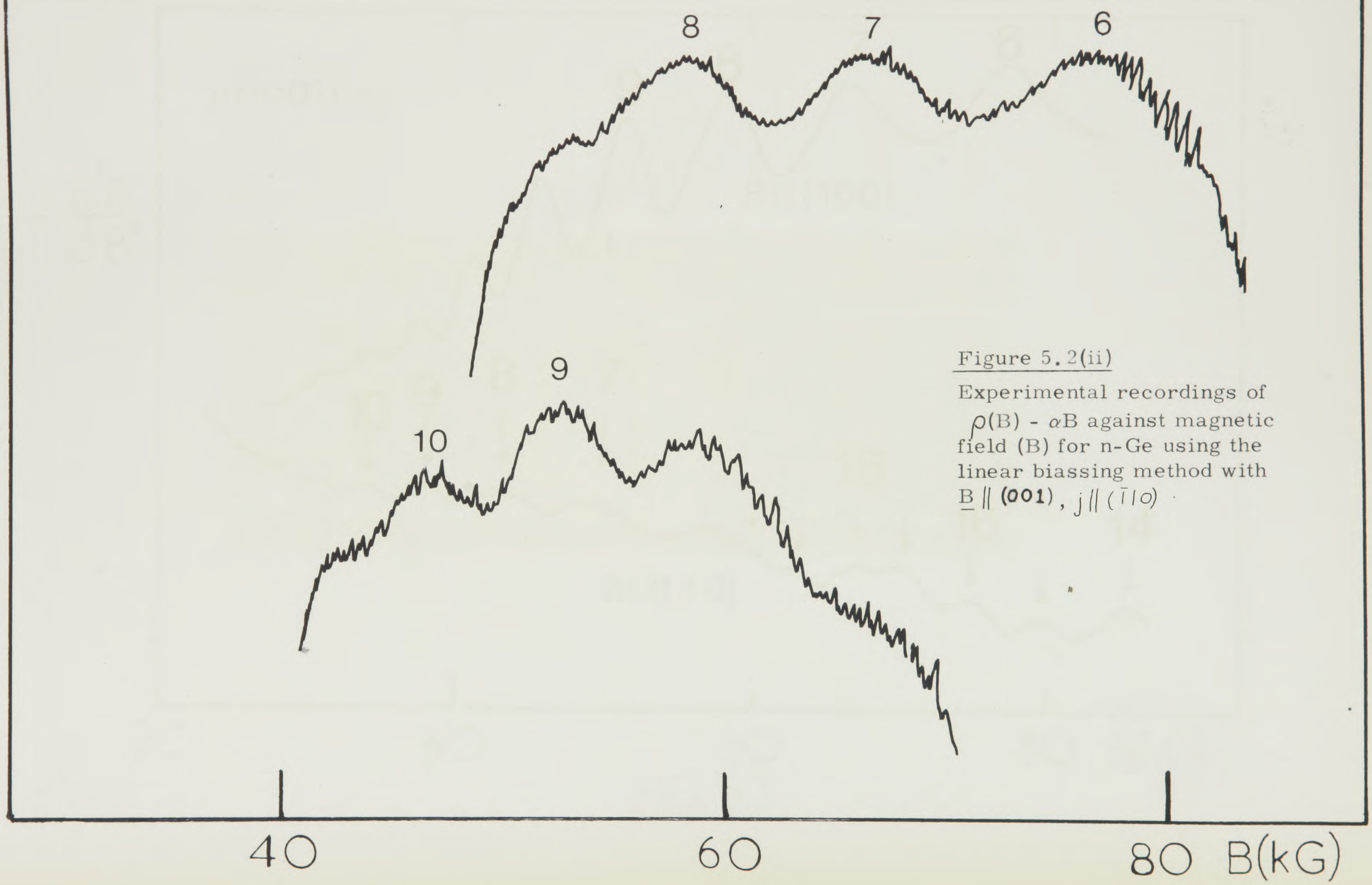


Figure 5.2(ii)

Experimental recordings of $\rho(B) - \alpha B$ against magnetic field (B) for n-Ge using the linear biassing method with $\underline{B} \parallel (001)$, $j \parallel (\bar{1}10)$.

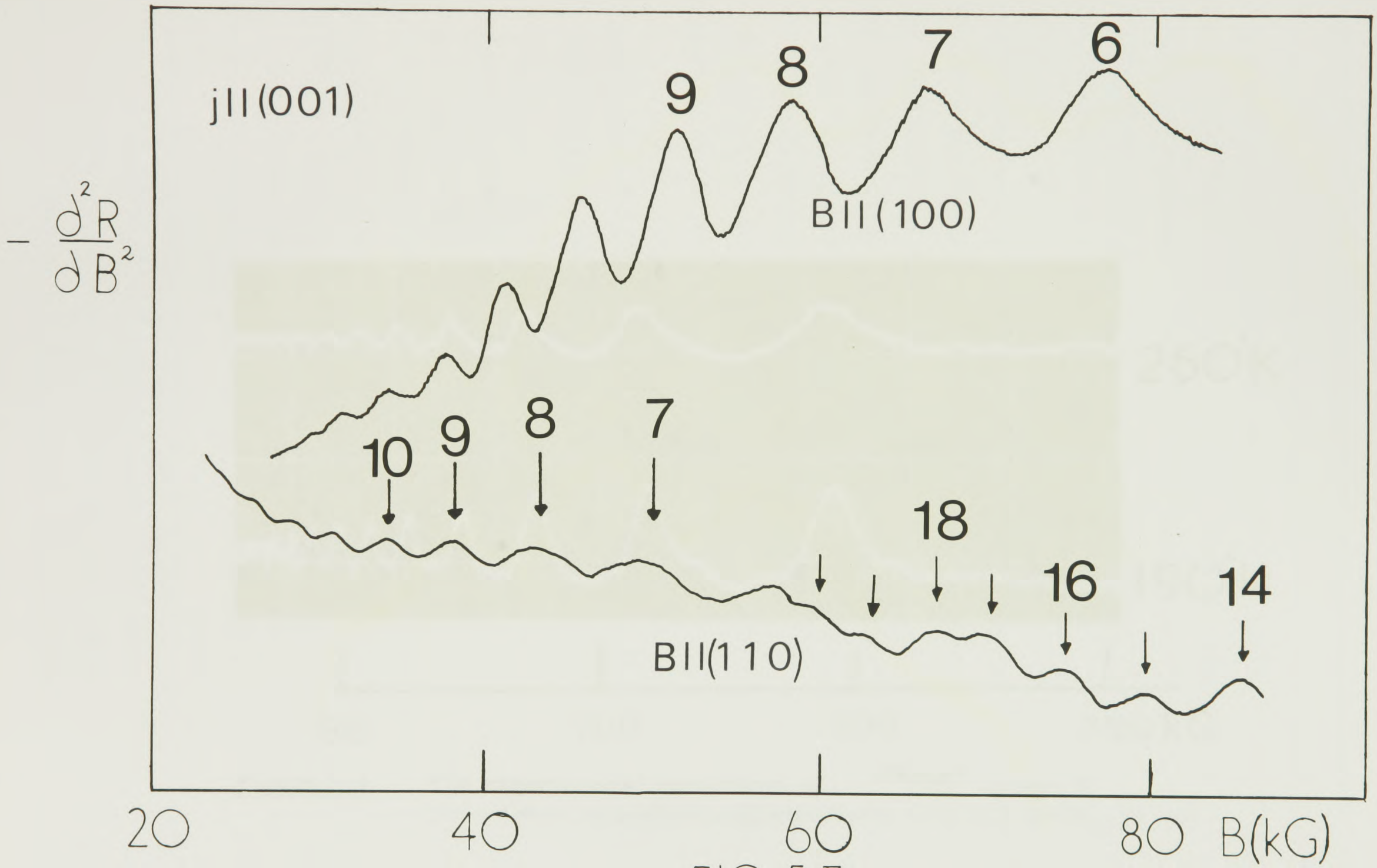

jII(001)
9
8
7
6
BII(100)
10
9
8
7
18
16
14
BII(110)
$-\frac{\partial^2 R}{\partial B^2}$
20
40
60
80
B(kG)

FIG. 5.3

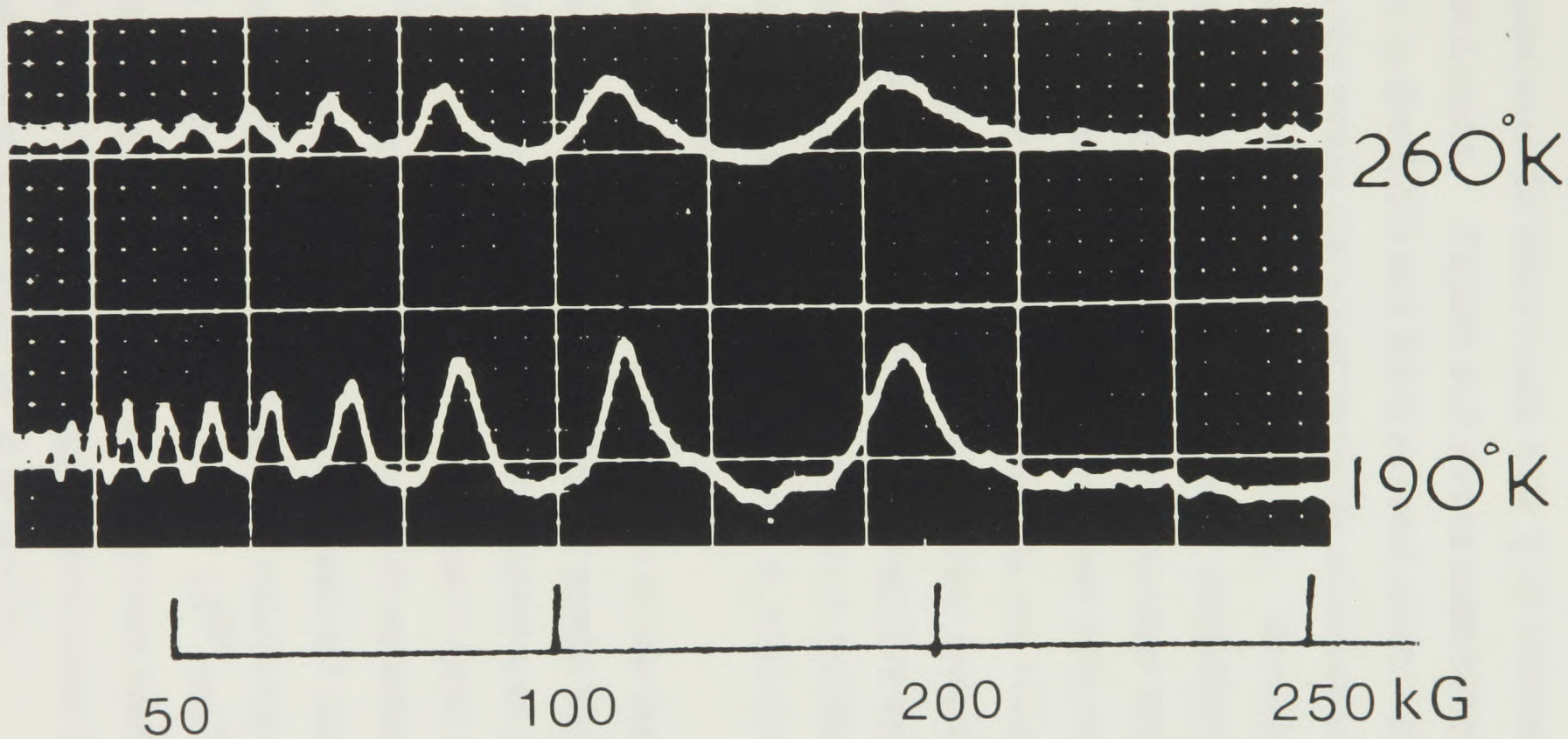


Figure 5.4 The experimental recordings of $-\partial^2 R/\partial B^2$ against B for n-Ge using pulsed magnetic fields with $\underline{B} \parallel (001)$, $j \parallel (T10)$.

Megagauss is strongly superimposed on it.

In order to investigate the magnetophonon peaks for a different current orientation, a second high purity sample (2), in which $N_D - N_A = 1 \times 10^{13}$ cm^{-3}, was cut with the current direction parallel to the (001) crystal axis and measurements were made with $\underline{B}$ at different orientations in the transverse (001) plane. Figure 5.3 shows experimental recordings taken with $\underline{B}$ parallel to the (100) and (110) crystal axes. The fundamental fields obtained from the peaks observed in these orientations agree with the corresponding values in sample 1 to within 1%. However, the amplitude of the peaks found in the less pure sample 2 were significantly weaker than those found in sample 1, being a factor of three smaller for $\underline{B} \parallel (100)$ at the same temperature. This result is in agreement with observations in InP (Chapter III of this thesis) and GaAs (Stradling and Wood, 1968a) that the amplitude of the peaks decreases with increasing ionised impurity content. A more interesting feature is that the relative amplitudes of the light and heavy electron series for $\underline{B} \parallel (110)$ are different for the two current orientations as can be seen by comparing figures 5.2(i) and 5.3(b). This result is discussed at the end of section 5.4.

An attempt was made to observe structure in the longitudinal magnetoresistance of both samples 1 and 2 but no peaks were visible in either sample at fields below 90 kG. The noise level was such that peaks of amplitude $\Delta\rho/\rho_0$ (where ρ_0 is the zero field resistance) greater than 5×10^{-5} would have been detected. In an effort to repeat the experiments of Sokolov and Tsidil'kovskii who observed magnetophonon extrema in the longitudinal magnetoresistance of relatively impure germanium, a third sample in which $N_D - N_A \simeq 10^{15}$ cm^{-3} was prepared with the current direction parallel to $(\bar{1}10)$. No peaks could be observed in either its transverse or longitudinal magnetoresistance at fields below 90 kG over the temperaturerange from 20°K to 150°K.

5.3 The Interpretation of the data and the determination of effective mass

In order to derive precise values of the electronic effective mass by means of the magnetophonon effect, the optic phonon frequency must be known accurately over the temperature range of interest. The most

accurate value for the optic phonon modes in germanium close to the centre of the Brillouin zone has recently been obtained by Ray et al. (1971) from Raman scattering experiments between 2K and 770K and it is this value which has been used to deduce the effective masses quoted in this and the next chapter. The phonon frequencies obtained by Ray and co-workers are about ½% higher than those used to calculate the effective masses in the original publication of the magnetophonon effect in n- and p-type germanium (Eaves et al. 1970). This earlier estimate of the optical phonon frequency was based on Raman data at 300°K (Parker et al. 1967) and neutron scattering experiments (Brockhouse and Dasannacharya, 1963) which indicated a decrease in the phonon frequency of 4½% on raising the temperature from 100K to 700K.

Figure 5.5 shows the effective mass deduced from the magnetophonon peak positions for values of θ (the angle between $\underline{B}$ and (001)) from 0° to 90°. In the (001) direction the single series of peaks corresponds to an effective mass of 0.138 m_0. As θ is increased from zero, there are three different cyclotron masses lying on the curves α, β and γ in figure 5.5. Although over a large range of values of θ, a series of peaks can be found corresponding to each of the three effective masses, the dominant series is that giving an effective mass lying on curve α. The probable cause of this is that the cyclotron masses on curve α correspond to two equivalent ellipsoids whereas the β and γ mass values correspond to one ellipsoid each. For angles of θ up to about 15° (see fig. 5.2a and b) the traces consist of a well defined series of peaks with a gradually increasing effective mass which become progressively distorted by the presence of higher and lower effective mass series. For larger angles, $20° \lesssim \theta \lesssim 40°$, the three mass values are well separated and a series of peaks marked by ↓ in fig. 5.2 are strongly superposed on the α peaks at fields above 50 kG. The data becomes more difficult to interpret when B is close to the (111) direction. Unfortunately, it was impossible to orient $\underline{B}$ sufficiently accurately along the (111) direction and obtain a trace in which only two magnetophonon series appeared. A misorientation of only 1° from the (111) direction causes the effective masses on the α and γ curves to differ by 0.01 m_0 and leads

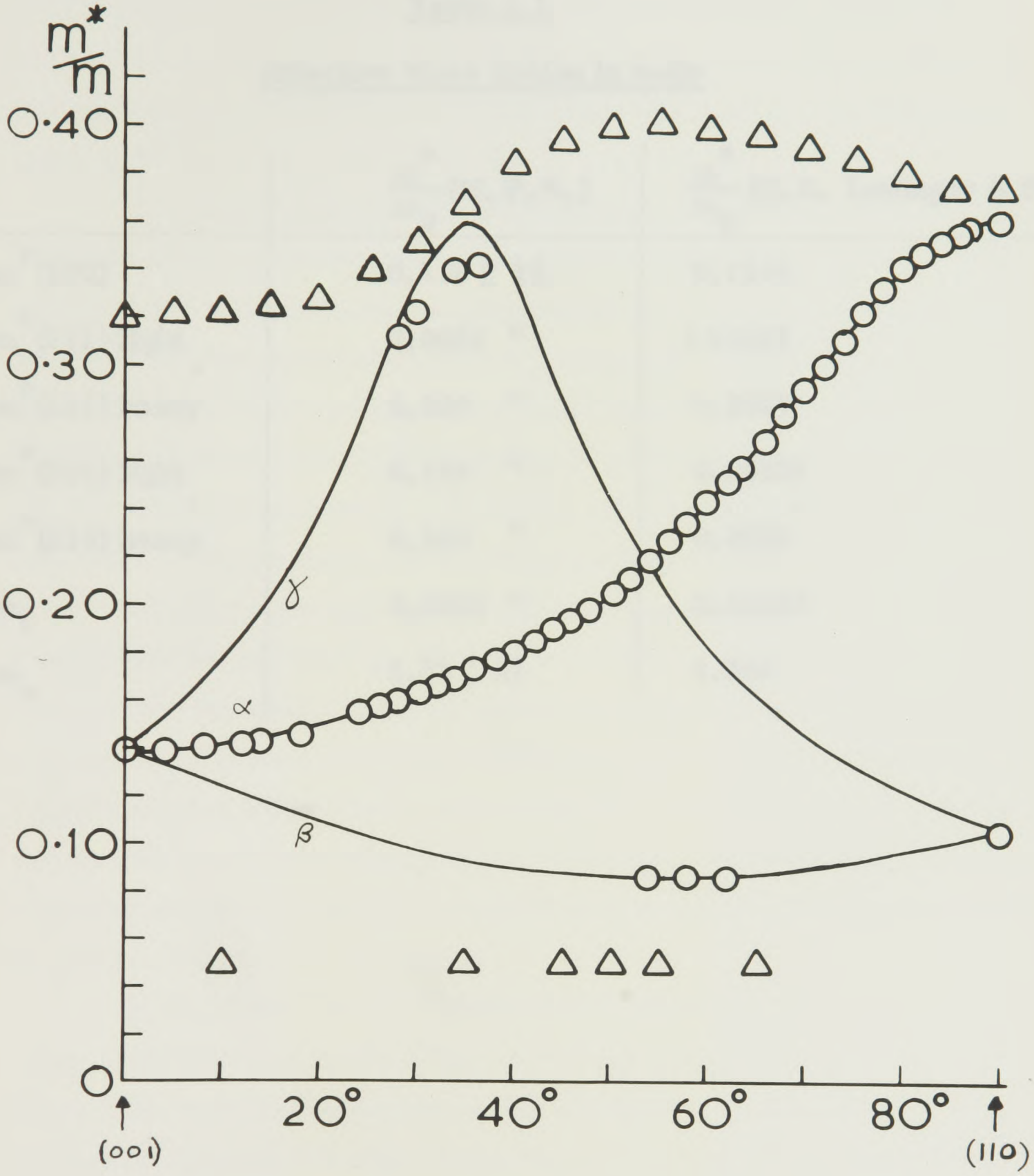


Figure 5.5 The variation of the electron (o) and hole (△) effective masses deduced from equation 5.1 with angle between magnetic field and the (001) direction. The solid curves show theoretical electron mass assuming $m_l = 1.51$ and $m_t = 0.086$.

Table 5.1

Effective Mass Ratios in n-Ge

	$\frac{m^*}{m_0}$ (M.P.R.)	$\frac{m^*}{m_0}$ (C.R. Levinger & Frankl, 1961)
$m^*(100)$	0.138 ± 1%	0.1346
$m^*(111)$ light	0.0858 "	0.08152
$m^*(111)$ heavy	0.220 "	0.2057
$m^*(110)$ light	0.105 "	0.09875
$m^*(110)$ heavy	0.360 "	0.3598
m_t	0.0858 "	0.08152
m_e	1.51 ± 3%	1.588

to interference between the two magnetophonon series. In trace g of figure 5.2i destructive interference occurs at a field of about 50 kG indicating a misalignment from (111) of just under 1°. As θ is increased further, the interference effects continue until $\underline{B}$ becomes parallel to (110) where the two well separated series give effective masses of 0.360 m_0 and 0.105 m_0.

The magnetophonon effective masses are compared with those obtained from cyclotron resonance experiments in Table 5.1. Also shown in the table are the components of the effective mass tensor which have been calculated from the observed values of the light electron mass for B // (111) and the heavy mass for B // (110). Such an assignment of m_l and m_t in equation (5.1) yields effective masses which agree with the observed masses at the other orientation of $\underline{B}$ to within about 1%. The increase in the value deduced for m_t over that obtained from cyclotron resonance is due to non-parabolicity of the conduction band which should have an appreciable effect at the energy of an optical phonon into the band. The 5% increase of mass for this amount of energy into the band is in very good agreement with that obtained by Aggarwal et al (1967) from magneto-optical experiments. Although the error involved in estimating m_e is about 3%, the value deduced from magnetophonon resonance is significantly smaller than that obtained from cyclotron resonance experiments.

It was found that the peaks in the magnetophonon structure in n-type germanium had no observable temperature dependence in the range from 77K to 250K despite the relatively large non-parabolicity of the conduction band ellipsoids. This result is rather surprising in view of the considerable changes in peak position with temperature which have been observed in n-type InP and other III-V compounds. It appears to arise from the compensating effects as the temperature is increased of the decrease in frequency of the optical phonon and the increase of thermal excitation into the non-parabolic band. Thus as the temperature is increased from 77K to 250K, the phonon frequency should decrease by about 1½% and the effect of band non-parabolicity should increase the magnetic field positions of the peaks by about 2%. Taking both these

factors into account, it therefore appears that the band edge effective mass changes by less than 1% over the temperature range for which the peaks are visible. This result is supported by Aggarwal (1972) in some unpublished work which has extended his magneto-piezotransmission experiments up to room temperature.

For both samples 1 and 2 over the temperature range from 60°K to 250°K for which the peaks are visible, it is possible to assign the magnetophonon series to intra-valley scattering processes with a phonon frequency which corresponds to that at the zone centre. No peaks could be identified as arising from intervalley scattering and such processes are estimated to be at least an order of magnitude weaker than intravalley transitions. Although this result conflicts with the magnetophonon data of Tsidil'kovskii and co-workers it is in agreement with the analysis of the transport properties of germanium carried out by Paige (1964) and with the acousto-electric experiments of Weinreich et al. (1959) who estimate the ratio of inter-valley to intra-valley to be about 0.02.

It is difficult to reconcile the results presented in this chapter with those obtained by Tsidil'kovskii and co-workers. In the longitudinal orientation, Sokolov and Tsidil'kovskii (1967) observed strong peaks with an amplitude of several percent at a temperature of 20°K in samples with $N_D - N_A$ equal to 1.8×10^{15} cm^{-3} and 2×10^{16} cm^{-3}. No peaks could be observed in positions corresponding to an intravalley series and the data were interpreted entirely in terms of intervalley transitions between both equivalent and non-equivalent valleys. However, some peaks corresponding to certain harmonics of both series did not appear in the magnetoresistance curves. In the transverse orientation, Gluzman and Tsidil'kovskii using double differentiation techniques observed weak magnetophonon structure for $\underline{B} \parallel$ (100) and (110) over the temperature range from 40K to 340K. The electron concentration at room temperature for this sample was 8.6×10^{14} cm^{-3}. In contrast to the relatively low temperatures employed in the longitudinal experiments, Gluzman and Tsidil'kovskii found that the optimum temperature for observing the transverse peaks was 120K. The extrema in the transverse orientation were interpreted in terms of inter- and intravalley series although neither provided an exact fit to the

experimentally observed peak positions and again certain harmonics did not appear in the magnetoresistance.

One of the strangest features of the Russian data is the large amplitude of the longitudinal peaks since in other materials (Stradling and Wood, 1968; Eaves et al 1970) such peaks are an order of magnitude weaker than those observed in the transverse orientation. In addition, the temperature at which the peaks were observed is considerably lower than that at which the cold electron magnetophonon structure normally disappears due to the freeze-out of the optic phonon mode. Attempts have been made at Oxford to observe magnetophonon structure in the longitudinal magnetoresistance of three samples with $N_D-N_A = 2 \times 10^{12}$, 1×10^{13} and 2×10^{15} cm^{-3} but no peaks can be seen at fields up to 90 kG. No explanation can at present be given for the considerable discrepancies between the two sets of data but it is possible that the presence of certain impurities are required to induce the intervalley transitions observed by the Russians. This suggestion gains some support from the fact that more peaks appear in the relatively impure Russian sample with $N_D - N_A = 2 \times 10^{16}$ cm^{-3} than in the sample with $N_D-N_A = 1.8 \times 10^{15}$ cm^{-3}.

5.4 The line-shape and amplitude of the magnetophonon peaks

An interesting feature of the peaks, which is particularly evident in the (001) orientation, is the sharpening of the maxima at magnetic fields above about 50kG. This can be seen in trace a of figure 5.2 and is even more evident in fig. 5.4 which was obtained by using pulsed fields. The sharpening of the high field maxima has previously been observed by Stradling and Wood (1970) in high purity n-type InSb and GaAs, but in these materials the effect is pronounced only for extrema with N = 4 or less. The high field peaks in Figure 2(a) also show an asymmetric broadening on the high magnetic field side which is due to the non-parabolicity of the conduction band. Because of this non-parabolicity the Landau level transitions, M = O to M = N, M = 1 to M = N + 1, etc, which when weighted by the Boltzmann factor make up the N^{th} magnetophonon peak, occur at progressively increasing fields. When added together such a series of transitions leads to an asymmetric line-shape similar to that

observed in the high field peaks along the (001) direction.

At lower magnetic fields the magnetophonon oscillations can be fitted by the formula

$$\Delta\rho \sim \exp\left(-\gamma\frac{\omega_e}{\omega_c}\right)\cos\left(\frac{2\pi\omega_e}{\omega_c}\right) \qquad (5.5)$$

for $\underline{B}$ along the (001) direction and also for B // (110) where no beating effects occur. At the optimum temperature in the purest sample the value of γ was 0.49 for $\underline{B}$ // (001) and 0.40 for the heavy electron series with $\underline{B}$ // (110). Such a low value of γ and the consequent large number of peaks observed is due to the very high purity of the material used in the experiments as Stradling and Wood (1968a) have shown that γ increases with increasing ionised impurity concentration. In addition, the non-polar nature of germanium may be a contributing factor to the relatively small damping of the series following the prediction by Dworin (1965) that the number of peaks observed should decrease with increasing values of the Frohlich coupling constant (α). This assertion is supported by comparing the highest observable N-values in Ge with those found in other materials. Thus, at the present time, in n-type germanium, the highest observable magnetophonon harmonic is N = 23 for B // (001) and N = 27 for B // (110). As will be discussed in the next chapter, extensive magnetophonon structure is also observable in p-type Ge where, for $\underline{B}$ // (110), peaks up to N = 40 have been observed in the heavy hole series. These values compare with the highest observable harmonics of N = 15 in GaAs (α = 0.06), N = 11 in InP (α = 0.12), N = 8 in CdTe (α = 0.4) and N = 6 in CdSe (α = 0.45), whereas in the strongly polar compound AgBr (α = 2), experiments to detect magnetophonon structure have proved unsuccessful (Jenkin, 1972).

The magnetophonon peaks were observable over the temperature range from 60K to 250K in the highest purity specimen, sample 1. Figure 5.6 shows the variation with temperature of the 7^{th} harmonic for $\underline{B}$ // (001) and the 14^{th} harmonic of the heavy electron series for $\underline{B}$ // (110). The amplitudes are defined as $\Delta\rho/\rho_0$ where ρ_0 is

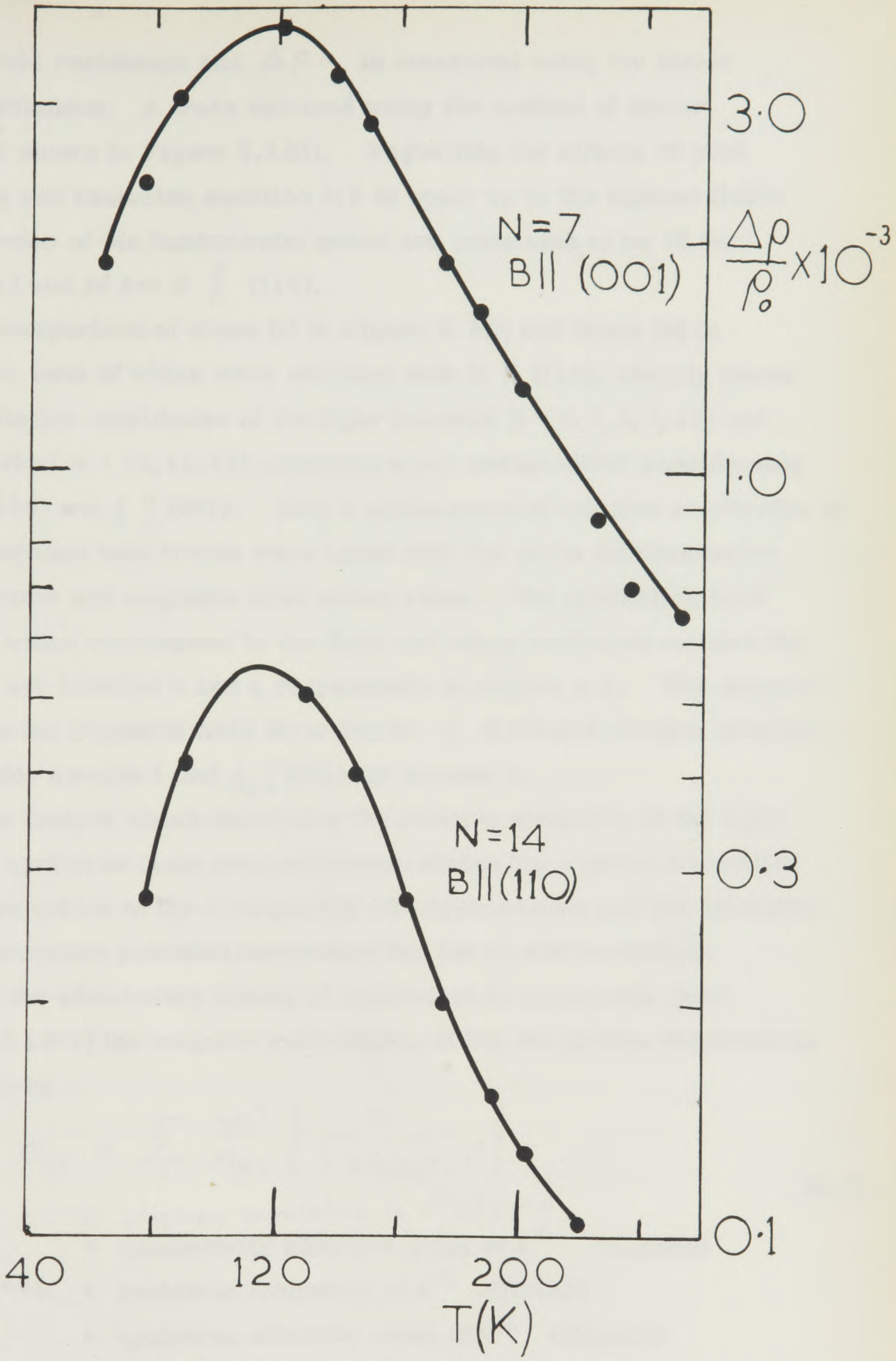


Figure 5.6 The temperature dependence of the magneto-phonon amplitudes in n-Ge for the single series with B || (001) and the heavy electron series with B || (110). $\Delta\rho$ is measured from the linear biassing traces, ρ_o is the zero field resistance.

the zero field resistance and $\Delta\rho$ is measured using the linear biassing technique. A trace obtained using the method of linear biassing is shown in Figure 5.2(ii). Neglecting the effects of peak sharpening and assuming equation 5.5 to apply up to the highest fields the amplitudes of the fundamental peaks are estimated to be 7% for $B \parallel (001)$ and 8% for $B \parallel (110)$.

A comparison of trace (i) in Figure 5.2(i) and trace (b) in Figure 5.3, both of which were obtained with $B \parallel (110)$, clearly shows that the relative amplitudes of the light (marked N = 6, 7, 8, 9, 10) and heavy (marked N = 14, 16, 18) cyclotron mass series differ considerably for $\underline{J} \parallel (\bar{1}10)$ and $\underline{J} \parallel (001)$. Such a comparison of relative amplitudes is justified because both traces were taken with the same differentiation time constants and magnetic field sweep rates. The conduction band ellipsoids which correspond to the light and heavy cyclotron masses for $B \parallel (110)$ are labelled b and a respectively in Figure 5.1. The diagram also shows the magnetic field direction $B \parallel (110)$ and current direction $\underline{J}_1 \parallel (\bar{1}10)$ for sample 1 and $\underline{J}_2 \parallel (001)$ for sample 2.

The factors which determine the relative strengths of the light and heavy cyclotron mass magnetophonon series for a given orientation of $\underline{J}$ are the values of the conductivity effective masses and the strengths of the deformation potential interaction for the a- and b- valleys.

By the elementary theory of conduction in a magnetic field (c.f. Kittel 1963) the magneto conductivity of the conduction electrons in Ge is given by

$$\sigma_{xx} = \sum_i \frac{n_i e^2}{m_{\sigma i}} \left[\frac{\tau_i}{1 + (\omega_{ci}\tau_i)^2} \right] \qquad (5.6)$$

where n_i = electron population in i^{th} ellipsoid
$m_{\sigma i}$ = conductivity effective mass of i^{th} ellipsoid
$\omega_{ci} = eB/m_{ci}$ = cyclotron frequency of i^{th} ellipsoid
m_{ci} = cyclotron effective mass of i^{th} ellipsoid
τ_i = relaxation time of i^{th} ellipsoid

At high magnetic fields $\omega_c \tau \gg 1$ and

$$\sigma_{xx} \simeq \sum_i \frac{n_i e^2}{m_{\sigma i}} \frac{1}{\omega_{ci}^2} \left(\frac{1}{\tau_i}\right) = \frac{1}{B^2} \sum_i \left(\frac{m_c^2 n}{m_\sigma \tau}\right)_i \qquad (5.7)$$

For B || (110) there are two types of ellipsoid corresponding to light electron (b-valleys) and heavy electron (a-valleys) effective masses so that

$$\sigma_{xx} \simeq \frac{1}{B^2}\left[\frac{m_{ca}^2}{m_{\sigma a}}\left(\frac{n}{\tau}\right)_a + \frac{m_{cb}^2}{m_{\sigma a}}\left(\frac{n}{\tau}\right)_b\right] \qquad (5.8)$$

With $\underline{J}_2$ || (001), $m_{\sigma a} = m_{\sigma b}$

$$\therefore \quad \sigma_{xx}(J_2) \simeq \frac{1}{B^2 m_\sigma}\left[m_{ca}^2\left(\frac{n}{\tau}\right)_a + m_{cb}^2\left(\frac{n}{\tau}\right)_b\right]$$

Since $m_{ca}/m_0 = 0.360$ and $m_{cb}/m_0 = 0.105$

$$\sigma_{xx}(J_2) \sim \left[12\left(\frac{n}{\tau}\right)_a + \left(\frac{n}{\tau}\right)_b\right] \qquad (5.9)$$

$n_a \neq n_b$ due to the quantum transfer effect (Love and Wei, 1961).

With $\underline{J}_1$ || ($\bar{1}10$), $m_{\sigma a}/m_0 = 0.23$, $m_{\sigma b}/m_0 = 0.086$

$$\sigma_{xx}(J_1) \sim \left[4.5\left(\frac{n}{\tau}\right)_a + \left(\frac{n}{\tau}\right)_b\right] \qquad (5.10)$$

Comparison of equations (5.9) and (5.10) shows that if the scattering rates in the a- and b-valleys were equal then the contribution to the magnetoconductivity of the heavy cyclotron electrons (a) relative to that of the light cyclotron electrons (b) would be greater for the current direction $\underline{J}_2$ than for $\underline{J}_1$. The relatively greater amplitude of the heavy cyclotron mass series in the $\underline{J}_1$ direction indicates that the scattering rate for the a- and b-valleys is anisotropic for different orientations of $\underline{J}$ relative to the crystalline axes. An investigation of the effect of anisotropic deformation potential scattering on the light and heavy electron magnetophonon series would therefore serve as a test of recent theoretical treatments on non polar phonon scattering in multivalley semiconductors (Lawaetz, 1969).

CHAPTER 6

The Magnetophonon Effect in p-Ge and p-GaAs

6.1 Introduction

Studies of the magnetophonon effect in n-type III-V and II-VI semiconductors have demonstrated that by applying a correction for band non-parabolicity, an accurate estimate can be made of the conduction band effective mass. Such a precise interpretation of the magnetophonon data is possible because the Landau levels for a spherical conduction band are given accurately by equation (1.2) except for a small correction due to band non-parabolicity. The equation, however, does not apply to the hole states in unstrained cubic crystals where the light and heavy hole valence bands are degenerate at the centre of the Brillouin zone. The effective mass theory of Luttinger and Kohn (1955, 1956) showed that as a result of this degeneracy, the energy separation of the Landau levels at the bottom of each valence band is markedly non-uniform. In the cyclotron resonance experiments on p-type Si and Ge (Fletcher et al., 1955; Hensel, 1962) which followed this theoretical work, many of the resonance lines appeared to result from transitions between the anomalously spaced low energy Landau levels but a complete interpretation of the data was not possible until the description of the hole states was extended to include the effects of finite k_B. The first calculations of the behaviour of the Landau levels in the valence bands of Ge and Si (Wallis and Bowlden, 1960; Evtuhov, 1962; Okazaki, 1962) for values of $k_B \neq 0$ showed that one of the heavy hole Landau level series was considerably distorted from the simple parabolic variation given by equation 1.2, with the appearance of energy minima at finite k_B and local maxima in energy at $k_B = 0$. The profound influence of such effects on the cyclotron resonance spectra of Ge was demonstrated by Hensel and Suzuki (1970) who showed that most of the lines which they observed originated from transitions with $k_B \neq 0$.

The experiments described in this chapter show that the irregular energy separation and k_B-dependence of the Landau levels associated with degenerate valence bands is also reflected in the complex nature of the magnetophonon resonance spectra of p-type Ge and GaAs. In p-type Ge, the anisotropy of the hole effective masses has been investigated for a range of orientations of the magnetic field in the (110) crystal plane and

the variation of amplitude and position of the magnetophonon peaks has been studied over the temperature range from 60 K to 240 K. However, the most interesting feature arising out of the data is the complex splitting of the heavy hole peaks at magnetic fields above about 50 kG. Such splitting has not been observed in the magnetophonon structure of any n-type semiconductors and, as will be discussed in section 3 of this chapter, its likely origin is the complex nature of the hole Landau levels. Although the magnetophonon structure in p-GaAs is much weaker than that observed in germanium, by using fields up to 350 kG it is possible to obtain a series of six light hole maxima from which an effective mass is obtained in good agreement with cyclotron resonance data. At fields above about 200 kG additional peaks appear in the magnetoresistance of p-GaAs which arise from transitions in the heavy hole valence band.

6.2 The Experimental Data in p-Ge

The germanium samples used for most of the experiments were cut from a slice of very high purity material with $N_A - N_D = 3 \times 10^{12} cm^{-3}$. The first observation of magnetophonon structure was made at Oxford using fields of up to 90 kG on a sample from the very high purity slice in which the current direction was parallel to the $(\bar{1}10)$ crystal axis. Typical experimental recordings of $-\frac{\partial^2 R}{\partial B^2}$ obtained in the transverse orientation at a temperature of about 120 K for various orientations of $\underline{B}$ with respect to the crystal axes are shown in Figure 6.1. At fields above about 35 kG magnetophonon peaks due to transitions within the heavy hole valence band are observed and grow rapidly with increasing magnetic field. The lowest field peak which can be observed corresponds to an N-value of about 40. At fields below about 40 kG a much weaker series of peaks appears which can be attributed to transitions within the light hole valence band. These peaks have harmonic number N varying from 6 to 11, the higher field maxima being obscured by the stronger heavy hole series although, as can be seen from curve e of Figure 6.1, the N = 3, 4 and 5 maxima are observable as the envelope of the heavy hole oscillations.

In order to study the anisotropy of the transverse magnetophonon

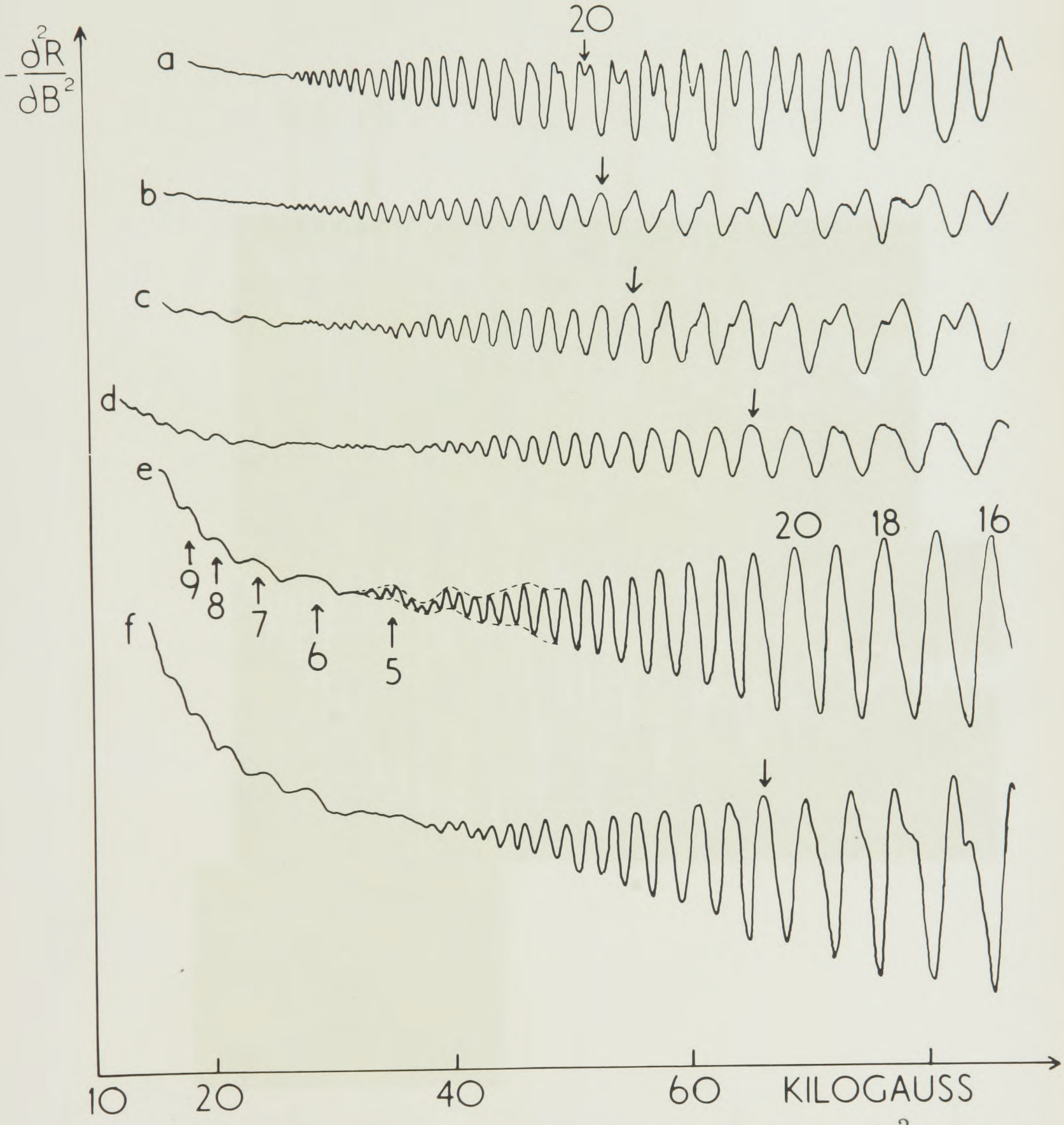


Figure 6.1 The experimental recordings in p-Ge of $-\frac{\partial^2 R}{\partial B^2}$ versus B at the following orientations of B in the transverse $(\bar{1}10)$ plane:- (a) (001) (b) (001) + 15^o (c) (001) + 25^o (d) (001) + 40^o (e) (111) (f) (001) + 75^o. The downward arrows mark the position of the N=20 peak for the heavy hole series. The upward arrows mark the positions of 5 light hole peaks for B || (111). The sample temperature is 120 K, $j \parallel (\bar{1}10)$.

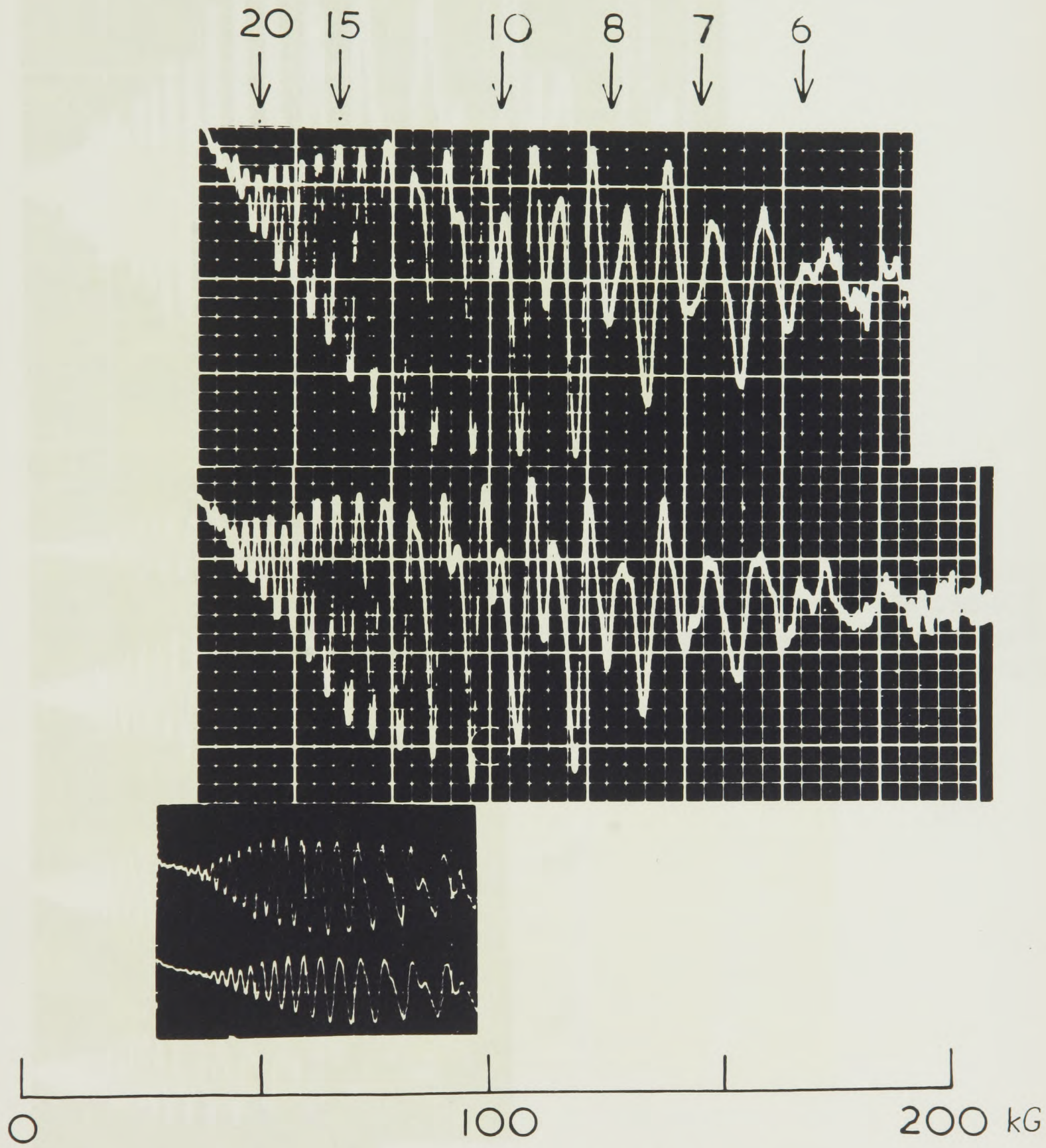


Figure 6.2 The experimental recordings in p-Ge with $\underline{B} \parallel (001)$ using pulsed magnetic fields at a sample temperature of 100K, $j \parallel (\bar{1}10)$.

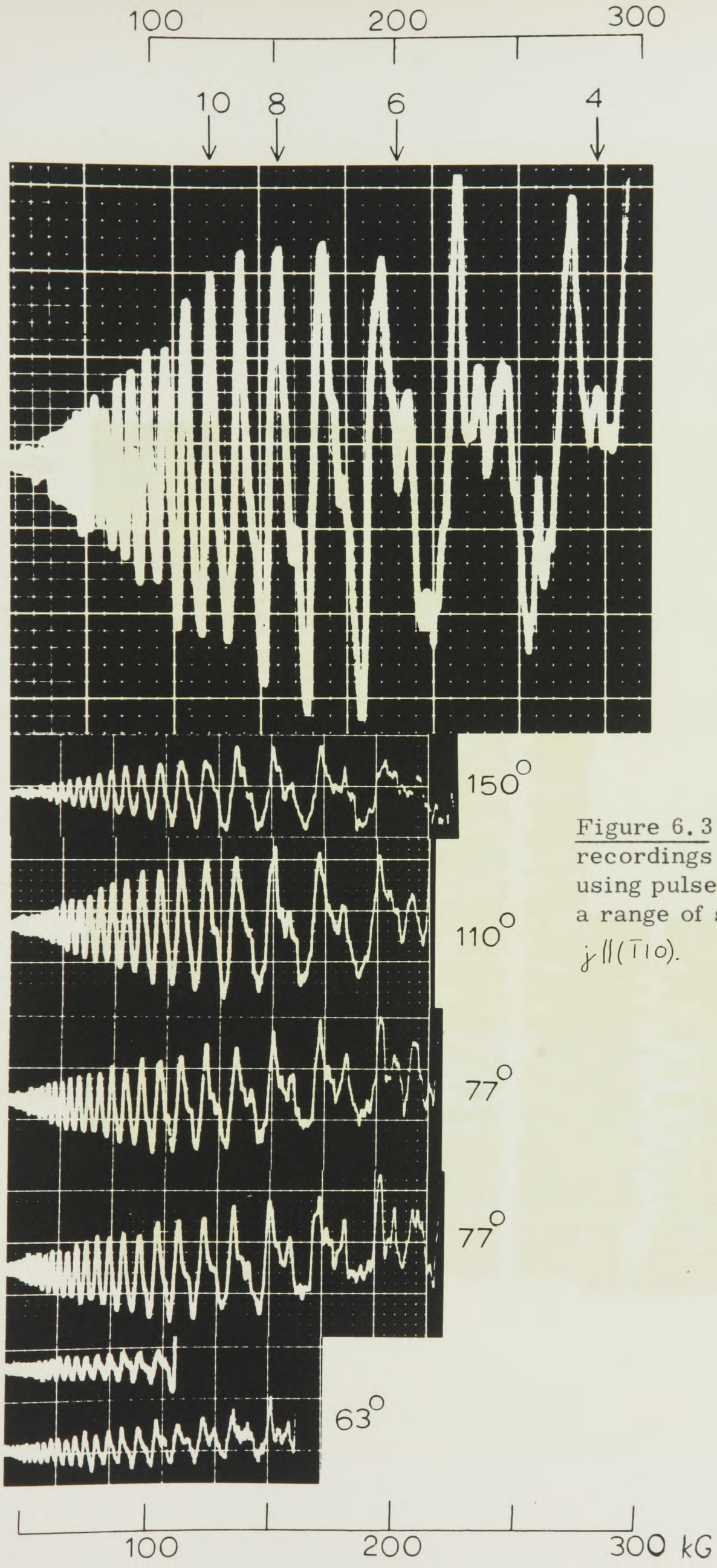


Figure 6.3 The experimental recordings in p-Ge with B || (111) using pulsed magnetic fields for a range of sample temperatures, $j \parallel (\bar{1}10)$.

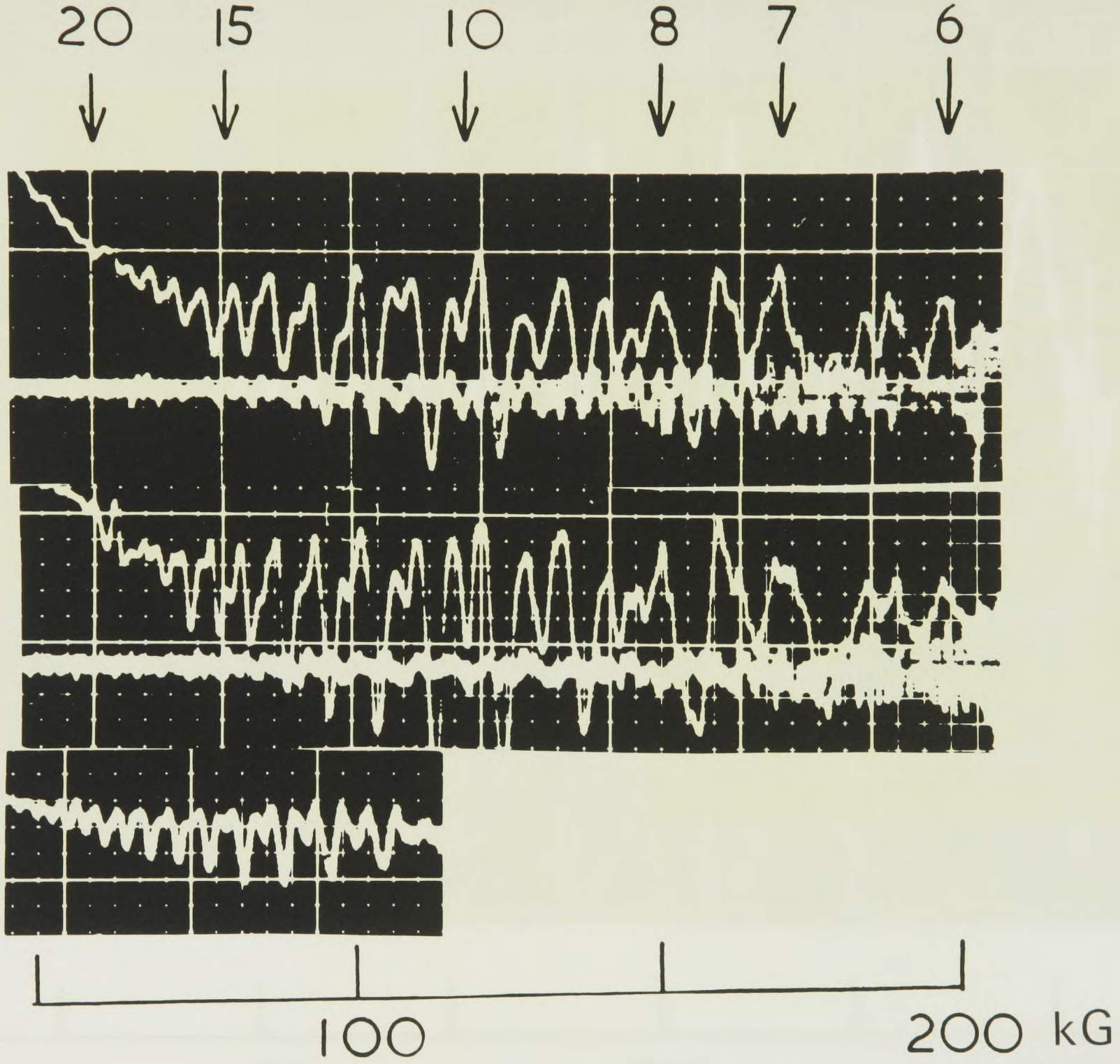


Figure 6.4 The experimental recordings in p-Ge with B ∥ (110) using pulsed magnetic fields at a sample temperature of 100 K, $j \parallel (\bar{1}10)$

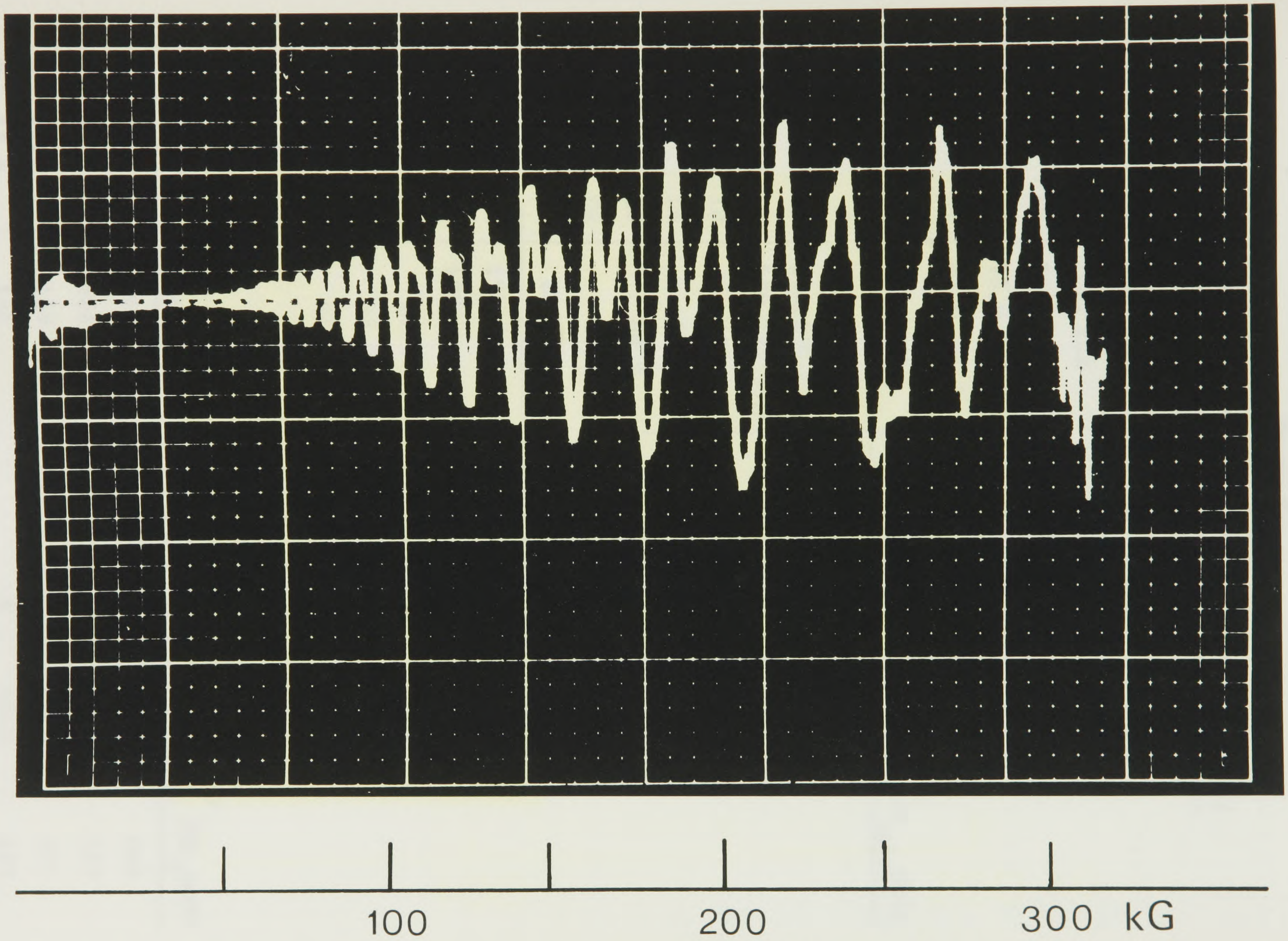


Figure 6.5 The experimental recordings in p-Ge with B ∥ (110) for a sample with $N_A - N_D = 2 \times 10^{13}$ cm^{-3} at a temperature of 100 K, $j \parallel (\bar{1}10)$.

Table 6.1: The peak positions in p-Ge for the three main symmetry directions

Heavy Holes

B // (001)	N	B_N(kG)	NB_N(MG)	ΔB(kG)
	4	257, 224	1.03, 0.90	33
	7	150, 139	1.05, 0.97	11
	8	131, 122	1.05, 0.98	9
	10	106, 101	1.06, 1.01	5
	14	75.0, 72.8	1.05, 1.01	2.2
	20	52.0, 51.1	1.04, 1.02	0.9

B // (111)	N	B_N(kG)	NB_N(MG)	$\Delta B = B_{max} - B_{min}$(kG)
	4	299, 285, 272	1.20, 1.14, 1.09	27
	5	244, 235, 227	1.22, 1.17, 1.14	17
	7	180, 174, 170	1.26, 1.22, 1.19	10
	10	123	1.23	-
	14	91.1	1.28	-
	20	65.2	1.30	-
	28	47.4	1.32	-

B // (110)	N	B_N(kG)	NB_N(MG)	Δ B
	7	170, 158	1.19, 1.11	12
	10	122, 116	1.22, 1.16	6
	14	88.0	1.24	-
	20	62.2	1.24	-
	24	51.2	1.23	-

Light Holes

B // (001)

N	B_N(kG)	NB_N(kG)
6	27.5	165
7	23.7	164
8	19.9	159
9	17.8	160

B // (111)

N	B_N(kG)	NB_N(kG)
6	26.7	160
7	22.5	157
8	19.6	157
9	17.5	157

peaks, a series of recordings of $-\frac{\partial^2 R}{\partial B^2}$ were obtained at 5° angular intervals for orientations of $\underline{B}$ between the (001) and (110) crystal axes. The heavy hole peaks showed the characteristic anisotropy of the heavy hole band with peaks of the same N-value being about 20% lower in field for B $\|$ (001) than for B $\|$ (111). The light hole peaks were also slightly anisotropic by an amount, about 2% , which was just greater than the error involved in determining the peak positions. The striking feature of the traces in Figure 6.1 is that for most orientations of B, the heavy hole maxima split into two components of approximately equal strength for peaks having $N \lesssim 20$. At fields below 90 kG the splitting was most pronounced with $\underline{B}$ along the (001) direction whereas in an angular range of about 10° on either side of the (111) direction no splitting was observable.

By using the pulsed magnetic fields available at the University of Toulouse, it was found that the splitting developed even more complex structure above 100 kG. Figures 6.2, 6.3 and 6.4 show the experimental recordings of $-\frac{\partial^2 R}{\partial B^2}$ versus B for three samples cut from the very high purity slice with $\underline{B}$ oriented parallel to the (001), (111) and (110) crystal axes respectively. In the (001) direction, the doublet structure is clearly visible for peaks up to N = 4 and, in addition, there appears to be a further weak splitting at high fields as can be seen on the N = 6 peak in Figure 6.2. The higher fields available with the Toulouse pulsed system shows that the splitting also develops along the (111) direction above 100 kG. Although the positions of the peaks for B $\|$ (111) remains unchanged over the temperature range from 60 K to 200 K it appears that the resolution of the structure improves as the temperature is lowered and below 80 K the peaks with $N < 8$ split into a triplet structure which becomes increasingly well resolved at higher magnetic fields. The traces in Figure 6.4 indicate that when B is oriented parallel to the (110) crystal axis the splitting develops in a rather irregular fashion. Thus the N = 6 and N = 8 peaks show a clearly resolved triplet structure whereas the N = 7 and N = 9 peaks appear to be doublets. The field positions of a range of peaks observed in the three main symmetry directions are shown in Table 6.1.

In order to investigate the amplitude and splitting of the magneto-phonon extrema at higher impurity concentrations, some experiments were

Table 6.2: Comparison of effective masses deduced from magneto-phonon and cyclotron resonance

Hole, orientation	m^*/m_0(M.P.R.)	m/m_0(C.R. Levinger & Frankl, 1961)
heavy, B ‖ (001)	0.317	0.2825
" , B ‖ (111)	0.400	0.377
" , B ‖ (110)	0.373	-
light, B ‖ (001)*	0.049	0.04368
" , B ‖ (111)	0.048	0.04187

* This value was actually calculated with B oriented 10° from (001)

The field positions employed in the calculation of the magneto-phonon masses were measured to an accuracy of ±1%.

also performed on a less pure sample in which $N_A - N_D = 2 \times 10^{13}$ cm^{-3}. Measurements were again made for various orientations of $\underline{B}$ in the transverse $(\bar{1}10)$ plane. For a given orientation, the peak positions agreed with those obtained in the very pure sample but the magnetophonon structure was about a factor of 3 weaker in amplitude at the same temperature. Although no splitting could be observed at fields below 90 kG, for any orientation of the magnetic field with respect to the crystal axes, it became well resolved at higher fields as can be seen from the trace in Figure 6.5, taken with B $\|$ (110).

6.3 The Interpretation of the Magnetophonon Data in terms of the Valence Band Structure in Ge.

6.3.1 The Determination of the Hole Effective Masses

The original publication of the magnetophonon effect in p-Ge (Eaves et al. 1970) reported the observation of light and heavy hole peaks at magnetic fields below 90 kG for orientations of $\underline{B}$ in the (110) crystalline plane. Reference to Table 6.1 shows that for the magnetophonon harmonics in this field range, the product NB is constant to within less than 3% for all orientations of magnetic field. The accurate $^1/B$ periodicity justifies the assignment of a magnetophonon effective mass given by the equation

$$m^* = \frac{e\overline{NB}}{\omega_c} \qquad (6.1)$$

The values of m^* of the light and heavy holes which are derived from this equation are given in Table 6.2 for the three main symmetry directions and are plotted for various orientations of B in the (110) crystal plane in Figure 5.5 (see previous chapter). As was discussed in Chapter 5, the values of m^* quoted in this thesis have been deduced on the basis of recent measurements by Ray et al. (1971) who obtained a value of ω_c about $\frac{1}{2}$% higher than that used in the original publication of the magnetophonon effect in Ge.

Since the magnetophonon masses are calculated from peaks in the field range where $\hbar\omega_c/kT \ll 1$ and $\omega_c/\omega_c \ll 1$, they exhibit an anisotropy which agrees with that obtained from cyclotron resonance experiments (Levinger and Frankl, 1961; see Table 6.2) in

which the microwave transitions occur predominantly at high quantum number. The striking difference between the two sets of results is that the magnetophonon mass is considerably greater than that obtained from cyclotron resonance. This deviation mainly arises from the influence of the split-off valence band as the optical phonon energy ($\hbar\omega_\ell \simeq 0.05$ eV) is not negligible compared to the spin-orbit splitting ($\Delta = 0.28$ eV). The proximity of the split-off band introduces a relatively large k^4 term in the hole dispersion curve. Thus the energy of the light holes deduced from $\underline{k}.\underline{p}$ theory is (Johnson, 1967)

$$E_{v\ell} \simeq \frac{\hbar^2 k^2}{2m_\ell}\left(1+\frac{\hbar^2 k^2}{2m_\ell}\left[\frac{1}{2\Delta}+\frac{1}{E_G}\right]\right) \qquad (6.2)$$

where m_ℓ = the band edge effective mass

E_G = the direct energy gap

Δ = the spin-orbit splitting

By using the method described by Stradling and Wood (1968), the non-parabolicity correction to the magnetophonon mass is estimated to be 12% giving a band edge light hole mass of 0.044 for B $\parallel$ (001) with a value 2% lower for B $\parallel$ (111). These estimates are in good agreement with the results of cyclotron resonance experiments. It is likely that the increase in mass observed for the heavy holes compared to the low temperature cyclotron mass also arises from the effect of band non-parabolicity rather than from a change in the band-edge mass with temperature.

As was the case in n-type Ge, no change with temperature could be detected in the positions of the magnetophonon peaks. Any change for the light hole series was less than $\pm 1\%$ in the temperature range from 100 K to 170 K. For the heavy hole peaks the change was less than $\pm 1\%$ between 60 K and 240 K. It is likely that the lack of temperature dependence of the peak positions again arises from the compensating effects of the decrease of the optic phonon energy and the increase in thermal excitation into the non-parabolic band as was discussed in the previous chapter for n-Ge. Taking this into account it appears that the band edge effective mass of both light and heavy holes does not change appreciably over the temperature range studied.

6.3.2 Interpretation of the splitting of the magnetophonon peaks

This section attempts to explain the splitting of the heavy hole magnetophonon harmonics in terms of the detailed structure of the valence band Landau level scheme. The most accurate description at present available of the hole energy levels is that of Hensel and Suzuki (1970) who obtained the five parameters of the Luttinger Hamiltonian (Luttinger and Kohn, 1955, Luttinger, 1956) from a series of cyclotron resonance and combined resonance experiments and then calculated the hole eigenvalues with the inclusion of k_B. The Landau level energies which have been kindly supplied by Hensel are shown in Figure 6.6 for B $\parallel$ (001) and (111).

In his interpretation of the cyclotron resonance spectra, Hensel considered the critical points in the one dimensional joint density of states function $(\partial \mathcal{E}_{nn'}/\partial k_B)^{-1}$ where $\mathcal{E}_{nn'}(k_B)$ is the energy between Landau states n and n' with the same k_B value. For the complex series of levels shown in Figure 6.6, $\mathcal{E}_{nn'}$ varies with k_B producing critical points in the joint density of states when $\partial \mathcal{E}_{nn'}/\partial k_B = 0$, each of which contributes a resonance feature to the spectrum assuming that the transition is allowed and that the states are thermally populated with holes. The application of the joint density of states concept to magnetophonon resonance is greatly complicated by the fact that the transitions between Landau levels can involve phonons with finite wave vector $\underline{q}$ and hence are not necessarily vertical. In such a case the magnetophonon intensity will be represented by a double integral over k_B and q and a resonance will occur whenever the transition energy $\mathcal{E}_{nn'}$ is stationary with respect to both k_B and q, that is when

$$\frac{\partial \mathcal{E}_{nn'}}{\partial k_B} = \frac{\partial \mathcal{E}_{nn'}}{\partial q} = 0$$

In order to analyse the magnetophonon transitions it would be necessary to plot not only $\mathcal{E}_{nn'}$ versus k_B as Hensel has done for cyclotron resonance but extend the plot as a function of $q = \Delta k_B$. In addition, the effects of band non-parabolicity which are neglected by Hensel would have to be taken into account as magnetophonon transitions occur between

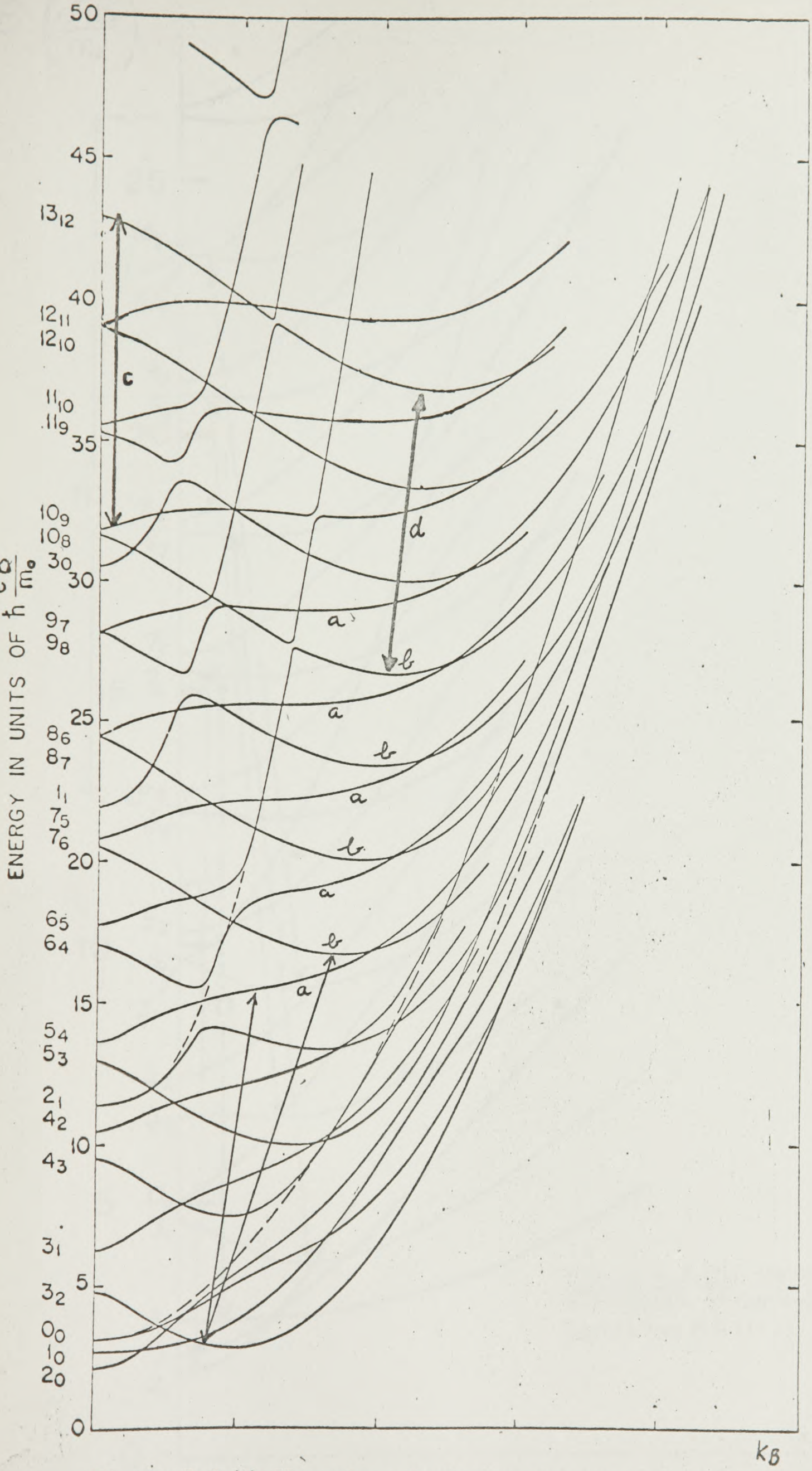


Figure 6.6 (i) Hensel's calculation of the hole Landau levels for B ∥ (001)

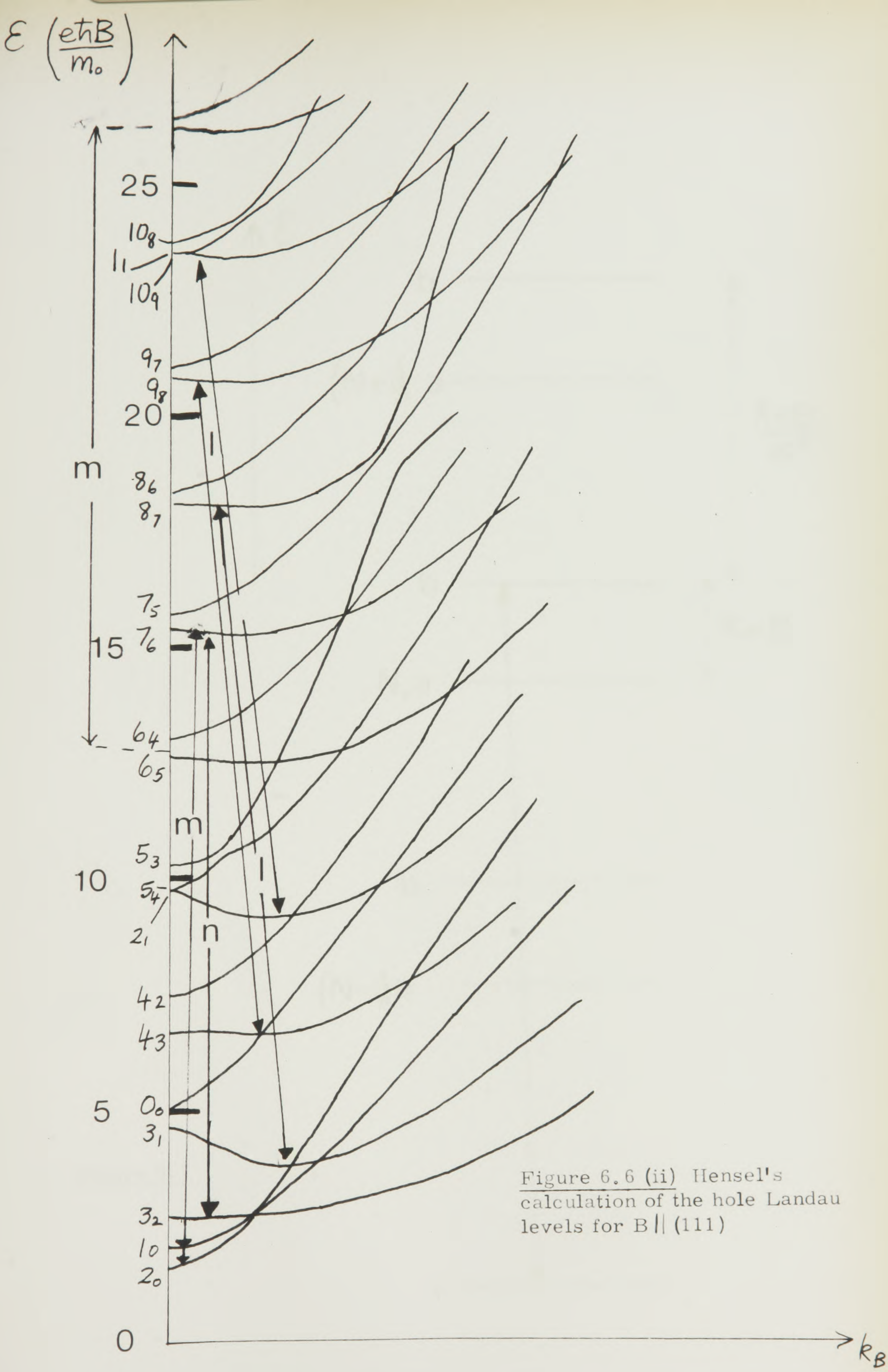


Figure 6.6 (ii) Hensel's calculation of the hole Landau levels for B || (111)

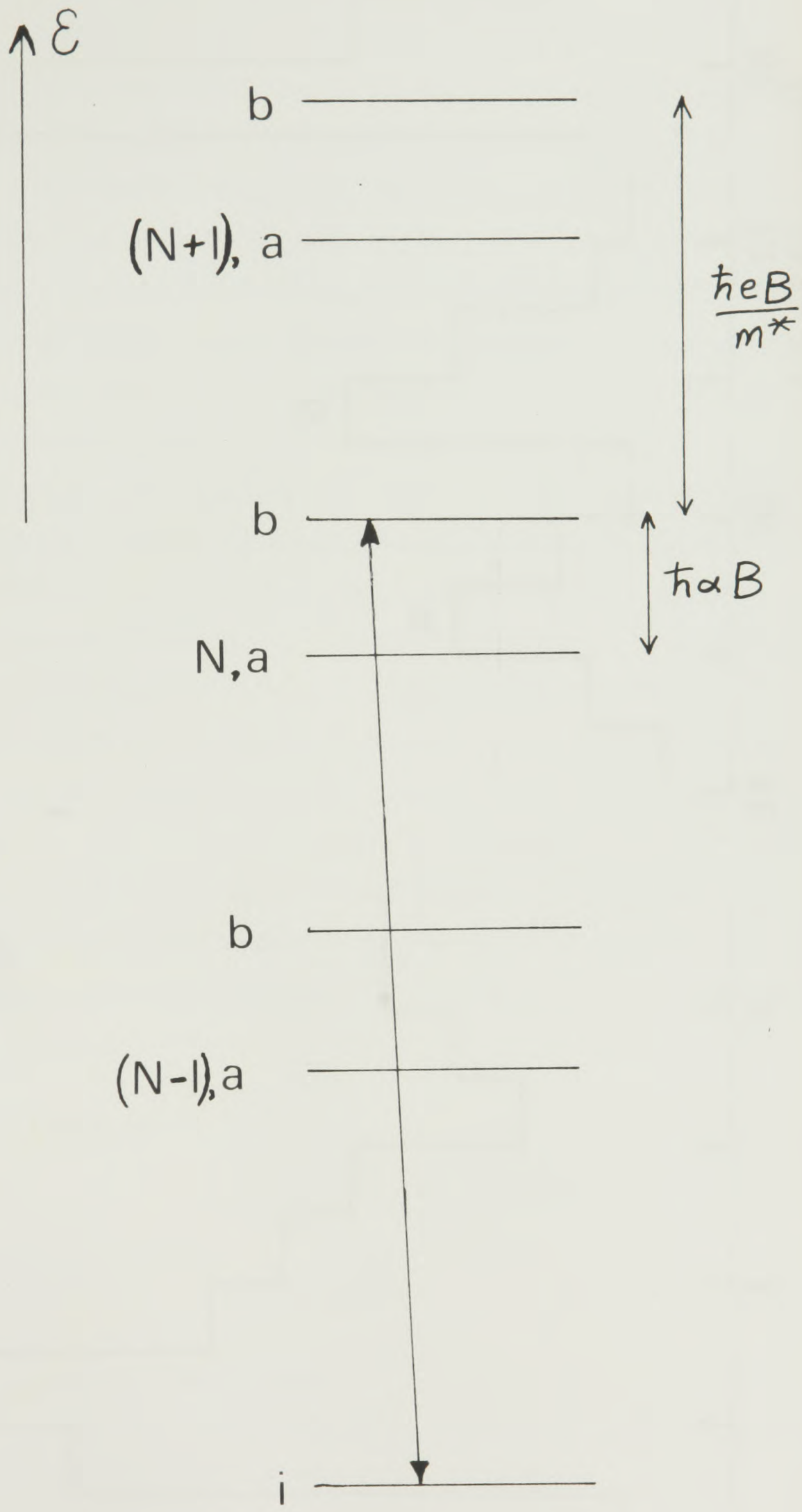
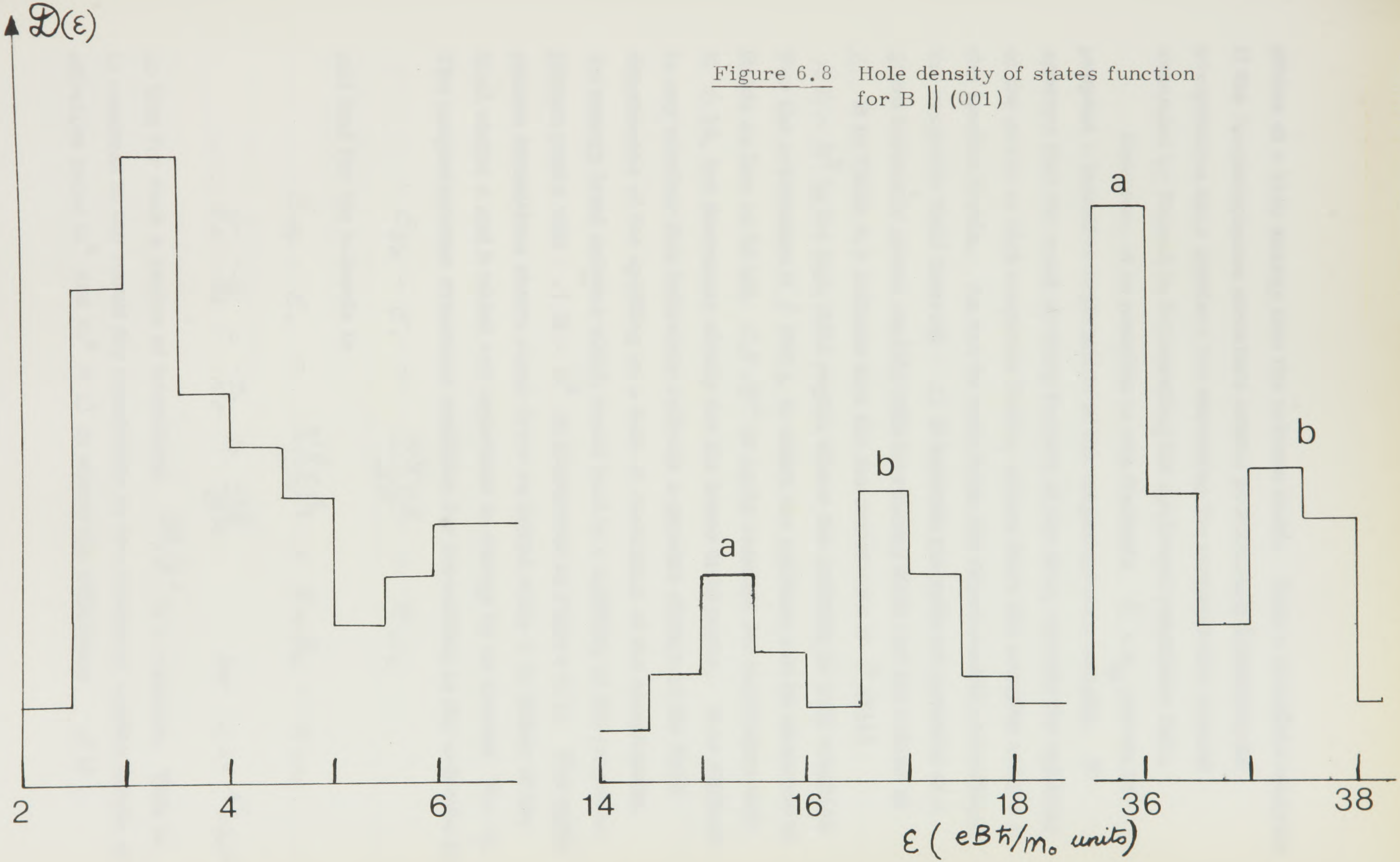


Figure 6.7

Figure 6.8 Hole density of states function for B || (001)



states at a high energy into the valence band. Such a complete analysis if the magnetophonon structure seems prohibitively laborious, the computation time involved far exceeding the considerable amount expended by Hensel in interpreting his cyclotron resonance data.

However, it is possible to use Hensel's $\mathcal{E} - k_B$ curves to propose a tentative explanation of the magnetophonon results. It appears that the most striking feature of the data, namely the splitting of the peaks at high magnetic fields, arises from the complex nature of the Landau levels. As can be seen from the experimental recordings, the magnetic field interval Δ B between the split components of a given harmonic grows rapidly with increasing field and the values of Δ B in Table 6.1 indicate that for the orientation B // (111) $\Delta B \sim B^2$ in the high field region where the splitting is well resolved. For the orientation B // (001), in which the splitting can be observed at fields as low as 50 kG, $\Delta B/B^2$ is again constant for harmonics with $N \lesssim 10$, but decreases slowly for the lower field peaks. It is difficult to say whether this behaviour reflects a genuine change in the field dependence of the splitting or a lack of resolution of the components. An energy level scheme which would lead to a splitting of the magnetophonon peaks with $\Delta B \sim B^2$ is illustrated in Figure 6.7. The optic phonon transitions shown occur from an initial state i to either of the final states a and b which are separated in energy by an amount $\hbar\alpha$ B. The magnetophonon resonance condition for transitions to the a-levels is

$$\mathcal{E}_{Na} - \mathcal{E}_i = \frac{N\hbar eB_a}{m^*} = \hbar\omega_e$$

and that for the b-levels is

$$\mathcal{E}_{Nb} - \mathcal{E}_i = \frac{N\hbar eB_b}{m^*} + \hbar\alpha B_b = \hbar\omega_e$$

$$\therefore \frac{1}{B_a} - \frac{1}{B_b} = -\frac{\alpha}{\omega_e} \simeq \frac{\Delta B}{B^2} \qquad \text{for } \alpha \ll Ne/m^*$$

so that for such a series of transitions $\Delta B/B^2$ is a constant. This is in contrast to the result for transitions in two classical Landau levels of effective mass m^* and $m^* + \Delta m$ where the difference Δ B

in resonance field satisfies the condition $\Delta B/B = \Delta m/m^*$. The illustration in Figure 6.7 is an over-simplification of magneto-phonon resonance as it neglects the dependence of the Landau level energies on k_B and takes no account of transitions involving initial states at higher energy. When considering how the holes are distributed in the complex Landau levels of Ge, it is profitable to calculate the hole density of states function defined as the number of states per unit energy range. The procedure adopted to obtain this function was to divide Hensel's graphs into small energy intervals $\Delta\mathcal{E}$ and then to measure the lengths Δk_i for each Landau level in the range from $\mathcal{E}$ to $\mathcal{E}+\Delta\mathcal{E}$. The density of hole states is then proportional to $\sum_i \Delta k_i$ summed over all the Landau levels. The value of $\mathcal{D}(\mathcal{E})$ obtained in this way is shown in Figure 6.8 for B // (001) as a function of energy in units of $\hbar eB/m_0$. As the Landau levels for this orientation fall into two well defined groups (marked a and b in Figure 6.6) whose critical points are well separated in energy, the density of states function for the higher energy levels shows two well resolved maxima separated by an energy of 1.3 $eB\hbar/m_0$. The second interesting feature of the Landau level configuration for B // (001) is that at an energy of about 3 $eB\hbar/m_0$, the critical points of the 2_0, 1_0, 0_0 and 3_2 Landau levels (Hensel's notation) are nearly degenerate and lead to a large peak in the density of states.

At a temperature of 100 K and at a magnetic field of 150 kG, an energy of kT corresponds to 8 $eB\hbar/m_0$ so that the majority of electrons occupy the lowest Landau levels and it is likely that the magnetophonon structure under such conditions is dominated by transitions which originate at states near the maximum in $\mathcal{D}(\mathcal{E})$ at an energy of 3 $e\hbar B/m_0$. Optic phonon scattering involving final states near the double peaks (a and b in Figure 6.8) in the density of states at higher energy would then lead to a splitting of the magnetophonon harmonics. Thus in the high magnetic field region, the transitions a and b in Figure 6.7 resemble the dominant magnetophonon scattering processes for B // (001). This interpretation appears to predict accurately the magnitude Δ B of the peak splitting in the (001) orientation: for the final states involved in the N = 4 harmonic,

the energy difference between the density of states maxima a and b in Figure 6.8 is 12% of the total energy involved in the transition. Similarly, the energy difference for the N = 8 transition is 6% of the optic phonon energy. By reference to Table 6.1, it can be seen that these percentage values are in excellent agreement with the experimentally observed splitting expressed as $\Delta B/B$.

The most difficult feature of the structure to explain is that the splitting for B // (001) appears to change very little in character over the magnetic field range from 60 to 240 kG and over the temperature range from 77 K to 150 K. At a temperature of 100 K, the ratio of the cyclotron energy to the thermal energy $\hbar\omega_c/kT \lesssim 3$ for $B \lesssim 100$ kG so that transitions involving initial states deep into the valence band make an increasingly important contribution to the magnetophonon intensity at relatively low fields. Thus the splitting of the low field peaks cannot be due entirely to transitions involving initial states near the peak in $\mathcal{D}(\mathcal{E})$ at an energy of $3\,e\hbar B/m_0$. Transitions of the type marked c and d in Figure 6.6(i) for which the initial and final states have high quantum numbers may explain the persistence of the splitting at relatively low magnetic fields. The transitions occur between critical points for which the energy interval corresponds to cyclotron masses of $0.29\ m_0$ and $0.30\ m_0$. (These mass values are derived from Hensel's curves and do not include the effects of non-parabolicity). Such an effective mass difference would yield a splitting $\Delta B/B = \Delta m/m = 3\%$ in fair agreement with that observed for peaks with N between 14 and 20. Thus it appears that the structure arising from transitions like a and b in Figure 6.6 for which the splitting satisfies $\Delta B \sim B^2$ develops with increasing magnetic field from a splitting due to transitions like c and d for which $\Delta B = \frac{\Delta m}{m} B$.

With B // (111), it is possible to give a tentative interpretation of the splitting of the high field harmonics into a triplet structure since it appears that the transitions which occur between critical points of the Landau levels fall into three groups which are clearly separated in energy. Figure 6.6(ii) shows the three types of transitions (labelled l, m, n) for the N = 5 harmonic. The magnetic fields at which l, m, n resonate with

the optic phonon energy are in the ratio 1 : 1.05 : 1.10 in fairly good agreement with the ratios of the field positions of the components of the N = 5 triplet which are given in Table 6.1. Despite this good agreement, it is impossible to explain an important feature of the magnetophonon structure for B // (111), namely the decrease of the product NB with decreasing N, in terms of Hensel's data. In addition, no explanation can be given for the irregular development of the splitting with B // (110) which was discussed in section 6.2.

To summarise, it is clear that the splitting of the heavy hole peaks in Ge requires further theoretical and experimental study. No calculations have been made of the matrix elements for the various transitions and in particular the effect of spin selection rules are unknown. A development of the magnetophonon experiments which might help with the interpretation of the peak splitting would be to emulate Hensel's technique of applying uniaxial stress, a method which has proved so successful in providing an interpretation of his cyclotron resonance data.

6.4 The Amplitudes of the Magnetophonon Structure

The amplitudes of the 16^{th} harmonic of the heavy hole peaks for B // (001) and (111) were measured using the linear biassing technique (see Chapter 2 for details) and are plotted in Figure 6.9 as a function of temperature. The graph also shows the amplitude of the 7^{th} harmonic of the light hole series for B // (111) over the temperature range for which it was visible. The empirical equation developed by Stradling and Wood (1968 and see Chapter 1, equation 1.12) to describe the amplitude of the magnetophonon peaks in n-type materials is inapplicable to the high field peaks in p-Ge due to the presence of splitting. However, the low field heavy hole peaks and also the light hole series fit the equation accurately and at a temperature of about 130 K yield the values of shown in Table 6.3.

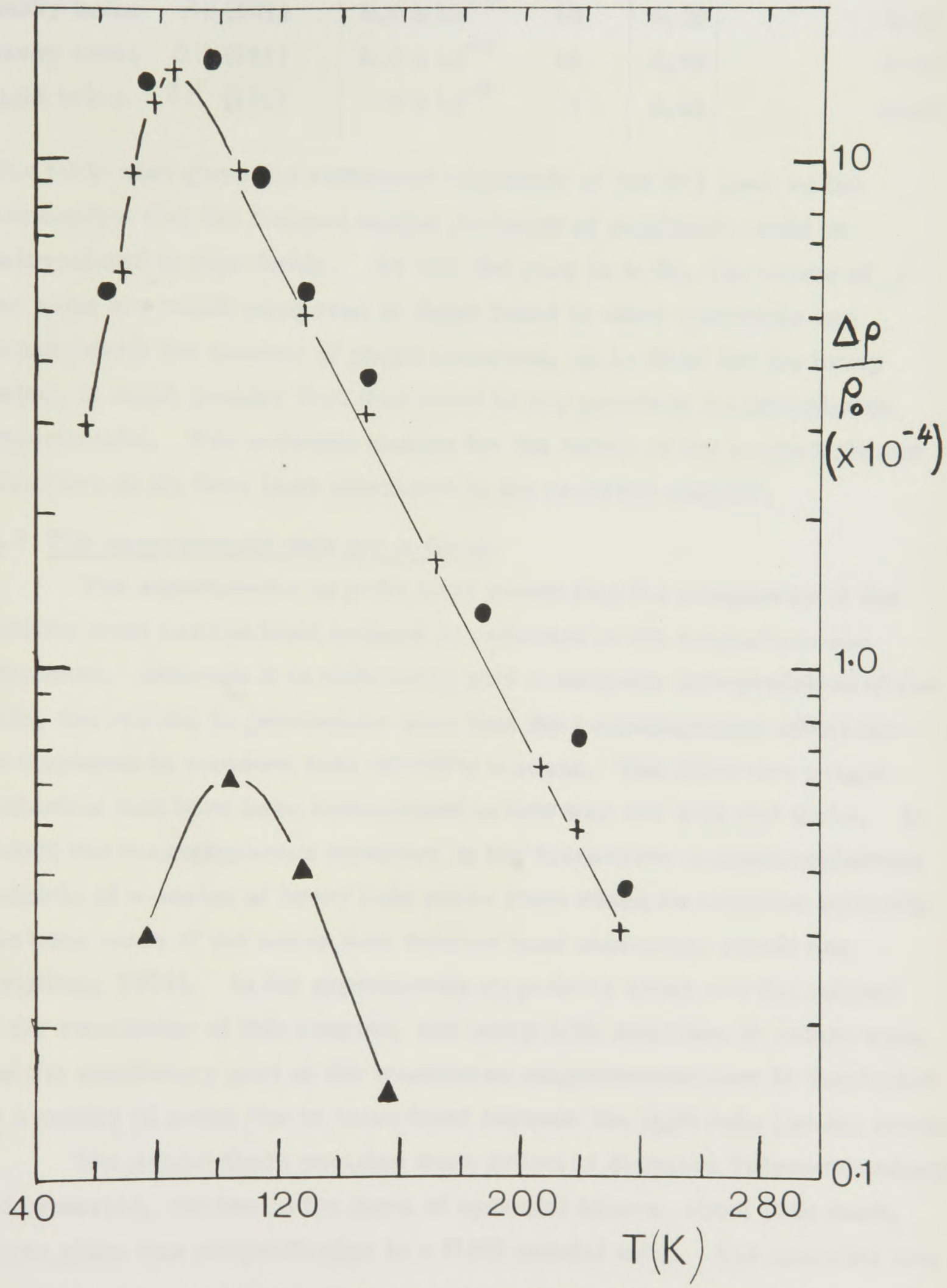


Figure 6.9 The Temperature dependence of the magneto-phonon amplitudes in p-Ge:-

(+) N = 16, heavy holes, B // (001)

(●) N = 16, heavy holes, B // (111)

(▲) N = 7, light holes, B // (111)

Table 6.3

(T = 130 K)

	Orientation	$\Delta\rho/\rho_o$	N	γ	(N=1 by extrapolation)
heavy holes	B|| (001)	5.0×10^{-4}	16	0.25	2.3%
heavy holes	B|| (111)	5.4×10^{-4}	16	0.28	3.5%
light holes	B|| (111)	4×10^{-5}	7	0.55	0.1%

The table also gives the estimated amplitude of the N=1 peak on the assumption that the damped cosine variation of amplitude could be extrapolated to high fields. As was the case in n-Ge, the values of γ for p-Ge are small compared to those found in other materials and consequently the number of peaks observed, up to N=40 for the heavy holes, is much greater than that found in any previous magnetophonon experiments. The probable causes for the extent of the magnetophonon structure in Ge have been discussed in the previous chapter.

6.5 The experimental data for p-GaAs

The experiments on p-Ge have shown that the complexity of the valence band Landau level scheme is reflected in the magnetophonon structure. Although it is difficult to give a complete interpretation of the data, the results in germanium show that the magnetophonon effect can be employed to measure hole effective masses. The other two p-type materials that have been investigated in this way are InSb and GaAs. In p-InSb the magnetophonon structure in the transverse magnetoresistance consists of a series of heavy hole peaks from which an accurate estimate has been made of the heavy hole valence band anisotropy (Hoult and Stradling, 1972). In the experiments on p-GaAs which are the subject of the remainder of this chapter, the heavy hole structure is rather weak and the oscillatory part of the transverse magnetoresistance is dominated by a series of peaks due to transitions between the light hole Landau levels.

The p-type GaAs samples were grown at Standard Telecommunications Laboratories, Harlow in the form of epitaxial layers, about 100μ thick, whose plane was perpendicular to a (100) crystal axis. The material was of

very high purity with $N_A - N_D = 6 \times 10^{14}$ cm^{-3} and had a mobility at 77 K of 7,500 cm^2/V.s. which increased steadily with decreasing temperature down to 50 K, below which carrier freeze-out occurred. The samples were cut with the long current carrying direction parallel to the $(\bar{1}10)$ crystal axis so that in the transverse orientation any anisotropy of the peaks could be studied for orientations of B parallel to the three major symmetry directions.

Magnetophonon structure was first observed using steady fields at Oxford where, with B // (110) and at a temperature of 110 K, three maxima were present in the magnetoresistance at fields of 54.8, 65.7 and 83.7 kG. The peaks are attributed to the 6th, 5th and 4th harmonics respectively of a light hole magnetophonon series with a fundamental of 330 kG. In order to confirm this interpretation, further experiments were performed using the higher magnetic fields available at Toulouse and Figure 6.10 shows experimental recordings taken with pulsed fields for B // (110). Maxima arising from the light hole series were observed at fields of 55.2 (N=6), 67.0 (N=5), 84.2 (N=4), 110.8 (N=3) and 167.1 kG (N=2) yielding a fundamental field in excellent agreement with that observed from the steady field traces. At fields above 200 kG, additional structure appears, the most prominent feature being a maximum at a field of 269 kG. The other weak maxima are almost certainly high-N harmonics of the heavy hole series. In an attempt to observe any anisotropy of the magnetophonon structure, further high field measurements were made with B parallel to the (001), (111) and (110) symmetry directions. These recordings are compared in Figure 6.11.

6.6 The Interpretation of the Magnetophonon Structure in p-GaAs

Although the magnetophonon structure appearing in p-GaAs is not as extensive as that found in p-Ge, probably due to the combined effect of increased ionised impurity scattering and the resonant polaron interaction in broadening the Landau levels, it is clear that a detailed knowledge of the Landau level structure and optic phonon scattering matrix elements is required for a complete interpretation of the data. However, the magnetophonon measurements permit an estimate to be made of the light hole effective mass. Substituting a fundamental field of 330 kG and an

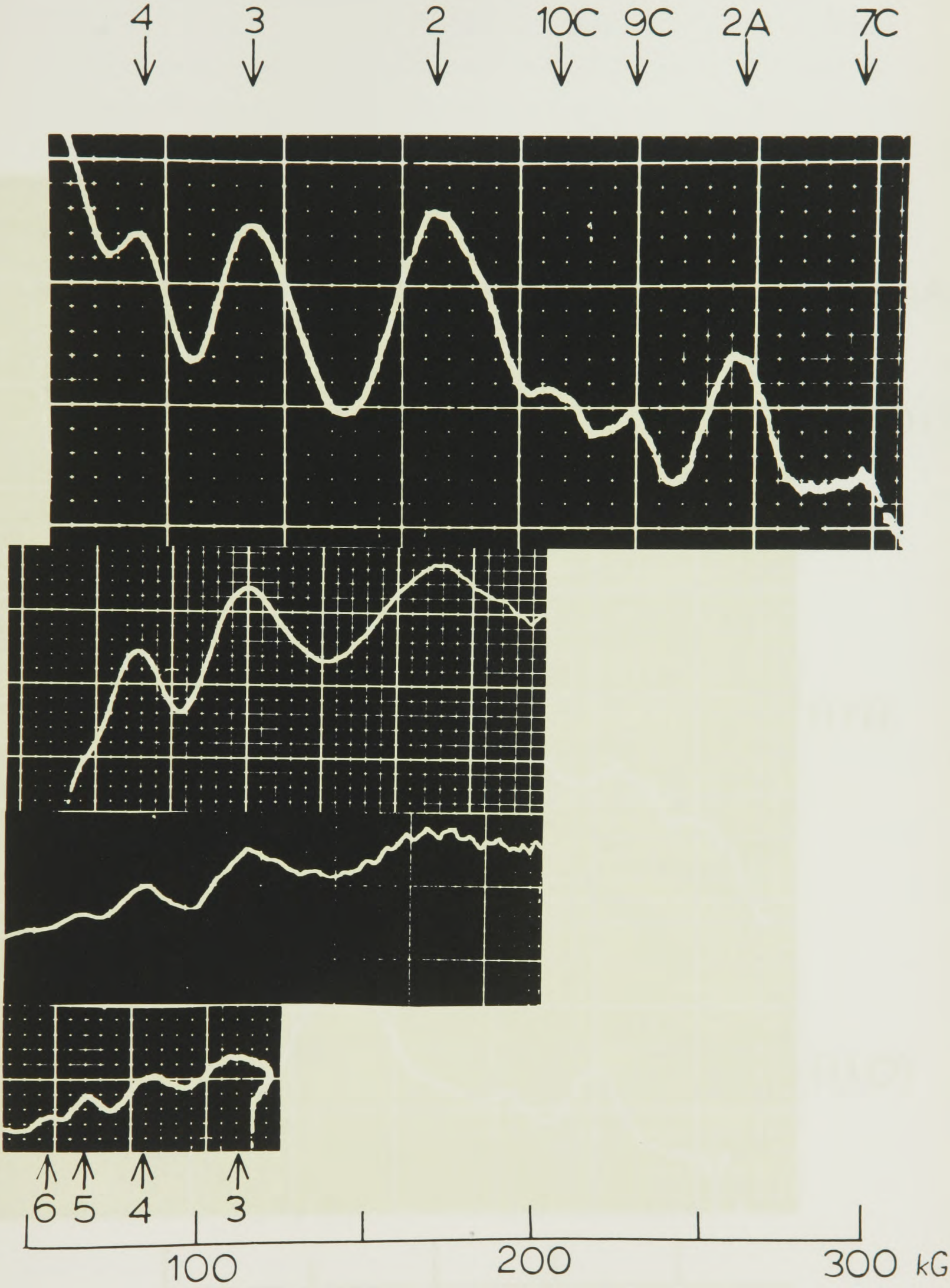


Figure 6.10 The experimental recordings of $-\partial^2 R/\partial B^2$ against B at 120 K for p-GaAs in the orientation $j \parallel (1\bar{1}0)$, B $\parallel$ (110). From right to left, the N = 7, 9 and 10 heavy hole peaks are separated by a stronger anomalous light hole peak and the N = 2 to 6 light hole peaks are seen at lower fields.

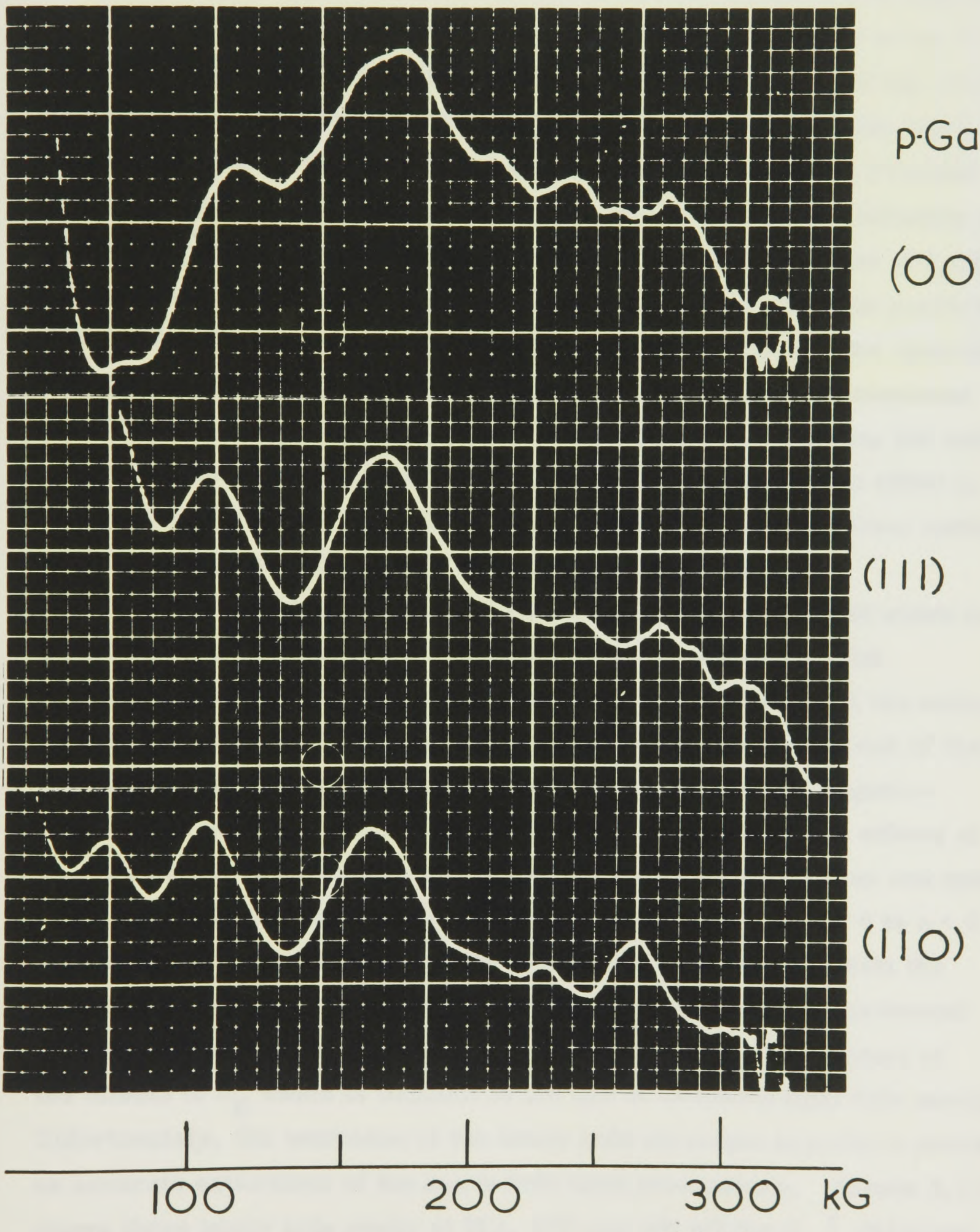


Figure 6.11 The experimental recordings of $-\partial^2 R/\partial B^2$ against B at 120 K for p-GaAs. From top to bottom, B is parallel to (001), (111), (110). In all three cases j // $(1\bar{1}0)$.

optical phonon at 120 K of 294 cm^{-1} (Iwasa, 1964; Mooradian and Wright, 1966) into equation 6.1 yields a light hole effective mass of 0.104 m_0. In order to estimate the effective mass at the bottom of the light hole band, corrections must be made for band non-parabolicity and the polaron effect. Using equation 6.2 (Johnson, 1967) the correction that should be applied to m^* to obtain the band edge effective mass is 10% as compared to the 3% correction deduced by Stradling and Wood (1968) for n-GaAs at the same temperature. The polaron correction for the light holes is also likely to be slightly greater than that applied to the electrons since the Frohlich coupling constant increases as the square root of the carrier effective mass. Estimating this correction to be 3%, a band edge effective mass of 0.091 m_0 is obtained. Although the error involved in measuring the peak positions from which the uncorrected mass m^* is derived is only 2%, the uncertainty concerning the effects of non-parabolicity and the polaron enhancement limit the accuracy of the band edge mass to about 5%. Allowing for such an error, the light hole mass deduced from the magnetophonon effect is in agreement with the value of 0.087 $m_0 \pm 0.005\ m_0$ obtained from cyclotron resonance experiments at 50 K by Mears and Stradling (1971).

The peak which occurs at a magnetic field of 269 kG and which is particularly prominent for B // (110) is probably associated with transitions between the anomalously spaced light hole levels at the bottom of the valence band. The only previous study that has been made of these levels in p-GaAs is that of Vrehen (1968) who analysed his magneto-optical data in terms of Luttinger-Kohn theory, neglecting the effects of k_B. From his data, Vrehen deduced the energies of the spin-up and spin-down light hole Landau levels. His values predict that the n = 0 to n = 2 Landau level transition of the spin-up ladder should resonate with the optical phonon energy at a field of 260 kG. This is in close agreement with the position of the observed peak at 269 kG despite the neglect of the effects of k_B which is implicit in the use of Vrehen's light hole energies. Unfortunately, the weakness of the heavy hole structure in p-GaAs prevents an accurate estimation of the heavy hole band parameters. Figure 6.10 shows three heavy hole peaks at 213, 235 and 305 kG for B // (110) and it is likely that a further peak is obscured by the anomalous light hole

peak at 269 kG. Although the positions of the peaks appear to shift as the orientation of B is changed (see Figure 6.11), it is difficult to estimate values of effective mass due to the uncertainty in the assignment of N-values to the peaks.

An interesting feature of the magnetophonon data for both p-type materials is the relative prominence of the light hole peaks. At first sight this result is rather surprising since for Ge and GaAs the density of light holes is about three times smaller than that for the heavy holes. The persistence of the light hole peaks in the field region where the heavy hole series is damped out probably mirrors the behaviour of the two density of states functions. Thus at low fields the singularities in $D(\varepsilon)_{h.h.}$ for the heavy holes are completely smeared out whereas the light hole Landau levels are more widely spaced in energy so that the corresponding $D(\varepsilon)_{l.h.}$ retains its oscillatory form.

CHAPTER 7

The Warm Electron Magnetophon Effect in n-InP

7.1 Introduction

A feature common to the experiments described in the earlier chapters of this thesis is that at temperatures below about 50K, the magnetophonon structure in the magnetoresistance disappears into the noise background. This fall-off in amplitude reflects the decreasing importance of optical-phonon scattering in limiting the electron mobility which as the temperature is reduced becomes increasingly dominated by ionised impurity scattering. However, even when the lattice temperature is well below 40K, magnetophonon peaks can be made to reappear by the application of an electric field sufficiently strong to raise the electron temperature a few degrees above that of the lattice. This chapter describes the observation of such hot electron magnetophonon structure in n-InP at lattice temperatures of 11K and 20K.

Under warm electron conditions, a dynamic equilibrium is established in which the power gained by the electrons from the applied electric field is transmitted to the lattice by phonon emission processes. The wave vector of the phonon or group of phonons emitted in a particular energy relaxation event are restricted by the laws of energy and crystal momentum conservation. When a magnetic field of sufficient strength to produce well defined Landau levels is applied to the crystal, the density of electron states becomes an oscillatory function of energy, with a peak corresponding to the bottom of each Landau level. If the phonons which dominate the energy relaxation from the electrons to the lattice are approximately monoenergetic, then the strength of the link between the electrons and phonons will vary in an oscillatory manner as the magnetic field is changed. Provided that electron-electron interactions are sufficiently strong to maintain a Boltzmann distribution the mean electron temperature will show a corresponding oscillatory variation which will also be reflected in the electrical resistance of the sample. On the basis of elementary theory concerning the energy dependent relaxation time, if ionised impurity scattering is dominant in relaxing the electron momentum, a maximum should occur in the magneto-resistance at the resonance fields since at these points the mean electron

temperature should be a minimum. However, Yamada and Kurosawa (1968) have shown that in the non-ohmic region, the electron distribution function shows a pronounced decrease compared to the Boltzmann function at energies near the bottom of each Landau level. They claim that this distortion could lead to a mimimum in the magnetoresistance at the resonance field as is found experimentally in a number of semiconductors. A further factor to be taken into account if the electron distribution is not in equilibrium with the lattice is the possibility of the carrier concentration decreasing when the resonance condition is satisfied. This could arise either because the decrease in energy of the electron system at resonance lowers the probability of impact ionisation of any electrons trapped on the donor sites, or because of an increase in the recombination rate of carriers at the donors accompanied by emission of optical phonons.

Magnetophonon structure was first observed under hot electron conditions in the non-linear current-voltage characteristics of n-InSb at 4K (Kotera et al., 1966). The first observation of hot electron magnetophonon peaks in the magnetoresistance at low temperatures was in n-GaAs (Stradling and Wood, 1968b) and since then further observations have been made in n-type InSb, InAs, CdTe (Stradling et al. 1970) and in InP (this thesis). More recently, hot electron effects have been reported at a temperature of 77K in the magnetoresistance of InSb at electric fields of up to 50V/cm (Curby and Ferry, 1972) and in the non-linear coefficient of electron mobility at relatively low electric fields ($\sim$ 1V/cm) using highly sensitive third harmonic detection techniques (Hamaguchi et al. 1972). In both experiments the hot electron peaks are slightly displaced to higher magnetic fields relative to the peak positions reported at low temperatures by Stradling et al. It is likely that this shift in the peak positions reflects the increased effect of conduction band non-parabolicity at a temperature of 77K. An additional factor may be that the mechanism for energy relaxation by optical phonon emission is different at the two temperatures. Thus whereas at low temperatures optic phonon emission is accompanied by electron capture at a donor site, it is possible that at 77K inter-Landau level transitions are more

Figure 7.1 The warm electron structure in InP sample B at 11K with $\underline{j} \parallel \underline{B}$. The recordings were made at the following electric field strengths (measured in zero magnetic field):-
(a) 12 V/cm (b) 6.3 V/cm (c) 4.5 V/cm (d) 2.4 V/cm (e) 1.4 V/cm
(f) 1.1 V/cm (g) 0.65 V/cm (h) 0.2 V/cm.

Figure 7.2 The warm electron structure in sample C at 11 K with $j \parallel B$. The recordings were made at the following electric fields (measured in zero magnetic field):-
(a) 12 V/cm (b) 8.7 V/cm (c) 5.7 V/cm (d) 4.8 V/cm (e) 3.5 V/cm
(f) 2.4 V/cm (g) 1.8 V/cm (h) 1.6 V/cm (i) 1.1 V/cm (j) 0.5 V/cm.

Figure 7.3 The warm electron structure in sample C at 11 K with $j \perp B$. The recordings were made at the following electric fields (measured in zero magnetic field):-
(a) 8.7 V/cm (b) 4.8 V/cm (c) 3.5 V/cm (d) 2.4 V/cm (e) 2.1 V/cm
(f) 1.9 V/cm (g) 1.6 V/cm (h) 1.0 V/cm (i) 0.5 V/cm.

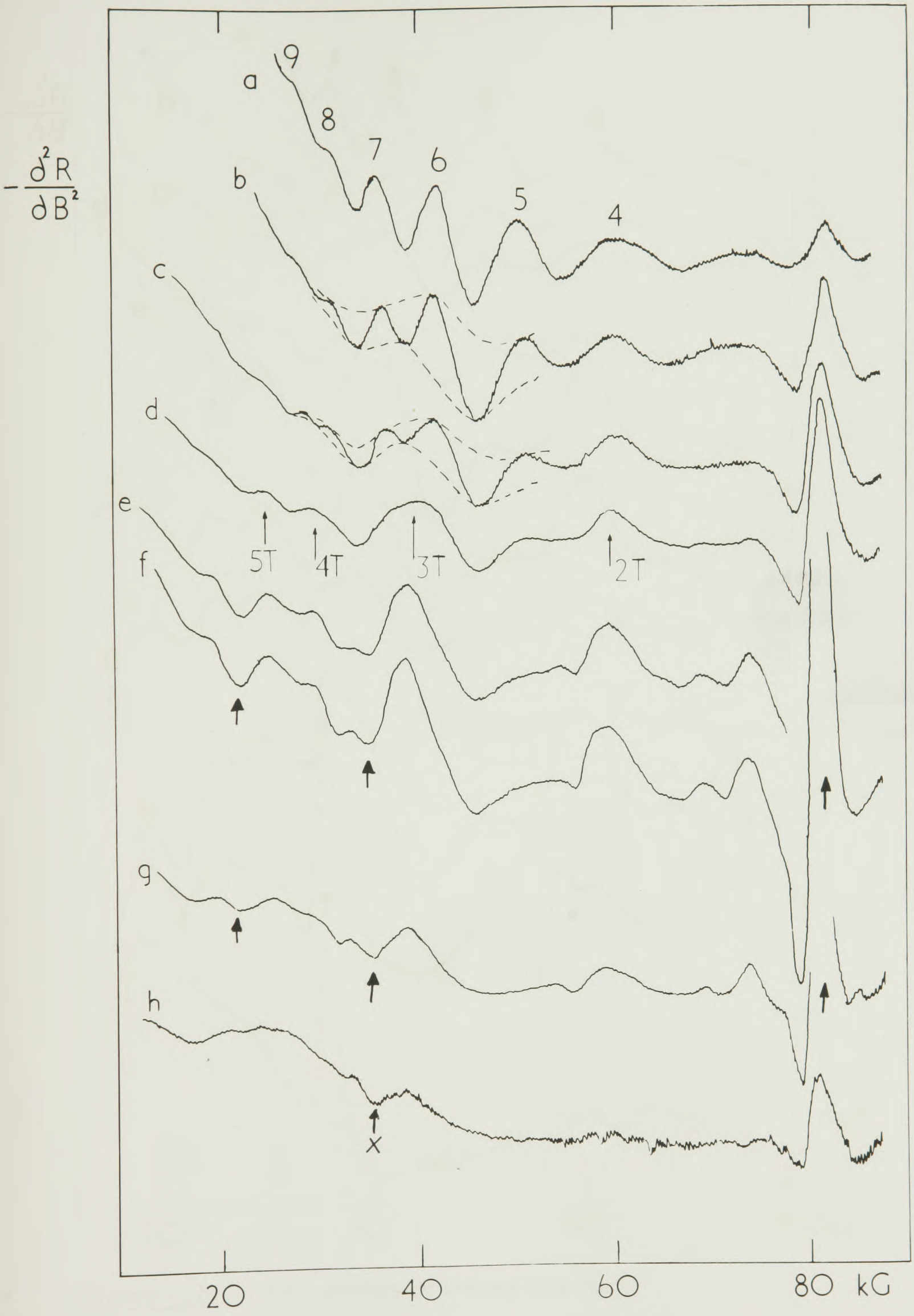


Figure 7.1 (for details of traces see text)

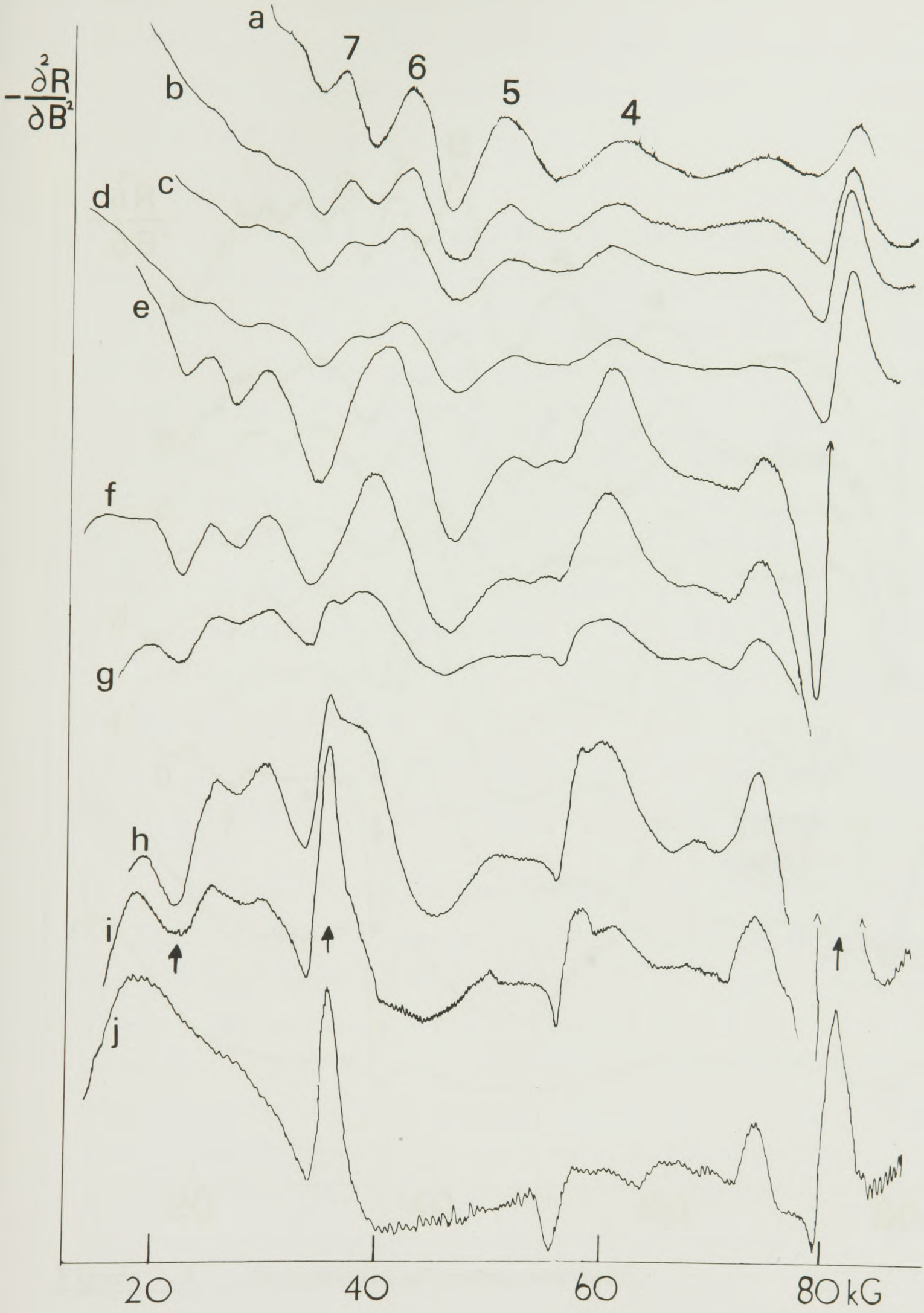


Figure 7.2 (for details of traces see text)

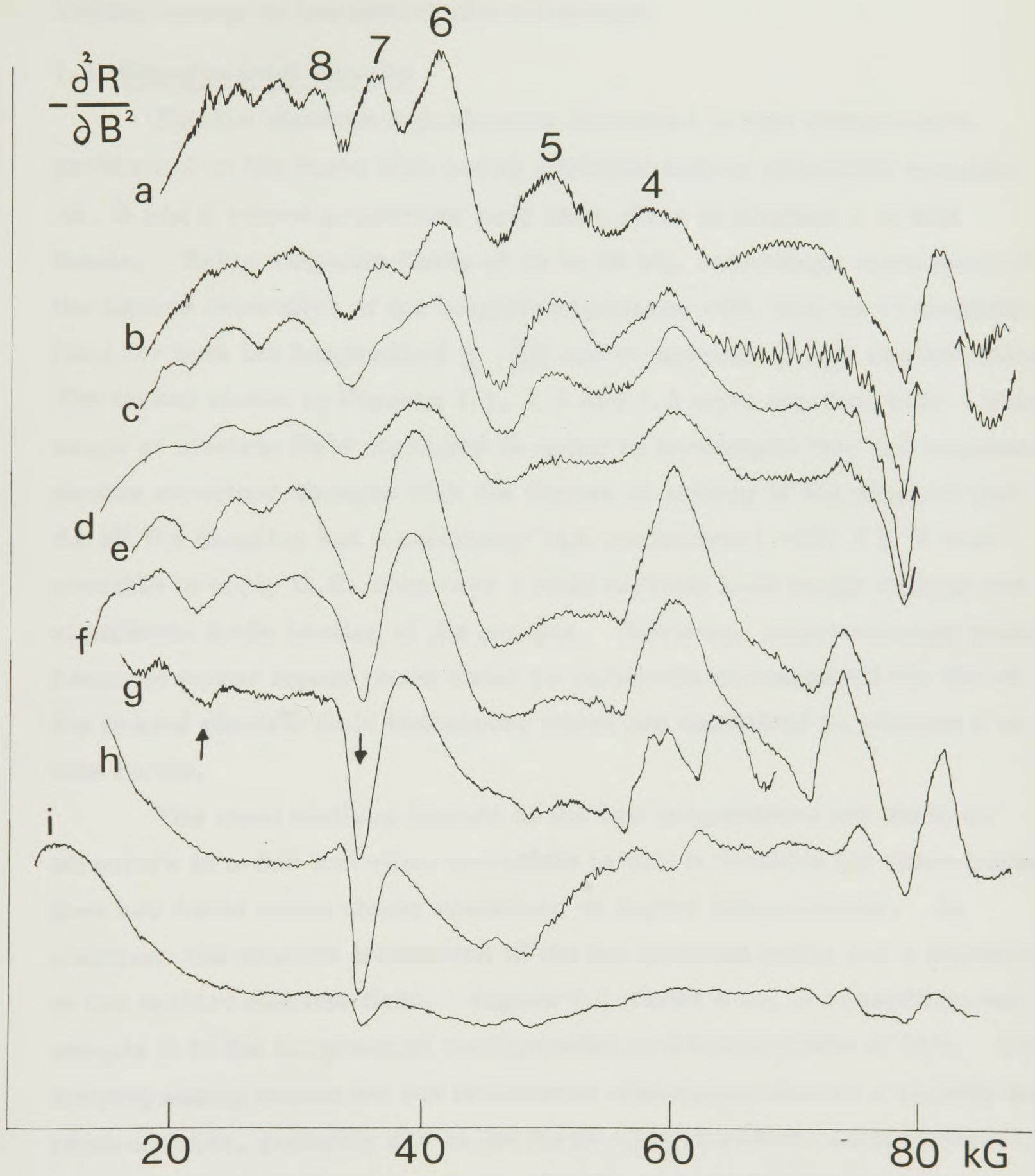


Figure 7.3 (for details of traces see text)

likely. As will be discussed in section 7.3.1 of this chapter, the fractional difference in the resonant magnetic field positions for the two types of relaxation process is given by the ratio of the donor binding energy to the optical phonon energy.

7.2 Experimental Results

The hot electron experiments described in this section were performed on the three high purity epitaxial indium phosphide samples A1, B and C whose properties have been given in Chapter 3 of this thesis. Using magnetic fields of up to 90 kG, recordings were made of the second derivative of the magnetoresistance with respect to magnetic field for both the longitudinal ($\underline{j} \parallel \underline{B}$) and transverse ($\underline{j} \perp \underline{B}$) configurations. The traces shown in Figures 7.1, 7.2 and 7.3 were obtained over a wide range of electric field strengths in order to investigate how the magneto-phonon structure changed with the degree of heating of the electron gas. As all the samples had a relatively high resistance ($\sim 10 k\Omega$), it was possible to apply D.C. bias over a wide electric field range without any significant Joule heating of the sample. However, measurements which required power inputs above about 10 milliwatts necessitated the use of the pulsed electric field techniques which are described in Chapter 2 of this thesis.

The most striking feature of the low temperature hot electron structure in n-InP and other materials is that it contains far more peaks than are found under ohmic conditions at higher temperatures. In addition, the relative intensities of the hot electron peaks are a function of the applied electric field. Figure 7.1 shows a set of recordings for sample B in the longitudinal configuration at a temperature of 11K. The corresponding traces for the transverse orientation showed a slightly higher level of noise, probably due to the large magnetoresistance background. However, the hot electron extrema for the two configurations had the same sign, approximately equal amplitudes and occurred at identical magnetic fields at least down to electric fields of about 0.5 V/cm below which all structure in the transverse magnetoresistance had disappeared into the noise background. In sample C, the recordings for the two magnetic

field configurations, shown in Figures 7.2 and 7.3, were again very similar. The only exception was the appearance at low electric fields of a strong peak at 35.5 kG which occurred as a maximum in ρ_{zz} and as a minimum in ρ_{xx}. The similarities of the results for the two configurations in contrast to the very great differences in peak positions and amplitudes which are observed in the ohmic magnetoresistance at higher temperatures is due to the fact that the hot electron magnetophonon extrema reflect energy relaxation rather than momentum relaxation processes.

As can be seen from all three sets of experimental recordings, the most prominent feature at the highest electric fields (5 V/cm - 16 V/cm) is a group of peaks numbered from 4 to 9 in Figures 8.1, 8.2 and 8.3 which, by their periodicity and steady variation in amplitude with increasing magnetic field, appear to form a magnetophonon series (A). The magnetic field positions of the maxima of this series are shown in Table 7.1. As the electric field is lowered, series A becomes increasingly distorted by the presence of a group of peaks which are characterised by a slower periodicity in $^1/B$. This structure (series B) is visible firstly as an envelope of the oscillations of series A, but as the electric field is decreased further to about 2.5 V/cm it becomes the dominant feature of the magnetoresistance curve. The maxima of this series, denoted by 2T, 3T, ... etc. in Figure 7.1, have the magnetic field positions shown in Table 7.1 which are periodic in $^1/B$ to within 2%.

Table 7.1

Series	T(K)	Orientation	Magnetic Field kG 2	3	4	5	6	7	8	9	10
ohmic	130	j B	160	106	81.7	65.2	54.2	46.3	40.4	35.6	31.9
non-ohmic series A	11,20	j B, j B	-	-	60.7	50.5	42.3	36.6	32.2	28.9	26.1
non-ohmic series B	11,20	" "	59.0	39.3	29.5	23.6	19.7	-	-	-	-

Although the peaks so far discussed can be fitted accurately to either series A or B, there are several features in the magnetoresistance curves which cannot be interpreted so easily. The most prominent of these peaks which occurs at a magnetic field of 82 kG has been observed in the magnetoresistance of all indium phosphide samples studied under hot electron conditions. The peak is clearly visible both at 11K and 20K but its amplitude relative to the peaks in series B appears to be slightly greater at the lower temperature where it can be observed over the electric field range from 0.1 V/cm to 16 V/cm. At electric fields below about 2V/cm, further peaks appear in the magnetoresistance which do not form an easily identifiable series. Of this structure, a minimum occuring at 21.5 kG is common to the recordings taken in the longitudinal and transverse configurations for samples A1, B and C. However, the extrema appearing in the magnetic field region from 32 kG to 40 kG are different for the three samples and also depend on the orientation of the magnetic field relative to the current direction. Thus in sample C there is a strong peak at a magnetic field of 35.5 kG which is a maximum for $\underline{j} \parallel \underline{B}$ and a minimum for $\underline{j} \perp \underline{B}$. Although this structure is present at low electric fields in both samples A1 and B, it is much weaker in amplitude than the corresponding peak in the magnetoresistance of sample C. Traces g and h of Figure 7.1 show the recordings for sample B at low electric fields. The structure occurring at a field of around 35 kG is rather complex and it is difficult to decide whether maxima or minima correspond to resonant features. However, the magnetic field position of the minimum at 35.5 kG (marked X in the figure) agrees exactly with that of the stronger peak which is found in sample C. To summarise, it appears that of the peaks in magnetoresistance which do not correspond to members of series A and B, those occurring at fields of 82.0, 35.5 and 21.5 kG are common to the recordings for all three InP samples.

7.3 The Interpretation of the Hot Electron Magnetophonon Structure

7.3.1 Structure arising from emission of L.O. phonons

The prominent series of peaks (series A) which is observed at relatively high electric fields can be attributed to an energy relaxation

process of the conduction electrons involving the emission of L.O. phonons. Table 7.1 compares the magnetic field positions of these peaks with those obtained in the transverse orientation in the ohmic region at higher temperatures. It is clear that the hot electron maxima are displaced to lower magnetic fields by about 20%. A shift of a similar nature has also been observed in n-GaAs (Stradling and Wood, 1968a) and n-CdTe (Stradling et al., 1970) and in both cases its magnitude correlates closely with the ratio of the donor binding energy to the optical phonon energy. This suggests that the energy loss mechanism by optical phonon emission which produces the extrema is associated with the capture of warm electrons at the donor impurity sites rather than with transitions between two Landau levels. Resistance maxima should therefore occur at magnetic fields given by

$$\hbar\omega_\ell = E_I(B) + N\hbar\omega_c \qquad N = 0,1,2\ldots \tag{7.1}$$

where $E_I(B)$ is the magnetic field dependent donor binding energy. At relatively low magnetic fields where

$$\gamma = \tfrac{1}{2}\hbar\omega_c / E_I(0) \ll 1$$

the impurity energy is given by

$$E_I(B) = E_I(0) + \tfrac{1}{2}\hbar\omega_c \tag{7.2}$$

For the shallow donor in InP, γ is approximately $\frac{1}{2}$ at a magnetic field of 60 kG and the binding energy predicted by equation (7.2) is about 5% too low (Larsen, 1968). This is a sufficiently accurate approximation to determine the peak positions and gives the resonance condition

$$\hbar\omega_\ell - E_I(0) = (N+\tfrac{1}{2})\hbar\omega_c = (N+\tfrac{1}{2})\frac{\hbar eB}{m^*}(1.t) \tag{7.3}$$

for the magnetic field positions B(low temp.) of the hot electron peaks. The resonance condition at higher temperatures is

$$\hbar\omega_e = \frac{N\hbar e}{m^*} B(h.t) \qquad (7.4)$$

Assuming the values of m^* to be equal, division of equation (7.3) by (7.4) gives

$$1 - E_I(0)/\hbar\omega_e = \frac{(N+\frac{1}{2})B(1.t)}{NB(h.t)} \qquad (7.5)$$

Neglecting the factor $\frac{1}{2}$ in equation (7.5), it can be seen that the fractional shift of the hot electron extrema to lower fields is $E_I(0)/\hbar\omega_e = 0.17$. Unfortunately, no calculations have yet been made of the optical polaron enhancement of the electron effective mass for a process which involves warm electron capture at a donor site. Hence, for the purpose of comparing equation (7.3) with the experimentally observed peak positions of series A, it is assumed that the magnetophonon mass m^* which is obtained from the transverse magnetophonon effect at 77K (Chapter 3 of this thesis and Eaves et al. 1971) is a sufficiently good approximation to the value of m^* which appears in equation (7.3). The magnetophonon mass m^* (77K) = 0.087 exceeds the low frequency cyclotron mass by 6% due to the effects of polaron enhancement and band non-parabolicity. As recent cyclotron resonance experiments have shown that the band-edge effective mass is independent of temperature below 50 K (Simmonds, 1972), the error involved in deducing equation (7.5) is likely to be small.

Figure 7.4 demonstrates the excellent fit which equation (7.5) provides for the magnetic field positions of the maxima of the hot electron series A. The theoretical line is calculated using an optical phonon frequency of 349.5 cm^{-1} (Mooradian and Wright, 1966) and a shallow donor binding energy of 61.0 cm^{-1} deduced from the photoconductivity experiments on sample B which are described in detail in the next chapter.

As was the case in the hot electron magnetophonon experiments in n-GaAs and CdTe, no series of peaks corresponding to equation (7.4) could be detected in the magnetoresistance of n-InP at low temperatures. A partial explanation for the absence of the series is that it requires electrons to be excited to a much higher threshold in energy compared to the series involving electron capture at the impurity site. This argument

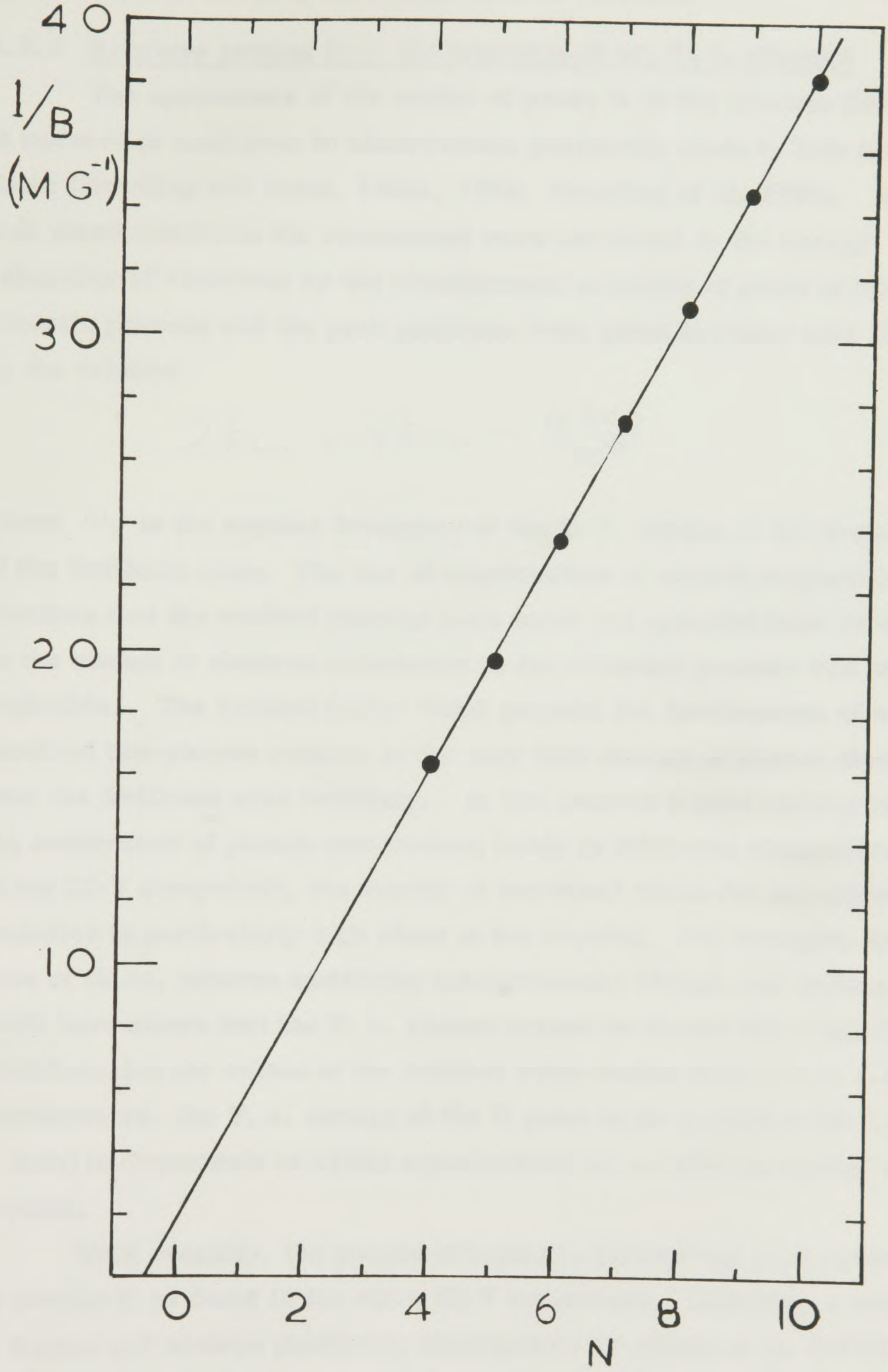


Figure 7.4 Plot of inverse magnetic field ($^1/B$) against peak number (N) for the hot electron magneto-phonon series A in InP. The straight line is given by the relation $\hbar\omega_1 - E_I(0) = (N+\frac{1}{2})\hbar\omega_c$.

is discussed in detail by Stradling and Wood (1968a).

7.3.2 Structure arising from the emission of two T.A. phonons

The appearance of the series of peaks B as the electric field is reduced is analogous to observations previously made in InSb and GaAs (Stradling and Wood, 1968a, 1970; Stradling et al. 1970). In both these materials the resonances were attributed to the energy relaxation of electrons by the simultaneous emission of pairs of transverse acoustic phonons and the peak positions were given to better than 2% by the relation

$$2\hbar\omega_t = N\hbar\omega_c = \frac{N\hbar eB}{m^*} \qquad (7.6)$$

where ω_t is the angular frequency of the T.A. phonon at the X-point of the Brillouin zone. The law of conservation of crystal momentum requires that the emitted phonons have equal and opposite wave vectors as the change of electron momentum in the emission process will be negligible. The critical factor which permits the development of well resolved two-phonon maxima is the very high density of phonon states near the Brillouin zone boundary. In this respect a good analogy is the occurrence of phonon combination bands in infra-red absorption. In the III-V compounds, the density of combined states for two-phonon emission is particularly high close to the X-point. For example, in the case of GaAs, neutron scattering measurements (Waugh and Dolling, 1963) have shown that the T.A. phonon branch is almost flat along the (100) direction for values of the reduced wave-vector from 0.6 to 1.0. Furthermore, the T.A. energy at the W point in GaAs (and at the L point in InSb) is degenerate to within experimental error with the energy at the X-point.

Until recently, the phonon energies in InP had not been determined as precisely as those in the other III-V compounds. However, a series of Raman and neutron scattering experiments by Alfrey et al. (1972) now give accurate values of the frequency of all the phonon modes at the X- and L- critical points of the Brillouin zone. In particular, the value they obtain for the frequency of the transverse acoustic phonon at the X-point

of 67 ± 1 cm^{-1} (8.3 meV = 2.00 THz) confirms the earlier estimates by Mitra (1963) from infra-red absorption and by Slack and Roberts (1970) from a comparison of the critical point energies of the III-V and II-VI zinc-blende compounds. In view of the agreement between recent determinations of the energy of the T.A.(X) phonon, it is clear that the interpretation of spectral emittance data by Stierwalt and Potter (1965) which gives $\hbar\omega$(T.A.X) = 20.1 meV is seriously at fault. Substituting values of the low frequency cyclotron mass at 9K of $m^* = 0.0803$ (Chamberlain et al. 1972a) and $\omega_t = 67.1\ cm^{-1}$ into equation (7.4) gives a fundamental field of 115 kG for the two-phonon series, in excellent agreement with the experimentally observed value of 118 kG for the maxima of the B-series. It is likely that the value of m^* that should be employed in equation (7.4) exceeds the band-edge low frequency mass by an amount due to the effect of band non-parabolicity and polaron enhancement. These correction probably amount to less than 5%.

As no complete neutron scattering data yet exist for the T.A. phonon energy along the (100) axis, it is impossible to deduce the phonon density of states function at an energy of $\hbar\omega_t$. However, a comparison of the velocity of the transverse acoustic waves and band edge phonon energies in InP and GaAs indicates that the T.A. dispersion curves for the two materials are very similar. Thus in GaAs, the expression

$$\omega = v_{T.A}\, k$$

where $v_{T.A}$ = T.A. phonon velocity
ω = " " frequency
$\hbar k$ = " " crystal momentum

when extrapolated to the zone boundary at the X-point gives an energy of 25 meV compared to the T.A.(X) phonon energy of 9.7 meV. In InP, the corresponding values are 22 meV and 8.3 meV. Hence it is likely that InP also possesses a T.A. dispersion curve in the (100) direction which is flat over a large part of the Brillouin zone.

The excellent fit which equation 7.6 provides for the maxima of series B confirms the interpretation of the series in terms of an energy

relaxation process which involves the emission of pairs of band-edge phonons. The increase in intensity of the peaks of series B relative to those of series A as the electric field is reduced can be explained by the much lower threshold in energy that is required for the emission of pairs of band-edge phonons from the T.A. branch compared to the threshold for single optic phonon emission. This permits two-phonon processes to dominate the energy relaxation at low electron temperatures. On the other hand, the energy release involved in the emission of pairs of band-edge phonons ($\sim$ 200 K for InP and GaAs) combined with the high density of states at the zone boundary is a considerably more effective energy relaxation process than that due to the emission of single acoustic phonons where the law of $\underline{k}$-conservation limits the energy loss per phonon to an equivalent of~1 ^{o}K.

The importance of electron interaction with pairs of band-edge acoustic phonons has recently been demonstrated by Ngai (1972) who, from a theoretical study of magneto-optical data, claims that the strength of the electron coupling to the 2 T.A.(L) multiphonon mode approaches that between electrons and L.O. phonons.

7.3.3 Unidentified Structure in the Magnetoresistance

A feature which is common to the hot electron measurements made in InSb, GaAs, CdTe (Stradling et al. 1970) and in InP is that the structure which appears in the magnetoresistance is considerably more complex than that observed at higher temperatures in the ohmic regime. Although it has proved possible to explain the origin of groups of peaks which are characterised by a $^{1}/B$ periodicity in terms of energy relaxation by phonon emission, there remains other structure in the magnetoresistance of all the materials investigated to date whose origin remains obscure. The major problem associated with the interpretation of these peaks is that they are irregularly spaced in magnetic field and it is therefore difficult to fit them to an equation analogous to (7.3) or (7.4) which are characteristic of a resonant scattering process between electron states in a magnetic field.

Structure very similar to the unidentified peaks which occur in n-InP

and other materials studied at Oxford (Stradling et al. (1970) has also been observed in the magnetoresistance of p-Te at 2K (von Klitzing and Landwehr, 1971). In these experiments no series could be identified as arising from resonant scattering processes involving the emission of an L.O. or two T.A. phonons. The tentative suggestion made by von Klitzing and Landwehr for the origin of the peaks involves the absorption of phonons by an unidentified donor which subsequently emits a photon of well-defined frequency. They claim that this monochromatic radiation would then interact with shallow impurity centres and produce resonant features in the magnetoresistance by means of a photoconductivity mechanism. A process which involves the excitation of a donor has also been suggested to explain a series of peaks, closely periodic in $^1/B$ with a fundamental field of 24 kG, which has recently been observed in the warm electron magnetoresistance of high purity n-GaAs (Hoult, 1972). In the proposed mechanism, electrons excited into the conduction band by the applied electric field can relax to lower energy Landau states by inelastically scattering from a neutral donor site which is thereby excited from the 1s ground state to the lowest lying $2p_{-1}$ excited state. In GaAs, the energy of the shallow donor 1s to $2p_{-1}$ transition is almost independent of magnetic field between 10 and 30 kG so that the resonance condition

$$N\hbar\omega_c = E(1s \rightarrow 2p_{-1}) \qquad (7.7)$$

gives a series of peaks which are closely periodic in $^1/B$ and characterised by a fundamental field in agreement with the observed value of 24 kG to within the limit of experimental accuracy.

In order to investigate the possibility of an interaction between the conduction electrons and neutral donors giving rise to the unidentified structure in InP, it is necessary to know precisely the excited state energies of the impurities present in the samples. These values are obtained from the photoconductivity experiments in the next chapter which reveal the presence of two shallow donor species whose mean binding energy is $E_I(0) = 61.0\ cm^{-1}$. The photoconductivity spectra also yield directly the magnetic field dependent 1s to $2p_{\pm 1,0}$ transition energies

for magnetic fields of up to 20 kG which are plotted in Figure 7.5. The curves are extrapolated to higher magnetic fields on the basis of Larsen's calculations of the eigenvalues of a hydrogenic donor in a magnetic field (Larsen 1968, Stillman et al.1969). The figure also includes the magnetic field dependant donor binding energy (Larsen 1968, Cabib et al. 1971)

$$E_I(B) = E(N = 0, k_B = 0) - E(1s) \qquad (7.8)$$

where $E(N = 0, k_B = 0)$ is the energy of the lowest lying Landau state. The curves in Figure 7.5 which intersect the impurity state transition energies correspond to integral numbers of Landau level spacings

$$E = N\hbar\omega_c \qquad (7.9)$$

From the intersections marked a, b and c in Figure 7.5 it can be seen that the resonances of the series given by equation 7.7 which Hoult has observed in GaAs would occur at fields of 36, 18, 13 ... kG in InP. The position of the fundamental of this series corresponds closely with that of the peak at 35.5 kG which has been observed in the warm electron magnetoresistance of all three samples of InP studied to date. Even in the purest samples of InP, no resonant structure can be observed at fields below 20 kG so that the higher harmonics of the series are unobservable. Hence, at the present time it is impossible to positively identify a series in InP which corresponds to equation (7.7).

The other group of intersections in Figure 7.5 (marked l, m, n) which are of interest satisfy the condition

$$E_I(B) = N\hbar\omega_c \qquad (7.10)$$

As the impurity binding energy $E_I(B)$ has a relatively large variation with magnetic field intensity, this series is aperiodic in $^1/B$. The resonant fields of the first three harmonics occur at 82, 34 and 21 kG and agree closely with the positions of the strong maximum at 82.0 kG and the weaker extrema at 35.5 and 21.5 kG which are common to all three InP samples. This close coincidence of magnetic fields suggests that the peaks may be caused by a resonant process which involves the energy

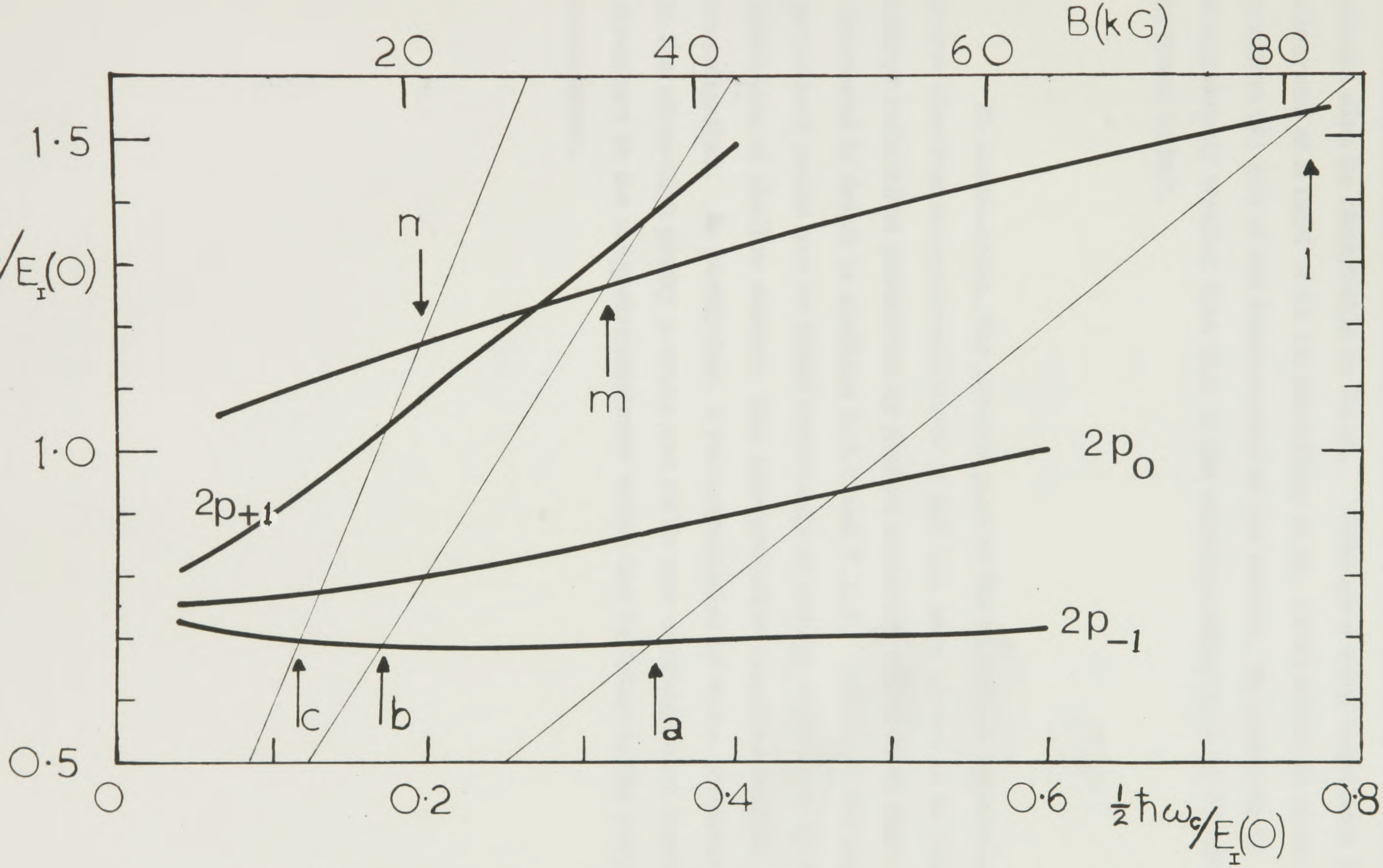


Figure 7.5 Magnetic field dependence of shallow donor transition energies in InP. The bold lines give the energies of the 1s to $2p_{-1}$, 1s to $2p_0$, 1s to $2p_{+1}$ and 1s to lowest Landau state transitions. The fine lines correspond to the energies $\hbar\omega_c$, $2\hbar\omega_c$, $3\hbar\omega_c$.

relaxation of warm electrons by the impact ionisation of a neutral donor. In such an inelastic scattering event the donor is excited from the 1s ground state to the lowest energy continuum state. If this interpretation is correct, a series of peaks given by equation (7.10) should also be observable in GaAs. Although a weak maximum has been observed at a field of 54 kG (Stradling et al. 1970) which is close to the position (51 kG) of the fundamental of the series, its intensity is considerably weaker than that of the corresponding peak at 82 kG which is found in InP.

To summarise, the greater part of the structure appearing in the warm electron magnetoresistance of InP has been shown to be due to the energy relaxation processes by phonon emission which have been discussed in detail in sections 7.3.1 and 7.3.2. Although the remaining prominent peaks can be fitted accurately to energy relaxation by impact ionisation of shallow donors, this interpretation requires further investigation. In particular, a re-examination of warm electron effects in the ultra-high purity n-GaAs and CdTe now available may reveal new structure in the magnetoresistance which can be fitted to the proposed mechanism.

CHAPTER 8

Infra-red photoconductivity in n-InP

8.1 Introduction

The previous chapter showed that warm electron capture at shallow donor sites accompanied by optical phonon emission is an important mechanism of energy relaxation in n-InP. In this chapter the energies of the shallow donor states are obtained from a series of photoconductivity experiments using a Fourier transform spectrometer and two types of cryostat designed for infra-red optical work at temperatures down to 1.2 K. Measurements have been made on a number of samples of different impurity concentrations prepared at the Royal Radar Establishment, Malvern and the Allen Clarke Research Centre of the Plessey Company, Towcester. The photoconductivity spectra reveal fine structure in the 1s to 2p transitions of the shallow donor states due to the presence of two impurity species whose ground states are separated in energy by an amount equivalent to 0.7 cm^{-1}. The widths of the photoconductivity peaks have been studied as a function of magnetic field and impurity content and are found to agree with the mechanisms responsible for line broadening which have been suggested by Larsen (1972). In addition to structure arising from transitions between donor states, a line has been observed in the photoconductivity spectrum at a frequency of 33.8 cm^{-1}. The intensity of this peak appears to be directly related to the line-width of the shallow donor transitions.

The advances in recent years of the techniques for the preparation of very high purity III-V semiconductor crystals has made possible a study of the properties of shallow donor impurities in these materials to a precision approaching that obtained in the elemental semiconductors Ge and Si (see Faulkner, 1969, for a comprehensive list of references). The first attempts to identify the chemical shifts of particular donors in GaAs was made by Summers et al. (1970) who worked at zero magnetic field with relatively impure material. The energy difference of 0.2 meV which they reported between different donor types was considerably larger than that subsequently observed by Fetterman et al. (1971) at Lincoln Laboratory of the Massachusetts Institute of Technology and more recently by Stradling et al. (1972) at

Oxford. The Lincoln group have also studied the magnetic field dependence of the energy separation between different donor types in GaAs and have shown that the perturbations which give rise to the relative shifts of the ground state energies are of short range compared to the hydrogenic Bohr radius a_o and are centred at the donor site. In addition, by studying the magnetic field variation of the energy difference $E(1s \rightarrow 2p_0) - E(1s \rightarrow 2p_{-1})$ which is independent of these central cell corrections, Stillman et al. (1971) were able to make a precise verification of the effective mass theory. They showed that for fields of up to 55 kG, the theory is accurate to 0.15% although the electric fields due to randomly distributed charged impurities can cause appreciable perturbations of the donor levels.

Larsen (1972) has made a theoretical study of the broadening mechanisms which may contribute to the observed line-widths and concludes that in addition to the Stark broadening of the impurity levels, the quadrupolar interaction of the excited states with random electric field gradients may be a significant broadening mechanism. To consider the effect of Coulomb fields produced by remote charged impurity centres on a neutral donor, it can be assumed that the electric potential $\varphi(r)$ at the centre of the donor has a slow spatial variation so that it can be expanded into the first few terms of a Taylor series

$$\varphi(r) = \varphi(0) + (\nabla\varphi)_{r=0} \cdot \underline{r} + \frac{1}{2}\sum_i x_i^2 \left(\frac{\partial^2\varphi}{\partial x_i^2}\right)_{r=0}$$

Using 1st order perturbation theory, the energy shift of the 1^{th} donor level with eigenfunction $|1\rangle$ is

$$\begin{aligned}\Delta E_\ell^{(1)} &= \langle \ell|\varphi(r)|\ell\rangle = \varphi(0) + \frac{1}{2}\sum_i \langle \ell|x_i^2|\ell\rangle \left(\frac{\partial^2\varphi}{\partial x_i^2}\right)_{r=0} \\ &= \varphi(0) + \frac{1}{4}\langle \ell|3z^2 - r^2|\ell\rangle \left(\frac{\partial^2\varphi}{\partial z^2}\right)_{r=0} \\ &= \varphi(0) + \frac{1}{4} Q_\ell \left(\frac{\partial \mathcal{E}_z}{\partial z}\right)_{r=0}\end{aligned} \qquad (8.1)$$

where $\mathcal{E} = \nabla\varphi$ is the electric field and Q_1 is the electric quadrupole moment of state $|1\rangle$. It is assumed that $|1\rangle$ is cylindrically symmetric about the z-axis and has a definite parity.* If the charged impurities are randomly distributed throughout the crystal then $\partial\mathcal{E}_z/\partial z$ has a Lorentzian distribution. Larsen has calculated the broadening which results from the quadrupole term in equation (8.1) for a range of magnetic field values and has shown that it disappears for the $2p_{\pm 1}$ states in GaAs at a magnetic field of about 55 kG. In InP, the quadrupole moment of the $2p_{\pm 1}$ states is zero at a field of about 100 kG.

Larsen has shown that the other significant contribution to the line-width arises from the second order Stark shift given by

$$\Delta E_\ell^{(2)} = e^2 \sum_j \frac{|\langle \ell | \underline{\mathcal{E}} \cdot \underline{r} | j \rangle|^2}{E_\ell - E_j} \qquad (8.2)$$

Thus the Stark effect causes the 2s state to repel the $2p_{+1}$ and $2p_{-1}$ states with a consequent increase in the apparent Zeeman splitting. As a result of the random nature of the electric field produced by the charged impurities, these states are broadened as well as shifted by the perturbation given in equation (8.2) and hence the $1s \rightarrow 2p_{+1}$ and $1s \rightarrow 2p_{-1}$ lines should have asymmetric tails on their high and low wave number sides respectively. Such line-shapes have been observed in GaAs (Stillman et al. 1971; Stradling et al. 1972) and in the InP spectra discussed in this chapter.

8.2 The apparatus for the photoconductivity experiments

Both molecular gas lasers and Fourier transform spectrometers have recently been used extensively to study the photoconductivity of shallow donor impurities. The respective advantages of the two types of spectrometer are complementary. Thus the high power levels at fixed frequencies provided by lasers are invaluable in the investigation of weak transitions such as those between the excited states of donors (Chamberlain et al. 1972) whereas the broad band spectrum available with Fourier transform spectrometers enables the complete frequency spectrum of lines to be determined in applications where the signal to noise ratio is such that the high power levels of the lasers are not essential.

* This is justified since the wave-function extends over many lattice spacings.

The Fourier transform instrument used in the experiments described in this chapter is a Beckmann R.I.I.C., FS720. The details of its construction and mode of operation have been summarised in recent texts on infra-red physics (Bell, 1972; Kimmitt, 1970). The f/1.7 beam at the exit slit of the spectrometer is focussed into a circular image of diameter 1 cm and is then transmitted by means of a brass light pipe (internal diameter = 12 mm; length = 1 metre) and a plane aluminised glass mirror to either of two cryostats. The designs of the two Dewar vessels are shown schematically in Figures 8.1 and 8.2.

In the design illustrated in Figure 8.1, the semiconductor specimen is mounted at the end of an electroformed copper cold finger which provides the thermal link to the helium bath. The cold finger is securely bolted onto the base of the helium bath by means of austenitic stainless steel screws which have approximately the same coefficient of expansion as copper. It was found that the heat link from the cold finger to the helium can was significantly improved by coating the two surfaces in contact with a layer of electro-deposited indium. Two alternative types of cold finger have been designed for use with the spectrometer. The first is in the form of a cylindrical tube with an internal diameter of 12 mm and provides a continuous light path through the cryostat. This arrangement enables transmission experiments to be performed using either a Golay detector mounted at the top of the Dewar vessel or else a cooled detector thermally linked to the helium bath in space D (see Figure 8.1).

The second type of cold finger is designed specifically for photo-conductivity experiments and is shown in the inset of Figure 8.1. The infra-red radiation is focussed by means of a copper cone into a hollow spherical cavity which contains the semiconductor sample. The sphere is composed of two hemispherical bowls with polished surfaces which were bored out of two interlocking blocks of copper. The use of such an integrating sphere increases the total radiation incident on the sample. In addition, since the angle of incidence of the radiation striking the sample is partially randomised, the occurrence of Fabry-Perot interference effects which can arise from multiple internal reflections at the surfaces of parallel sided samples is considerably reduced.

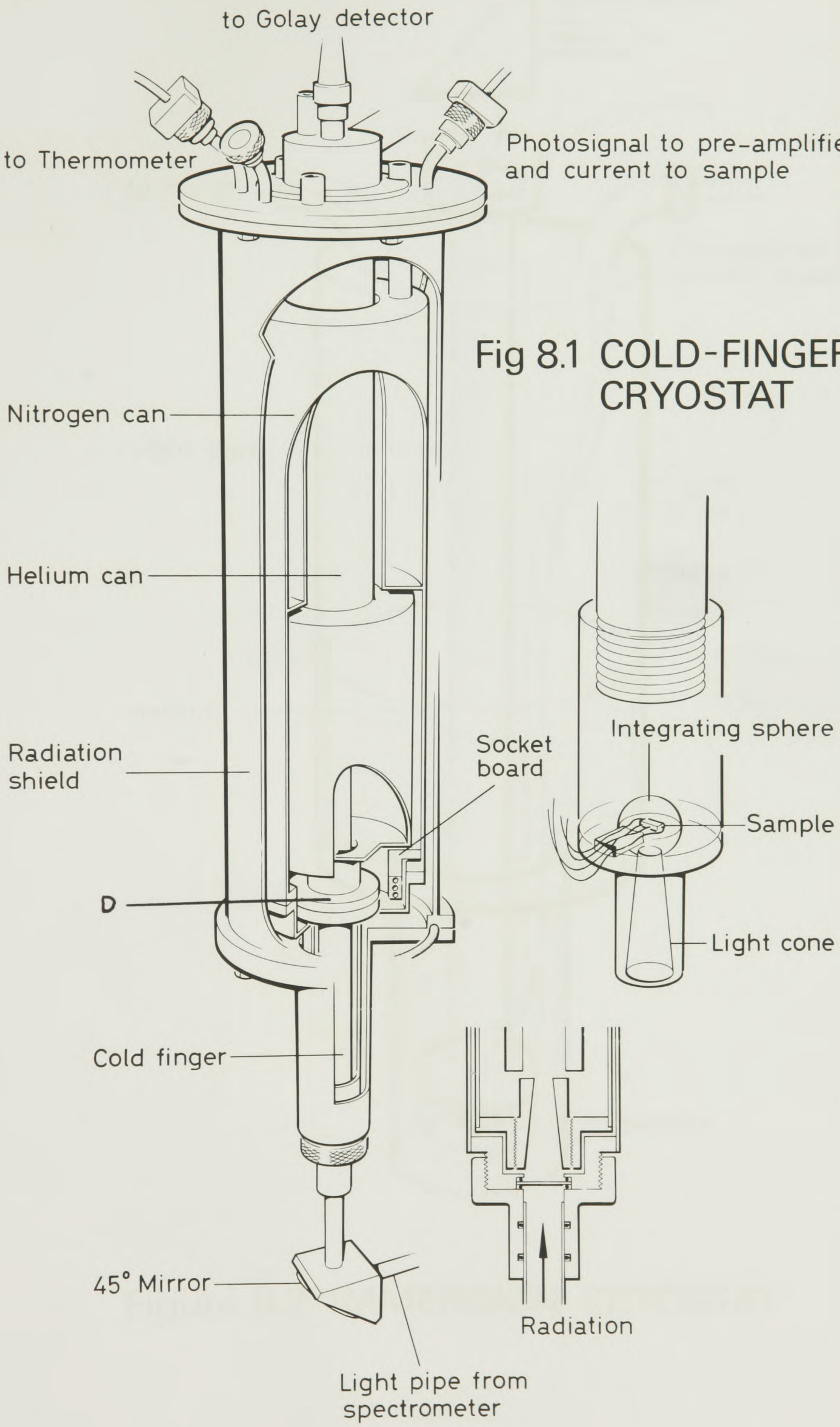


Fig 8.1 COLD-FINGER CRYOSTAT

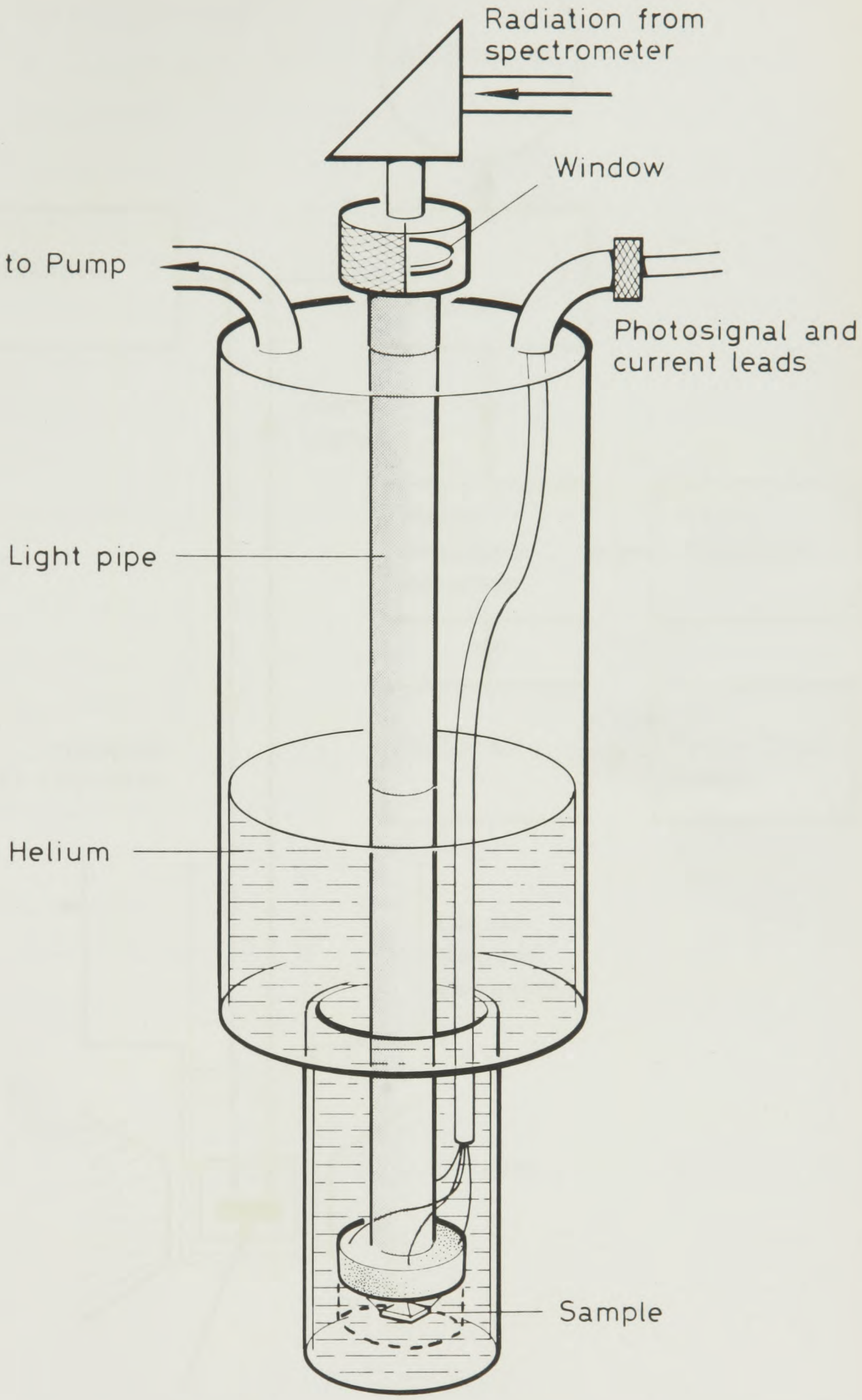


Figure 8.2 IMMERSION CRYOSTAT

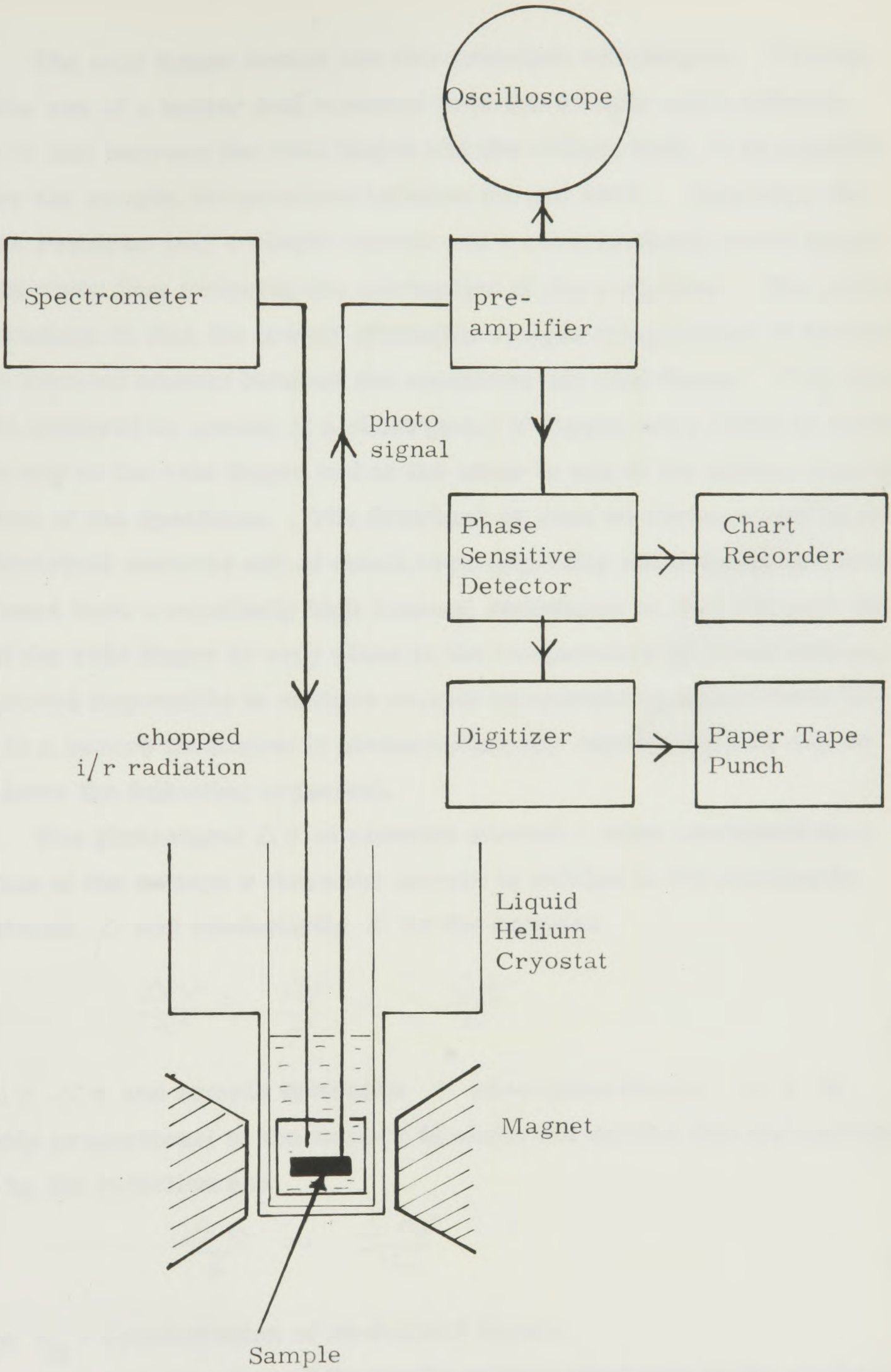


Figure 8.3 Block diagram of the apparatus employed in the infra red photoconductivity experiments

The cold finger design has two principal advantages. Firstly, with the use of a heater coil mounted near the sample and a suitable thermal link between the cold finger and the helium bath, it is possible to vary the sample temperature between 6K and 300K. Secondly, the system requires only a single mirror and a comparatively short length of light pipe, thus reducing the attenuation of the radiation. The principal disadvantage is that the lowest attainable sample temperature is limited by the thermal contact between the specimen and cold finger. This heat link is achieved by means of a short piece of copper wire which is soldered at one end to the cold finger and at the other to one of the indium electrical contacts of the specimen. The drawback of such an arrangement is that the electrical contacts are of small area (typically about $\frac{1}{2}$ mm in diameter) and hence have a relatively high thermal resistance so that although the end of the cold finger is very close to the temperature of liquid helium, it has proved impossible to achieve sample temperatures below about 6K. This is a severe limitation in photoconductivity experiments as can be seen from the following argument.

The photosignal Δv at constant current i when expressed as a fraction of the voltage v down the sample is related to the changes in resistance ρ and conductivity σ by the equation

$$\frac{\Delta v}{v} = \frac{\Delta \rho}{\rho} = -\frac{\Delta \sigma}{\sigma} \qquad (8.4)$$

If $\Delta v \ll v$ and sample thickness $\ll$ absorption length, $\Delta \sigma$ is directly proportional to the number of electrons excited into the conduction band by the radiation and

$$\frac{\Delta \sigma}{\sigma} \sim \frac{I n_d}{n_c} \qquad (8.5)$$

where n_d = concentration of un-ionised donors

n_c = concentration of thermally excited electrons in the conduction band

I = intensity of radiation

From Equations (8.4) and (8.5)

$$\Delta v \sim \frac{v I n_d}{n_c}$$

In practice, the value of applied voltage v is limited to about 1 V/cm since at higher electric fields severe noise is generated in the sample, probably due to the onset of impact ionisation of neutral donors. At temperatures below 10K, the value of n_d is roughly constant as the majority of electrons are already frozen out onto donor impurities. Hence the factor which determines the magnitude of $\triangle$ v is the concentration of conduction electrons, n_c which is exponentially dependant on temperature. Thus in InP, n_c increases by more than an order of magnitude as the temperature is reduced from 6K to 4K. For this reason a second cryostat, shown in Figure 8.2, was constructed with the sample mounted on a P.T.F.E. ring at the end of a stainless steel light-pipe and immersed in the liquid helium refrigerant. This system extends the working range for photoconductivity experiments down to pumped helium temperatures.

The schematic diagram in Figure 8.3 shows the lay-out of the spectrometer, cryostat and detection system. The infra-red radiation is mechanically chopped at a frequency of 1 Kc/s by means of rotation wheel and the photoresponse of the sample is measured using a standard four contact technique by passing a constant current through the two outer electrical contacts of the sample and amplifying the A.C. photovoltage generated between the two inner contacts with a low noise preamplifier. After further amplification, the signal is fed into a phase sensitive detector. The output interferogram is displayed on a chart recorder and simultaneously digitised and stored on paper tape. A subsequent Fourier transformation of the interferogram using the Oxford University I.C.L. 1906A Computer yields a graph plot of the photosignal as a function of wave-number (cm^{-1}).

8.3 Experimental Results and Discussion

The three samples of high purity epitaxial InP which were studied in the experiments described in this section have the properties summarised in Table 8.1.

Table 8.1

Sample	N_E(300K)	N_E(77K)	μ(300K)	μ(77K)
R.R.E.(B)	2×10^{15}cm^{-3}	1.4×10^{15}cm^{-3}	4,200cm^2/V.s	60,000cm^2/V.s
R.R.E.(D)	4×10^{14}cm^{-3}	3.7×10^{14}cm^{-3}	4,800cm^2/V.s	84,000cm^2/V.s
Plessey	3.6×10^{14}cm^{-3}	3.6×10^{14}cm^{-3}	3,700cm^2/V.s	52,000cm^2/V.s

The R.R.E. sample (B) was used in the magnetophonon experiments described in chapters 3 and 7 of this thesis.

The photoconductivity spectra for the three samples in zero magnetic field and at a field of 19 kG are shown in Figures 8.4, 8.5 and 8.6. The Zeeman-split 1s to 2p peaks in Figures 8.4 and 8.5 for the R.R.E. samples B and D reveal two dominant donor species which are present in approximately equal concentrations. The two donor types can just be detected in the zero field spectrum of sample B which yields 1s to 2p transition energies of 45.5 cm^{-1} and 46.1 cm^{-1}. Assuming that the impurity states are hydrogenic, the mean donor binding energy is estimated to be $\frac{4}{3}$ E(1s $\rightarrow$ 2p) = 61.0 cm^{-1}. Although the samples of InP are the purest available, the resolution of the component lines is considerably less than that obtained for high purity GaAs. The spectra shown in Figure 8.6 for the Plessey sample reveal only a single dominant component. In order to compare the donor energies in the three samples, the 1s to $2p_{-1}$ line was chosen since in the region of 20 kG the frequency of this transition reaches a minimum and is therefore insensitive to the calibration, homogeneity and stability of the applied magnetic field. The magnetic field variation of the 1s to $2p_{-1}$ peaks obtained for the three samples is shown in Figure 8.7. It is likely that the small frequency difference of about 0.1 cm^{-1} between the components a and b for different samples is due to the incomplete resolution of the peaks. Making allowance for this pulling effect of the overlapping lines, the true positions of the components at 20 kG are 40.65 cm^{-1}(a) and 41.35 cm^{-1}(b) with the single dominant donor in the Plessey sample being of type (a). The fine structure on the impurity lines has also been detected in experiments using infra-red gas lasers (Chamberlain et al. 1972, Stradling et al. 1972)

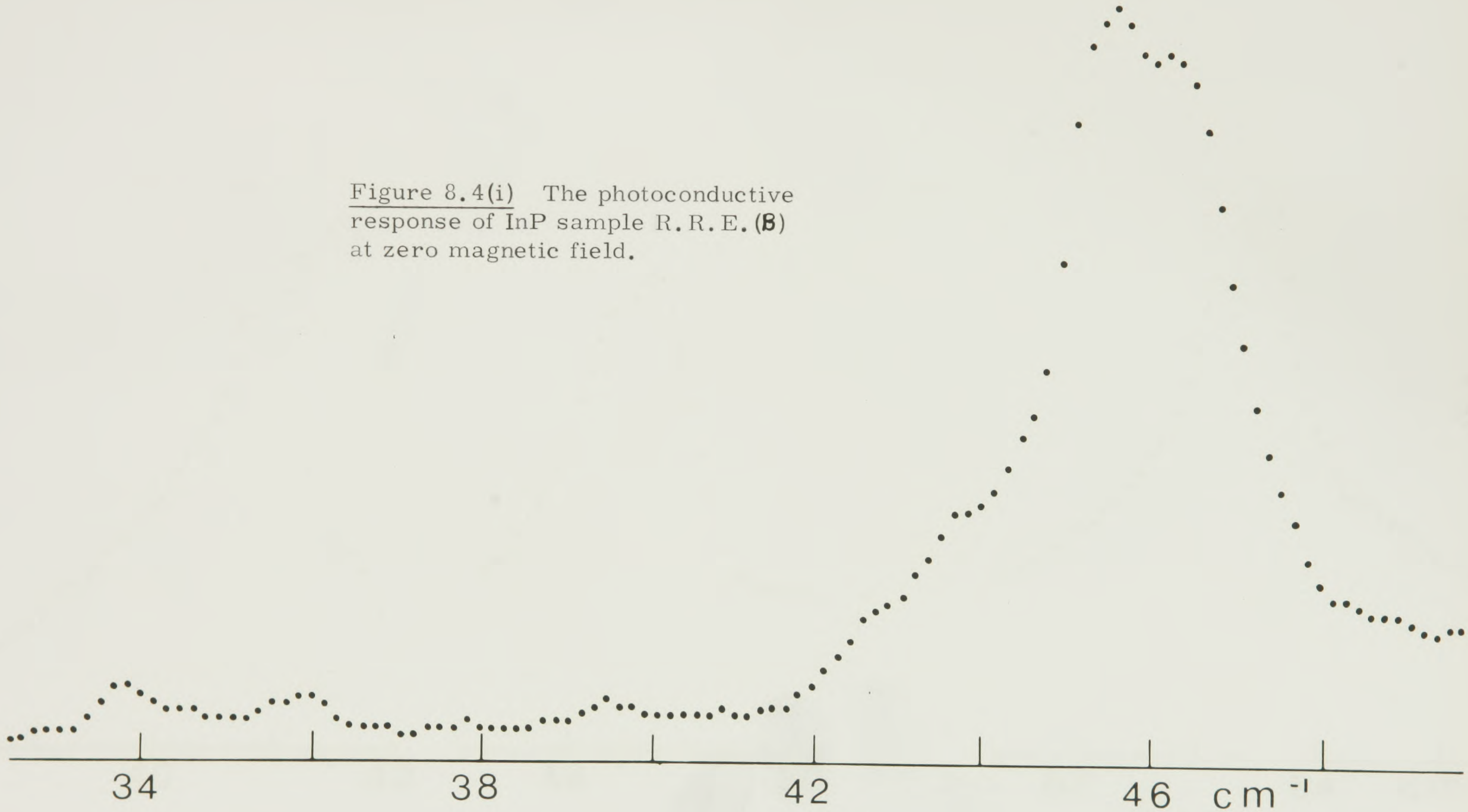


Figure 8.4(i) The photoconductive response of InP sample R.R.E.(B) at zero magnetic field.

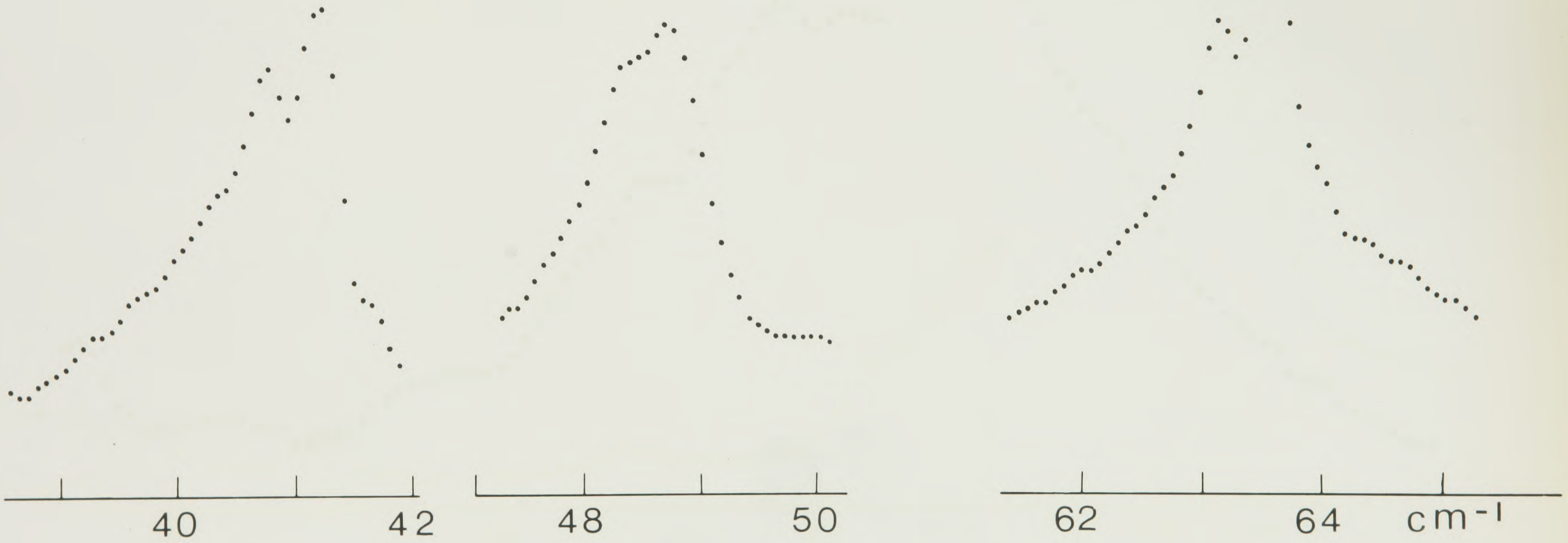
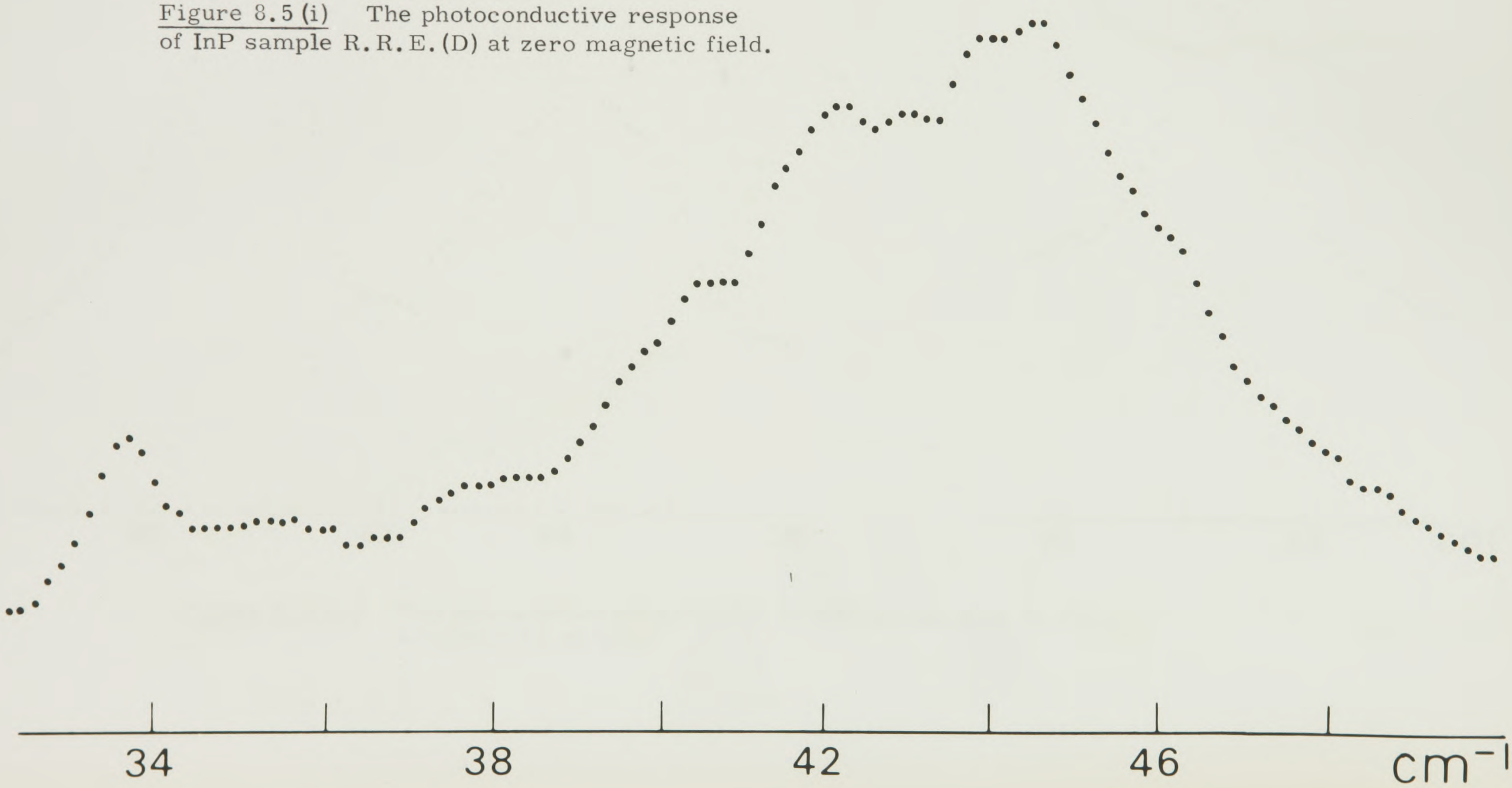


Figure 8.4(ii) The photoconductive response of InP sample R.R.E.(B) at a field of 19.42 kG.

Figure 8.5 (i) The photoconductive response of InP sample R.R.E.(D) at zero magnetic field.



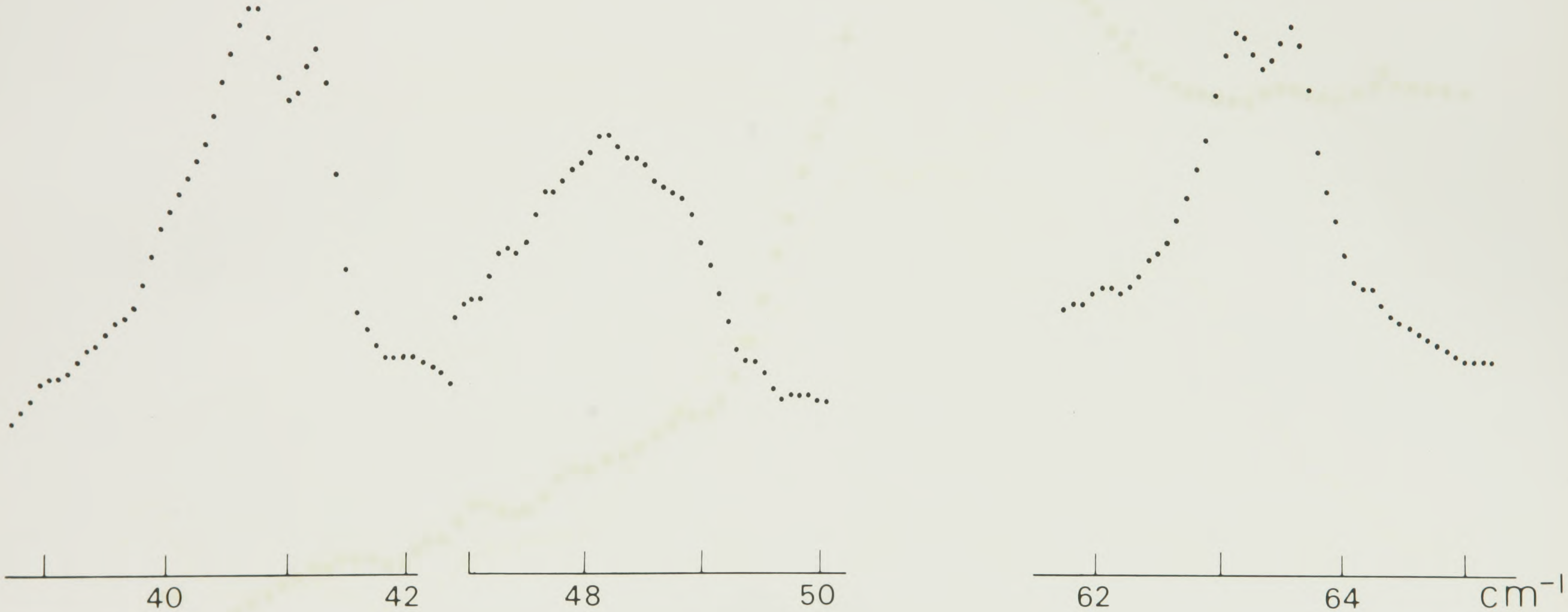


Figure 8.5 (ii) The photoconductive response of InP sample R.R.E.(D) at a field of 19.05 kG.

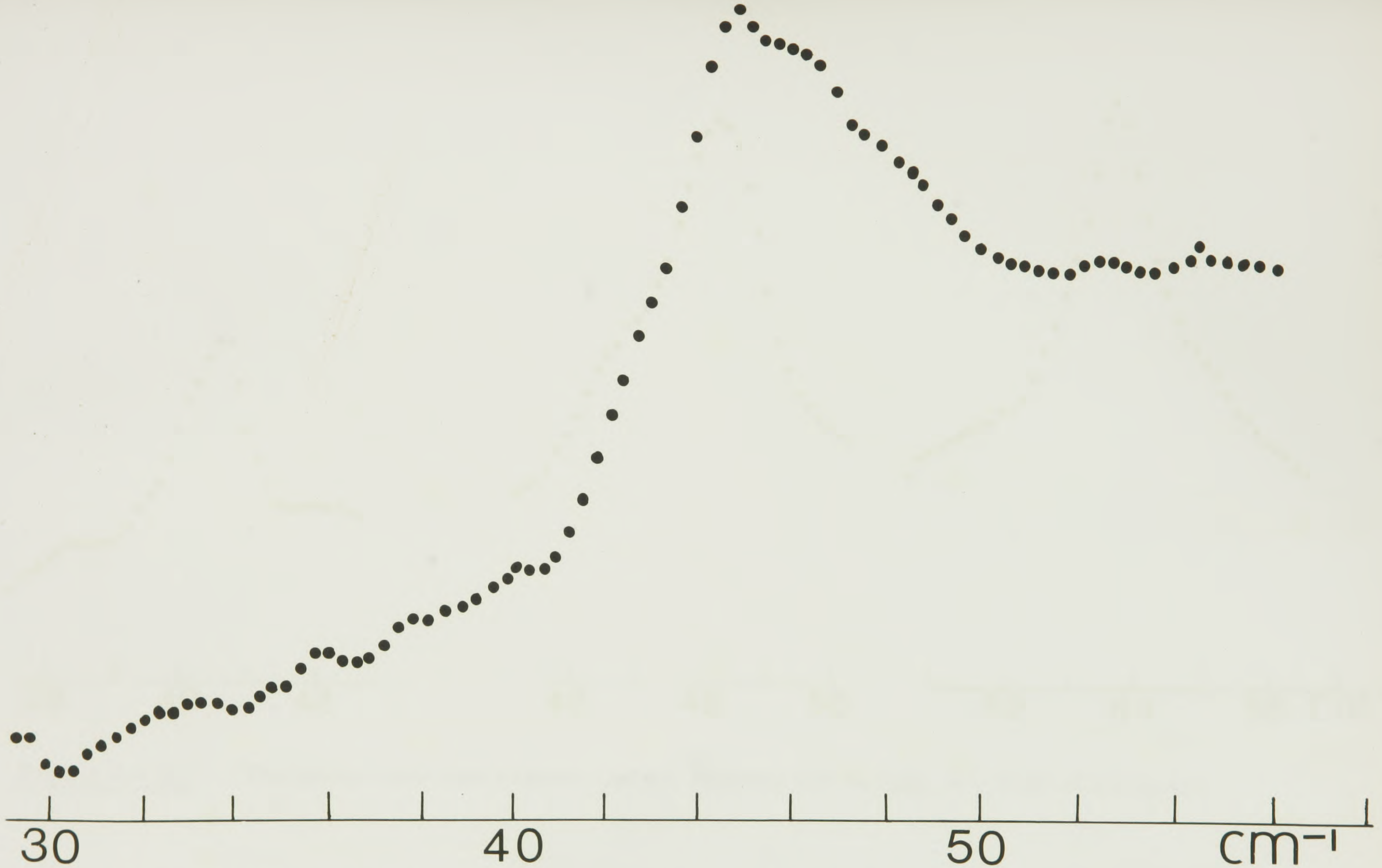


Figure 8.6 (i) The photoconductive response of the Plessey InP sample at zero magnetic field

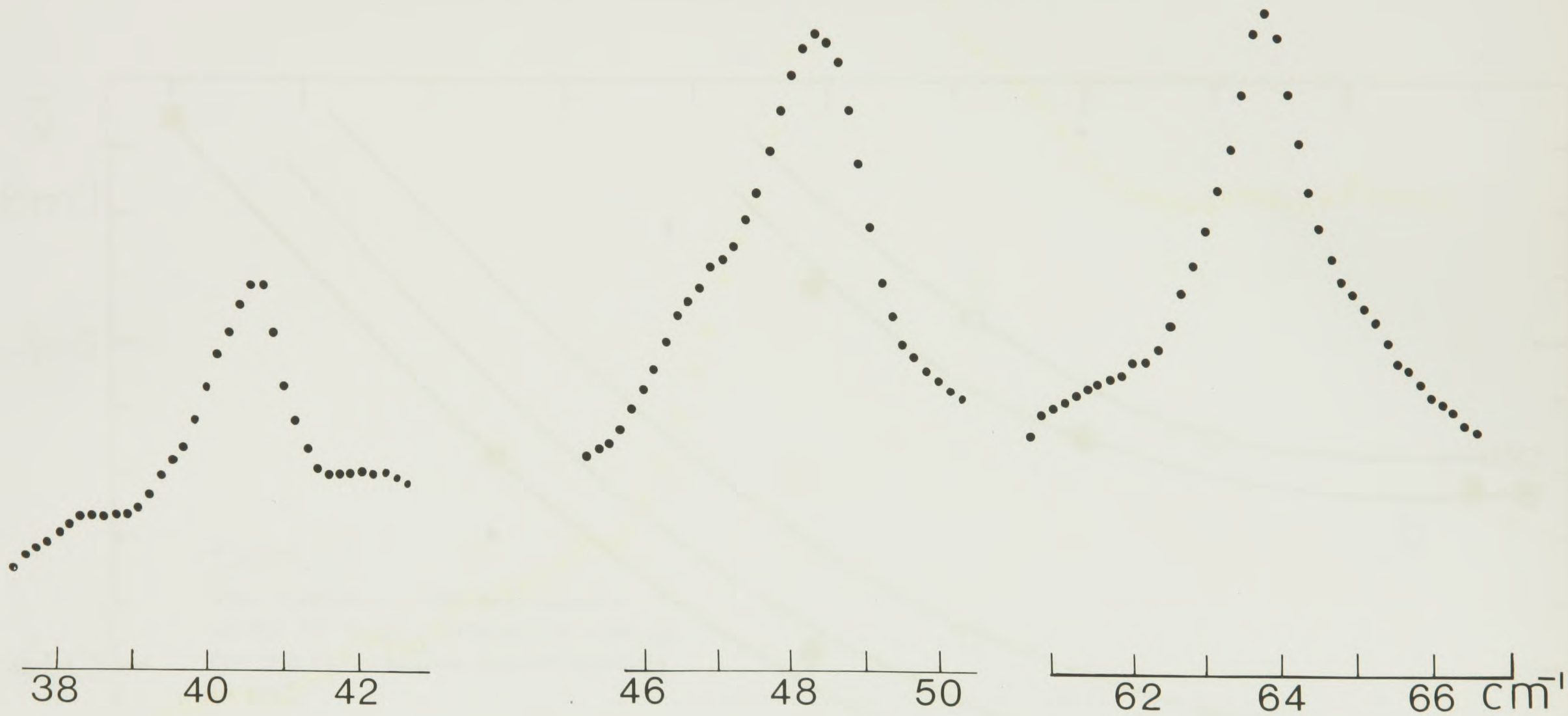


Figure 8.6 (ii) The photoconductive response of the Plessey InP sample at a field of 19.55 kG.

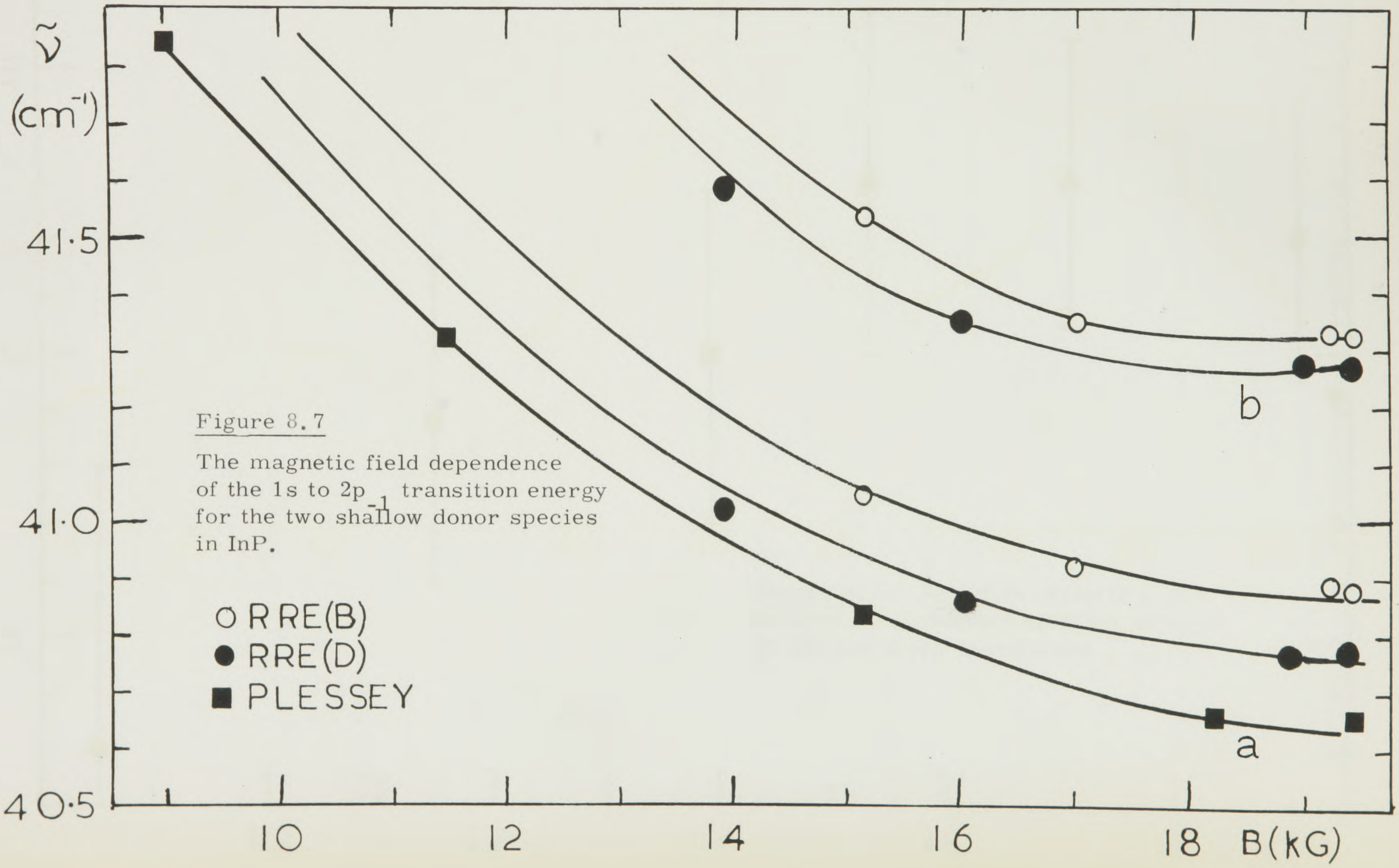


Figure 8.7

The magnetic field dependence of the 1s to $2p_{-1}$ transition energy for the two shallow donor species in InP.

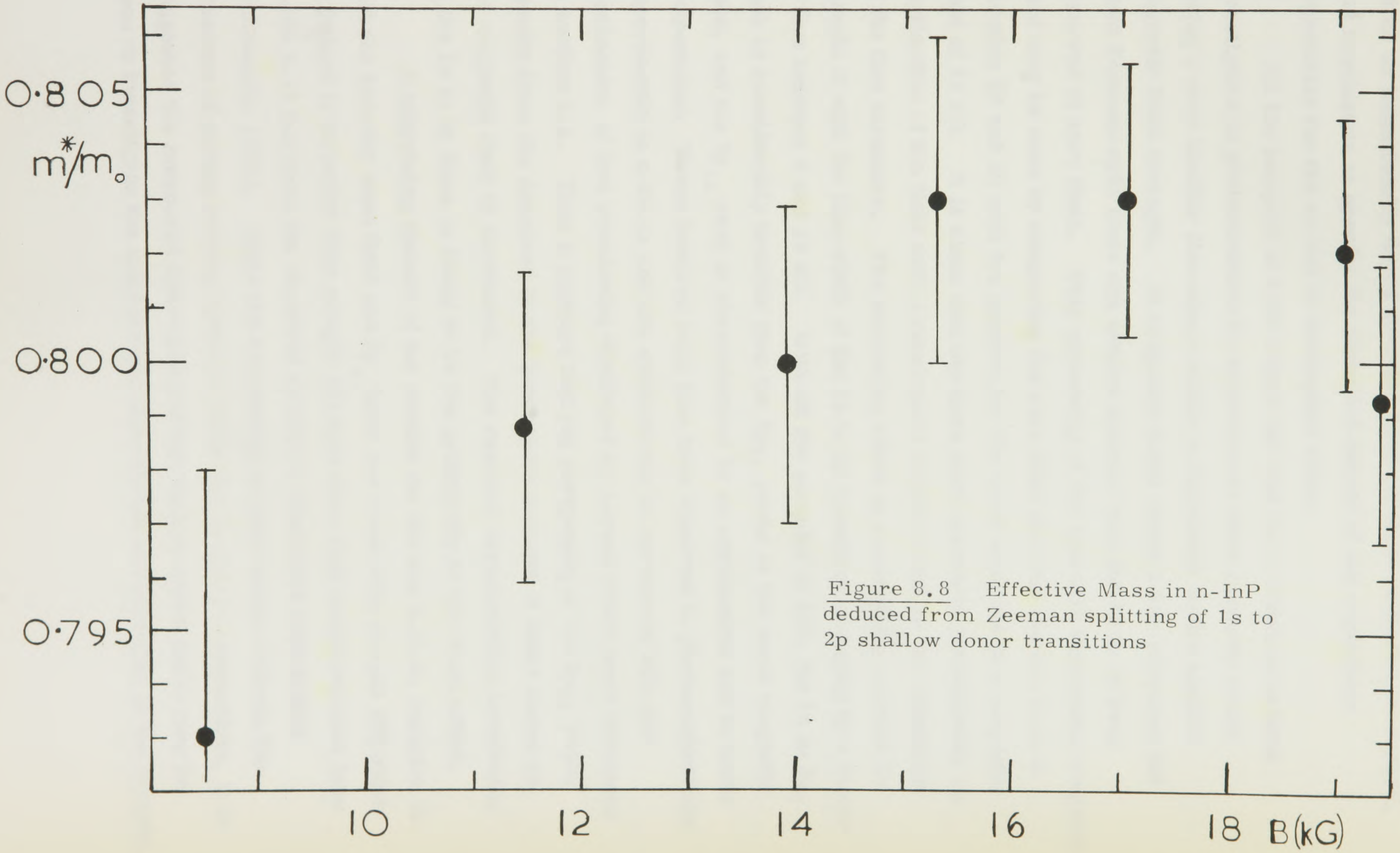


Figure 8.8 Effective Mass in n-InP deduced from Zeeman splitting of 1s to 2p shallow donor transitions

but as no intentionally doped samples have yet been prepared or studied, it is impossible to specify the chemical nature of the impurities responsible for the a- and b- component lines.

All the samples of both n-type InP and GaAs which have been investigated in photoconductivity experiments show impurity peaks having a very similar line-shape which is dependent on the applied magnetic field strength. At magnetic fields above a few kilogauss the three Zeeman-split lines are always sharper than the 1s to 2p peak observed at zero field. This narrowing of the line with increasing magnetic field may be seen by comparing the zero field data for the two R.R.E. samples (B and D) with the spectra for the same samples at a magnetic field of 19 kG. It is clear that the lines have narrowed considerably on application of the field with a consequent improvement in the resolution of the fine structure. The narrowing effect is particularly marked for sample D with the line-width of the 1s to 2p transition changing by a factor of five between 0 and 19 kG. With all the samples of InP, the 1s to $2p_o$ peak is considerably broader than the $2p_{\pm 1}$ peaks at the same magnetic field, and the $2p_{-1}$ peak is characterised by an asymmetric tail to lower frequencies. These features have also been observed in photoconductivity experiments in n-GaAs and are qualitatively in agreement with the mechanism of line broadening developed by Larsen which were discussed in section 8.2. Thus it appears that the sharpening of the $2p_{\pm 1}$ peaks results from the decrease in the quadrupole moment of these states as the magnetic field is increased. The residual asymmetrical broadening of the 1s to 2p lines is likely to be due principally to the Stark effect.

A surprising feature of the results for the two R.R.E. samples is that the broader zero field and $2p_o$ lines are found with sample (D) which is judged to be purer than sample (B) both from Hall measurements (see Table 8.1) and from the observed cyclotron resonance line-widths (Simmonds, 1972). Since the broadening of these peaks reflects the presence of strong random electric fields due to charged impurities, it is suggested the measured line-widths of the shallow donor peaks may be used to investigate the microscopic distribution of impurities in the sample.

Previous work on the Zeeman splitting of the 1s to 2p transitions by Chamberlain et al. (1971) have yielded a value of the conduction band effective mass ratio of 0.0810 ± 0.0005. As the resolution of the spectra presented in this chapter is considerably higher than that of this earlier work, a more precise estimate of the effective mass can now be made. Figure 8.8 shows the effective mass values calculated at various magnetic fields from the $2p_{\pm 1}$ peak positions of donor species b for the R.R.E. sample B. The value of m^* is given by the equation

$$E(2p_{+1}) - E(2p_{-1}) = \frac{\pm eB}{m^*} \qquad (8.6)$$

At fields below about 8 kG, it was difficult to estimate an accurate value of the effective mass because of the increased broadening of the $2p_{\pm 1}$ lines and their overlapping with the $2p_o$ peak. It is possible that the slightly lower mass value obtained at a field of 8.5 kG reflects the Stark perturbation on the $2p_{\pm 1}$ states which were observed by Stillman et al. (1971) in GaAs. The effective mass ratio of 0.0802 ± 0.0003 deduced from the Zeeman splitting at fields above 10 kG is in excellent agreement with other estimates as can be seen by reference to Table 3.2 of Chapter 3.

In addition to the peaks arising from transitions between states of the shallow donor impurities, the photoconductive response showed additional structure at a frequency of 33.8 cm^{-1}. This line, although visible in all three samples of InP, appeared to be strongest in sample D. It was impossible to detect any splitting or shift of the peak position with magnetic field although its amplitude relative to the 1s to 2p shallow donor peaks was suppressed at fields above a few kilogauss. A similar line has also been observed in the photoconductive response of GaAs (Stradling, 1972; Hoult, 1972) and CdTe (Simmonds, 1971). In all three materials the frequency of the peak corresponds to approximately 70% of the zero field 1s to 2p transition energy and its intensity appears to be directly related to the line-width of the shallow donor transitions. The peak is too well separated from the main 1s to 2p line to be attributable to a neutral donor transition and at present its origin cannot be explained. However, its association with broad lines suggests that it may result from the interaction of two or more impurities.

REFERENCES

Aggarwal, R.L., Zuteck, M.D. and Lax, B. Phys. Rev. Lett. 19, 236 (1967)

Aggarwal, R.L. private communication (1972)

Akselrod, M.M. and Tsidilkovskii, I.M. Zh. eksp. teor. Fiz. 9, 622 (Sov. Phys. JETP Lett. 9, 381) (1969)

Alfrey, G.F. and Borcherds, P.H. J. Phys. C. 5, 20, L275. (1972)

Argyres, P.N. and Roth, L.M. J. Phys. Chem. Solids 12, 89 (1959)

Askenazy, S., Leotin, J. and Ulmet, J.P. Phys. Lett. 29A, 9 (1969)

Askenazy, S. et al. Solid State Commun. 9, 729 (1971)

Barker, J.R. Phys. Lett. 33A, 8, 516 (1970)

Barker, J.R. J. Phys. C. Sol. St. Phys. 5, 1675 (1972)

Barker, J.R. private communication, to be published J. Phys. C. Sol. St. Phys. (1972a)

Bashirov, R.I., Mollaev, A. Yu., Siukaev, N.V. Sov. Phys. Solid State 13, 10, 2597 (1972)

Bashirov, R.I., Mollaev, A. Yu., Siukaev, N.V. Sov. Phys. Solid State 13, 11, 2892 (1972)

Bell, R.J. Introductory Fourier Transform Spectroscopy (Academic Press 1972)

Bernstein, L. and Beale, R.J. J. appl. Phys. 32, 122-3 (1961)

Brockhouse, B.N. and Dasannacharya, B.A. Solid State Commun. 1, 205 (1963)

Button, K.J. and Lax, B. Bull. Am. Phys. Soc. 15, 365 (1970)

Cabib, D., Fiorio, G. and Fabri E. Solid State Comm. 9, 1517 (1971) and to be published

Chamberlain, J.M., Ergun, H.B., Gehring, K.A. and Stradling, R.A. Solid State Comm. 9, 1563 (1971)

Chamberlain, J.M., Simmonds, P.E., Stradling, R.A. and Bradley, C.C. J. of Phys. C, 4, L38 (1971)

Chamberlain, J.M., Simmonds, P.E., Stradling, R.A. and Bradley, C.C. Solid State Comm. 11, 463 (1972)

Chamberlain, J.M., Simmonds, P.E., Stradling, R.A. and Bradley, C.C. Proc. Int. Conf. on Physics of Semiconductors, Warsaw (1972a) to be published

Curby, R.C. and Ferry, D.K. Proc. Int. Conf. on Physics of Semiconductors, Warsaw (1972) to be published

Dickey, D.H. and Larsen, D.M. Phys. Rev. Lett. 20, 65 (1968)

Dworin, L. Phys. Rev. 140, A1689 (1965)

Eaves, L., Stradling, R.A., Wood, R.A. Proc.Int.Conf. on Physics of Semiconductors (Boston), 816 (1970)

Eaves, L., Stradling, R.A., Askenazy, S., Leotin, J., Portal, J.C. and Ulmet, J.P. J.Phys.C. Sol.St.Phys. 4, L42 (1971)

Eaves, L., Stradling, R.A., Askenazy, S., Carrère, G., Leotin, J., Portal, J.C. and Ulmet, J.P. J.Phys. C. Sol.St. Phys. 5, L19 (1972)

Evtuhov, V. Phys.Rev. 125, 1869 (1962)

Fan, H.Y. Phys.Rev. 82, 6, 900 (1951)

Faulkner, R.A. Phys.Rev. 184, 713 (1969)

Fetterman, H.R., Larsen, D.M., Stillman, G.E., Tannenwald, P.E. and Waldman, J. Phys.Rev.Lett. 26, 975 (1971)

Fletcher, R.C., Yager, W.A. and Merritt, F.R. Phys.Rev. 100, 747 (1955)

Folberth, O.G. and Weiss, H., Z. Naturforsch 10A, 615 (1955)

Ginter, J. Phys.Stat.Solidi 8, K141 (1965)

Glicksman, N. and Weiser, K. J.Electrochem.Soc. 105, 728 (1958)

Gluzman, N.G. and Tsidilkovskii, I.M. Sov.Phys.Sol.Stat. 10, 2469 (1969a)

Gluzman, N.G. and Tsidilkovskii, I.M. Sov.Phys.Semicond. 2, 869, (1969b)

Gurevich, V.L. and Firsov, Y.A. Sov.Phys. J.E.T.P. 13, 137 (1961)

Gurevich, V.L. and Firsov, Y.A. Sov.Phys. J.E.T.P. 20, 489 (1964)

Hamaguchi, C., Shirakawa, T., Yamashita, T. and Nakai, J. Phys.Rev. Lett., 28, 1129 (1972)

Harper, P.G. et al. Proc.Int.Conf. on Physics of Semiconductors (Boston) 166, (1970)

Harper, P.G., Hodby, J.W., Stradling, R.A. to be published Rep.Prog. Phys. (1972)

Hensel, J.C. Proc.Int.Conf. on Physics of Semiconductors (Exeter) 281 (1962)

Hensel, J.C. and Suzuki, K. Proc.Int.Conf. on Physics of Semiconductors (Boston) 541 (1970)

Hickernell, F.S. and Gayton, W.R. J.Appl.Phys. 37, 462 (1966)

Hilsum, C. and Rees, H.C. Electron.Lett. 6, 277 (1970)

Hoult, R.A. private communication (1972)

Hoult, R.A. and Stradling, R.A. private communication (1972)

Iwasa, S., Balsev, I., Burstein, E. Proc.Int.Conf. on Physics of Semiconductors (Paris) New York: Academic Press, 1077 (1964)

Jenkin, G.T. D.Phil. Thesis, Oxford University (1972)

Johnson, E.J. Semiconductors and Semimetals 3, (Ed. Willardson and Beer) 153 (1967)

Kesemanly, F.P., Klotyn'sh, E.E., Mal'tsev, Yu. V., Nasledov, D.N. and Ukhanov, Yu. I. Sov.Phys.Solid.St. 6, 109 (1964)

Kharus, G.I. and Tsidilkovskii, I.M. Sov.Phys. Semiconductors 5, 534 (1971)

Kimmitt, M.F. Far Infra Red Techniques (Pion, London, 1970)

Kittel, C. Quantum Theory of Solid (New York: Wiley 1963)

von Klitzing, K. and Landwehr, G. Solid State Commun. 9, 1251 (1971)

Köhl, F. J.Phys.Chem.Solids 32, 2481 (1971)

Kotera, N., Komatsubara, K.F., Yamada, E. Proc.Int.Conf. on Physics of Semiconductors (Kyoto) 411, (1966)

Kubo, R., Miyake, S.J. and Hashitsume, N. Solid State Phys. (New York: Academic Press) 17, 269 (1965)

Kubo, S. and Onuki, M. J.Phys.Soc.Japan 20, 1280 (1965)

Langer, D.W., Park, Y.S. and Euwema, R.N. Phys.Rev. 152, 788 (1966)

Larsen, D.M. J.Phys.Chem.Sol. 29, 271 (1968)

Larsen, D.M. to be published (1972)

Lawaetz, P. Phys.Rev. 183, 730 (1969)

Lax, M. Bull.Am.Phys.Soc. 6, 109 (1961)

Levinger, B.W. and Frankl, D.J. Phys.Chem.Solids 20, 281 (1961)
Love, W.F. and Wei, W.F., Phys. Rev. 123, 67, (1961).
Luttinger, J.M. and Kohn, W. Phys.Rev. 97, 869 (1955)

Luttinger, J.M. Phys.Rev. 102, 1030 (1956)

Mahan, G.D. and Hopfield, J.J. Phys.Rev.Lett. 12, 241 (1964)

McCombe, B.D. and Kaplan, R. Phys.Rev.Lett. 21, 756 (1968)

Mears, A.L., Stradling, R.A. and Inall, E.K. J.Phys.C. Sol.St. Phys. 1, 821 (1968)

Mears, A.L. and Stradling, R.A. J.Phys.C. Solid St.Phys. 4, L22 (1971)

Mikaye, S.J. Phys.Rev. 170, 726 (1968)

Mitra, S.S. Phys.Rev. 132, 986 (1963)

Mitra, S.S. Proc.Int.Conf.Physics of Semiconductors (Kyoto) J.Phys. Soc.Japan 21 Suppl. 61-6 (1966)

Mooradian, A. and Wright, G.B. Solid St. Commum. 4, 431 (1966)

Moss, T.S. and Walton, A.R., Physica 25, 1142 (1959)

Newman, R. Phys.Rev. 111, 1518 (1958)

Ngai, K. private communication (1972)

Okazaki, M. J. Phys. Soc. Japan 17, 1865 (1962)

Paige, E. G. S. Prog. in Semiconductors (Heywood and Co. Ltd., London) 8, 1, (1964)

Palik, E. D. and Wallis, R. F. Phys. Rev. 123, 131 (1961)

Palmer, R. J. D. Phil. Thesis, Oxford University (1970)

Parker, J. H., Feldman, D. W. and Ashkin, M. Phys. Rev. 155, 712 (1967)

Parrish, J. F. et al. II-VI Semiconductor Compounds Int. Conf. ed. D. G. Thomas (New York: Benjamin) 1164 (1968)

Peterson, R. L. Phys. Rev. Lett. 28, 431 (1972)

Peterson, R. L. Phys. Rev. B5, 10, 3994 (1972)

Pitt, G. D. Solid St. Commum. 8, 1119 (1970)

Pollack, F. H., Higginbotham, C. W. and Cardona, M., Proc. Int. Conf. on Physics of Semiconductors (Kyoto) 20, (1966)

Prajoux, R., Gaetcher, J.-P., Askenazy, S. Conf. on High Magnetic Fields and their Applications (Nottingham) Inst. of Phys. and Phys. Soc. (1969)

Ray, R. K., Aggarwal, R. L., Lax, B. Proc. Int. Conf. on Light Scattering in Solids (Paris) Ed. Balkanski (1971)

Reynolds, D. C., Litton, C. W. and Collins, T. C. Phys. Rev. 177, 1161 (1969)

Roth, L. M. and Argyres, P. N. Semiconductors and Semimetals (Academic Press: New York) 1, 159 (1966)

Simmond, P. E. private communication (1972)

Slack, G. A. and Roberts, S. Phys. Rev. B 3, 2613 (1971)

Smith, D. T. B. Sc. Thesis, Oxford University (1967)

Sokolov, V. I. and Tsidilkovskii, I. M. Sov. Phys. Semiconductors 1, 695 (1967)

Stierwalt, D. L. and Potter, R. F., Phys. Rev. 137A, 1007 (1965)

Stillman, G. E., Wolfe, C. M. and Dimmock, J. O. Solid State Commun. 7, 921 (1969)

Stillman, G. E., Larsen, D. M., Wolfe, C. M. and Brandt, R. Solid State Commun. 9, 2245 (1971)

Stillman, G. E., Larsen, D. M. and Wolfe, C. M. Phys. Rev. Lett. 27, 15, 989 (1971)

Stradling, R. A. and Wood, R. A. Solid State Comm. 6, 701 (1968)

Stradling, R. A. and Wood, R. A., J. Phys. C. Solid. St. Phys. 1, 1711 (1968)

Stradling, R. A. and Wood, R. A., J. Phys. C. Solid. St. Phys. 3, L94 (1970)

Stradling, R.A. and Wood, R.A. J.Phys. C. Solid St. Phys. 3, 2425 (1970)

Stradling, R.A., Eaves, L., Hoult, R.A., Mears, A.L. and Wood, R.A. Proc.Int. Conf. on Physics of Semiconductors (Boston) 369 (1970)

Stradling, R.A. Proc. of Summer School on Semiconductors at McGill University (Wolters-Noordhoff Holland 1971)

Stradling, R.A., Eaves, L., Hoult, R.A., Miura, N., Simmonds, P.E. and Bradley, C.C. Proc.Int.Symposium on GaAs and related compounds (Boulder, Colorado) Publ: Inst. of Physics (1972)

Stradling, R.A. Proc.Int.Conf. on Physics of Semiconductors (Warsaw) to be published (1972)

Summers, C.J., Dingle, R., Hill, D.E. Phys.Rev. B1, 1603 (1970)

Vrehen, Q.H.F. J.Phys.Chem.Solids, 29, 129 (1967)

Wallis, R.F., Bowlden, H.J. Phys.Rev. 118, 456 (1960)

Waugh, J.L.T. and Dolling, G. Phys.Rev. 132, 2410 (1963)

Weinreich, G., Sanders, Jr. T.M., White, H.G. Phys.Rev. 114, 33 (1959)

Wheeler, R.G. and Dimmock, J.O. Phys.Rev. 125, 1805 (1962)

Wood, R.A. D.Phil. Thesis, Oxford University (1970)

Yamada, E. and Kurosawa, T. Proc.Int.Conf. on Physics of Semiconductors (Moscow) 805 (1968)